FISEVIER

Contents lists available at ScienceDirect

### Palaeogeography, Palaeoclimatology, Palaeoecology

journal homepage: www.elsevier.com/locate/palaeo



# The relationship between total organic carbon and bottom water redox state in North American black shales

Samantha R. Ritzer<sup>a,\*</sup>, Shane Schoepfer<sup>b</sup>, Bella Bussian<sup>c</sup>, Una C. Farrell<sup>d</sup>, Tiffani Fraser<sup>e</sup>, Charles M. Henderson<sup>f</sup>, Junyao Kang<sup>g</sup>, Chiza N. Mwinde<sup>h</sup>, Austin Patch<sup>i</sup>, Erik A. Sperling<sup>a,\*</sup>

- <sup>a</sup> Department of Earth and Planetary Sciences, Stanford University, Stanford, CA 94305, USA
- <sup>b</sup> Geoscience and Natural Resources, Western Carolina University, Cullowhee, NC 28723, USA
- Geology Department, Colorado College, Colorado Springs, CO 80903, USA
- <sup>d</sup> Department of Geology, Trinity College Dublin, Dublin, Ireland
- e Yukon Geological Survey, Government of Yukon, Whitehorse, YT Y1A 2C6, Canada
- <sup>f</sup> Department of Geosciences, University of Calgary, 2500 University Drive NW, Calgary, Alberta T2N 1N4, Canada
- g Department of Geosciences, Virginia Tech, Blacksburg, VA 24060, USA.
- <sup>h</sup> Department of the Geophysical Sciences, University of Chicago, Chicago, IL, 60637, USA
- i Department of Geography, Geology, Environment, and Planning, Indiana University of Pennsylvania, 1011 South Drive, Indiana, PA 15705, USA

#### ARTICLE INFO

Editor: B. Shen

Keywords: Euxinic Ferruginous Organic matter iron speciation Black shale

#### ABSTRACT

It is clear from modern analogue studies that O2-deficient conditions favor preservation of organic matter (OM) in fine-grained sedimentary rocks (black shales). It is also clear that appreciable productivity and OM flux to the sediment are required to establish and maintain these conditions. However, debates regarding redox controls on OM accumulation in black shales have mainly focused on oxic versus anoxic conditions, and the implications of different anoxic redox states remain unexplored. Here, we present detailed multi-proxy sedimentary geochemical studies of major Paleozoic and Mesozoic North American black shale units to elucidate their depositional redox conditions. This is the first broad-scale study to use a consistent geochemical methodology and to incorporate data from Fe-speciation - presently the only redox proxy able to clearly distinguish anoxic depositional conditions as ferruginous (H2S-limited) or euxinic (H2S-replete, Fe-limited). These data are coupled with total organic carbon (TOC), programmed pyrolysis, and redox-sensitive trace element proxies, with almost all measurements analyzed using the same geochemical methodology. Consistent with expectations based on previous geochemical and paleontological/ichnological studies, these analyses demonstrate that the study units were almost exclusively deposited under anoxic bottom waters. These analyses also demonstrate that there is wide variance in the prevalence of euxinic versus ferruginous conditions, with many North American black shale units deposited under predominantly ferruginous or oscillatory conditions. TOC is significantly higher under euxinic bottom waters in analyses of both preserved (present day) TOC and reconstructed initial TOC values, although sediments deposited under both redox states do have economically viable TOC content. While this correlation does not reveal the mechanism behind higher organic enrichment in euxinic environments, which may be different in different basins, it does open new research avenues regarding resource exploration and the biogeochemistry of ancient reducing environments.

#### 1. Introduction

Although organic-rich sedimentary rocks may be deposited in a wide range of settings (Trabucho-Alexandre, 2015a), their ultimate organic matter content is dependent upon a source (primary productivity or terrigenous input), a mechanism for flux to the sediment, and a

mechanism for preservation (Katz, 2005; Tyson, 2005). Questions of preservation (anoxia) versus productivity in the generation of organic-rich sedimentary units were heavily studied and debated during the 1970–1990s, and it was largely resolved that both factors were important, and the relative importance (along with sedimentation rate, i.e. Anttila et al. (2023)) can vary dramatically between different settings.

E-mail addresses: samritzer@gmail.com (S.R. Ritzer), esper@stanford.edu (E.A. Sperling).

https://doi.org/10.1016/j.palaeo.2024.112266

<sup>\*</sup> Corresponding authors.

Such questions are now worth revisiting using the modern sedimentary geochemical toolkit and our increased knowledge of the biogeochemical nature of anoxia.

Here, we conduct a comprehensive geochemical analysis of nine major North American black shale units and investigate the relationship between the inferred redox state of the bottom waters under which these shales, mudstones, and other fine-grained sediments were deposited and the total organic carbon (TOC) contents of the sediments. Throughout this paper, 'black shale' is used as a colloquial shorthand following Wignall (1994) for fine-grained sedimentary strata bearing appreciable organic matter (generally >0.5 wt%). Although we have not sampled every organic-rich shale in North America, to our knowledge this is the largest public geochemical dataset generated to date that utilizes generally consistent methodology across all sampled stratigraphy, thus allowing for direct comparison between stratigraphic units in a manner not previously possible.

A major focus of our research is the biogeochemical nature of anoxia, and more specifically, the proportions of ferruginous (anoxic, sulfidelimited, containing free ferrous iron) vs. euxinic (anoxic, iron-limited, containing free sulfide) conditions in the bottom waters of North American shale basins. While both conditions are anoxic, ferruginous conditions are limited by sulfide availability, and thus dissolved ferrous iron can persist in the water column. In contrast, under euxinic conditions, sulfate reduction in the water column produces hydrogen sulfide, which reacts readily with dissolved ferrous iron, stripping it from the system as pyrite (and/or other Fe-sulfide minerals) and allowing for free sulfide to accumulate in the water column. The factors that control the distribution of ferruginous and euxinic bottom waters are the relative availability of adequate levels of organic carbon, sulfate for reduction to sulfide, and reactive iron to form pyrite (Raiswell and Canfield, 2012). In a water column with sufficient sulfate availability, abundant organic carbon loading will eventually exhaust more energetically favorable electron acceptors (i.e., O2, NO3, Mn4+ and Fe3+) and drive the system to sulfate reduction, producing sulfides that effectively titrate out available reactive iron, leading to euxinic water column conditions (Johnston et al., 2010; Van De Velde et al., 2020).

In the present day, our oceans are well oxygenated, except for a few locally euxinic basins. With a proxy toolkit based on these modern euxinic analogues, ferruginous conditions have not often been specifically identified in paleoenvironmental studies. The assumption that anoxic conditions are usually also euxinic is typically based on the observation of notable quantities of pyrite in a black shale. However, iron geochemistry studies demonstrate that it is not simply pyrite contents, but rather the ratio between pyrite iron and other reactive iron phases (i.e., the iron speciation proxy, reviewed by Raiswell et al., 2018; Raiswell and Canfield, 2012) that effectively identifies whether ancient bottom waters were euxinic, or anoxic and non-sulfidic (ferruginous). Recent studies have shown that for much of Earth history, many organicrich black shales were deposited under ferruginous conditions (Canfield et al., 2008; Guilbaud et al., 2015; Planavsky et al., 2011; Poulton and Canfield, 2011; Sperling et al., 2015). While ferruginous conditions have most notably been identified in the Proterozoic, they are increasingly being recognized in the Phanerozoic as well (Hancock et al., 2019; LeRoy and Gill, 2019; Marz et al., 2008; Sperling et al., 2021; Young et al., 2020).

One issue with the identification of ancient ferruginous water columns is that, traditionally, many shale redox geochemical studies have utilized redox-sensitive trace metals (RSMs) as the primary proxy. These are metals that are soluble under oxygenated conditions, but under anoxic conditions become insoluble and/or can complex with organic carbon, sulfides, and other phases to become authigenically enriched in the sediment. Different elements are enriched at different redox potentials, via different mechanisms, and thus have the potential to yield important insights into paleoenvironmental conditions (reviewed by Tribovillard et al., 2006). Unfortunately, RSMs can also be ambiguous with respect to the nature of anoxic conditions. Specifically, while very

high enrichments in RSMs generally indicate deposition beneath euxinic bottom waters (e.g., Scott and Lyons, 2012), lower enrichments are non-unique and could represent 1) deposition under oxic conditions, 2) deposition under suboxic, ferruginous, or fluctuating conditions, or 3) deposition under persistent euxinic conditions, but with low aqueous trace metal concentrations due to basinal restriction or globally widespread reducing conditions (Algeo, 2004; Algeo and Rowe, 2012; Emerson and Huested, 1991; Gill et al., 2011; Scott et al., 2008). RSM trends can also be obscured by changes in detrital provenance (Cole et al., 2017) and/or by changes in sedimentation rate (Crombez et al., 2020).

In this study, we use a multi-proxy approach incorporating iron speciation and RSMs to test the redox state of bottom waters above deposited sediments. In this way, these proxies can serve as independent tests of redox state. Given the increasing frequency with which ferruginous conditions are currently being identified in the ancient black shale record, we perhaps not surprisingly find that many North American black shales are wholly or partially deposited under ferruginous bottom waters. We then combine these data with TOC and programmed pyrolysis analyses to investigate the relationship between TOC and redox state, using both present-day TOC values and reconstructed initial TOC values.

The relationship between TOC and euxinic versus ferruginous conditions has been investigated in individual Proterozoic basins (Johnston et al., 2010; Sperling et al., 2013), but not in a comparative study of Phanerozoic black shales or using initial TOC values. Understanding such relationships are important for debates about whether the development of ferruginous/anoxic and non-sulfidic conditions is more generally related to upwelling of deep-water Fe<sup>2+</sup> (Poulton et al., 2010) or relatively lower rates of organic carbon input (Johnston et al., 2010). These statistical analyses do not provide clear evidence of a single mechanism - as with the productivity versus preservation debate, the answer is probably 'both', with variable importance in different settings. However, the demonstrable correlations seen here between TOC and redox state provide important new insights into the economic development of these units and black shale biogeochemistry more broadly.

### 2. Geochemical background

#### 2.1. The iron speciation paleoredox proxy

The presence of iron is ubiquitous in sediments of all ages and can be found in a wide range of mineralogical configurations. The partitioning of total iron into these different phases can be useful in determining certain characteristics of pore and bottom water conditions. In this study, we quantify and interpret iron contents as a proxy for depositional and early diagenetic redox conditions at or around the sedimentwater interface following the logic and procedures originally set forth by Canfield (1989), Raiswell et al. (1994), and Raiswell and Canfield (1998), recently reviewed and updated by Poulton (2021) and Raiswell et al. (2018).

To briefly describe the basis for this proxy system, we begin with an initial assumption that in stratified marine systems, dissolved and nanoparticulate forms of iron are delivered to the basin depocenter via repeated cycles of reduction and oxidation (Raiswell and Canfield, 2012), a mechanism commonly referred to as the "iron shuttle" (Lyons and Severmann, 2006; Severmann et al., 2008) (Fig. 1). By this process, mobilized iron is transported across a chemocline from the marginal source area to the anoxic deep basin, where it is precipitated as syngenetic pyrite under sulfidic conditions or in the form of authigenic carbonates or oxides in sulfide-limited settings. The iron contents of ancient sediments are then quantified as a set of mineralogical pools, which are operationally-defined according to a mineral's reactivity towards dissolved sulfide. Here, we follow the sequential extraction procedure of Poulton and Canfield (2005) to quantify a set of mineralogical iron species which are considered to make up the 'highly-reactive' iron

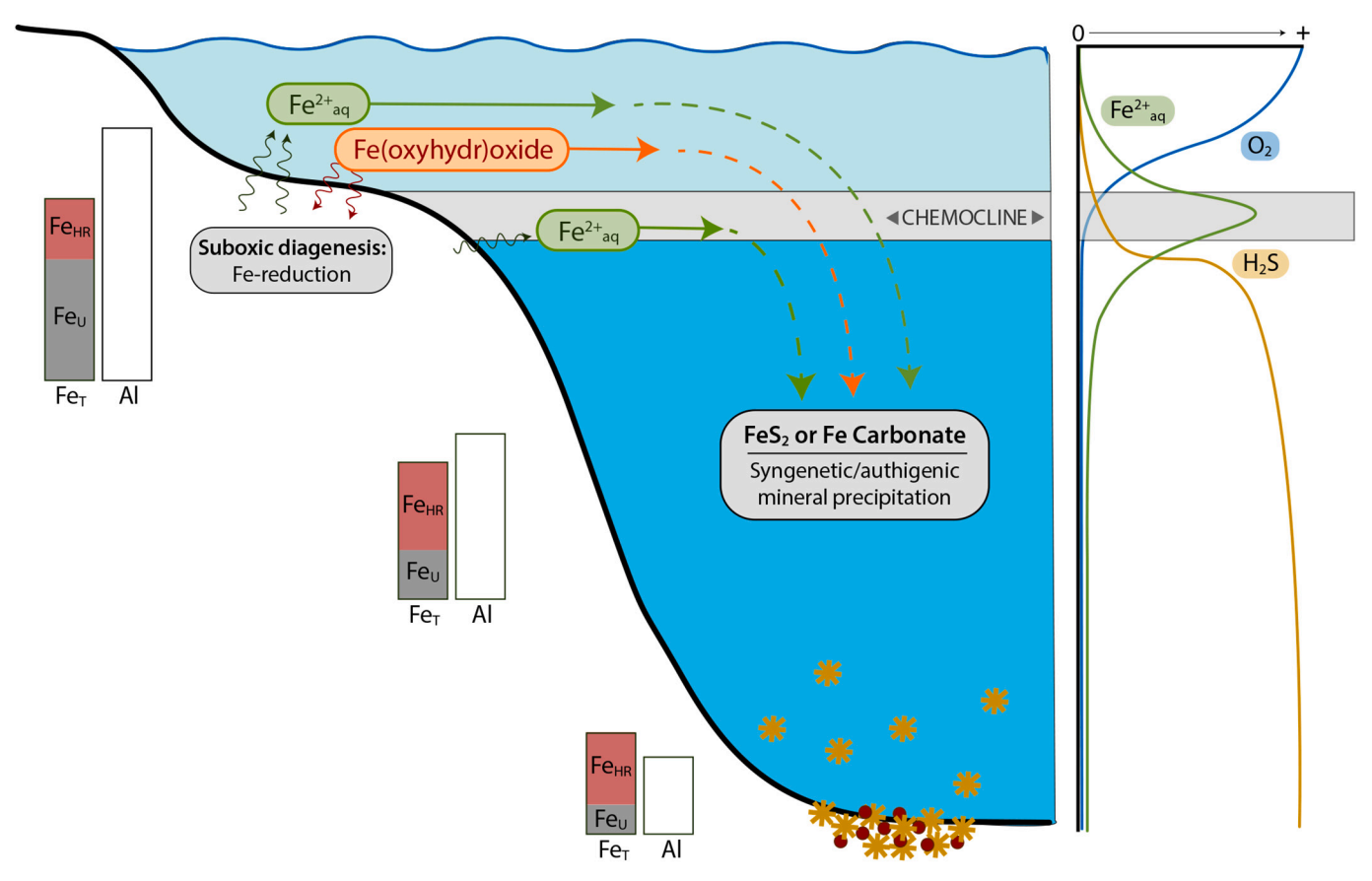


Fig. 1. Conceptual diagram of an operational iron shuttle within a stratified basin. In this system, reactive Fe ( $Fe_{HR}$ ; iron that is reactive to sulfide on early diagenetic timescales and/or participates in biogeochemical cycling) is released from shelf sediments to the sediment-water interface by suboxic diagenesis, where it will continue to be recycled. A portion of the  $Fe_{HR}$ , however, escapes recycling and is transported across a chemocline to the deep basin (Anderson and Raiswell, 2004; Raiswell and Canfield, 1998; Wijsman et al., 2001) to be rapidly precipitated with available sulfide as syngenetic pyrite under a euxinic water column (Anderson and Raiswell, 2004; Wijsman et al., 2001). If there is insufficient sulfide to match or exceed dissolved Fe concentrations below the chemocline (i.e., ferruginous conditions), precipitation of authigenic Fe-carbonate or Fe-oxide minerals will dominate, though the process is less efficient. Golden stars represent pyrite. Red dots represent iron carbonates forming in the sediment, although this is meant to schematically show where they would form in a ferruginous system, as iron carbonates would be pyritized in the depicted euxinic system.  $Fe_U$  is unreactive iron,  $Fe_T$  is total iron, and  $Fe_T = Fe_{HR} + Fe_U$ . Al is total aluminum. The relative proportions of total Fe and total Al are depicted by the height of the columns. After Lyons and Severmann (2006). (For interpretation of the references to color in this figure legend, the reader is referred to the web version of this article.)

(FeHR) fraction. This fraction is defined as:

$$\label{eq:Fehrestern} Fe_{HR} = Fe_{carb} + Fe_{ox} + Fe_{mag} + Fe_{py}.$$

and includes carbonate-associated iron ( $Fe_{carb}$ ), such as siderite and ankerite, reducible iron (oxyhydr)oxides ( $Fe_{ox}$ ), such as ferrihydrite, lepidocrocite, goethite, hematite and akaganeite, magnetite-bound iron ( $Fe_{mag}$ ), and pyrite-bound iron ( $Fe_{py}$ ). Note that although these pools are named based on the dominant mineral they are designed to extract, they are operational terms and the chemical extraction may be imperfect at the mineralogical level (Poulton and Canfield, 2005; Slotznick et al., 2020). The remaining portion of the total iron contents that is not included in  $Fe_{HR}$  is considered to be the 'unreactive' iron ( $Fe_{U}$ ) fraction and consists of residual iron silicate minerals that do not react with dissolved sulfide on early diagenetic timescales.

After the iron pools are quantified, the ratio of highly reactive iron to total iron content ( $Fe_{HR}/Fe_T$ ) can be used to draw inferences about paleoredox conditions, where reducing bottom-water environments will be enriched in highly reactive iron due to operation of the Fe shuttle. The ratio of pyrite-bound iron to highly reactive iron ( $Fe_{py}/Fe_{HR}$ ) can further distinguish euxinic (sulfide-replete, iron-limited) from ferruginous (sulfide-limited, iron-replete) conditions, as the mineralogy should reflect the relative availability of sulfide in the depositional system (Anderson and Raiswell, 2004; Lyons and Severmann, 2006; Marz et al., 2008; Poulton et al., 2004, 2010; Poulton, 2021; Poulton and Canfield, 2011; Poulton and Raiswell, 2002; Raiswell et al., 2001, 2018; Raiswell

and Canfield, 1998). We note that while the modern iron speciation proxy was developed to distinguish sulfidic from truly iron-rich conditions such as during deposition of Archean/Paleoproterozoic Banded Iron Formations (Poulton et al., 2004), it is unlikely that the Phanerozoic examples in this study were exceptionally iron-rich. Rather, and from a nomenclatural perspective as used in this paper, 'ferruginous' conditions simply indicate that sufficient reactive iron was available to titrate out any sulfide. 'Anoxic and non-sulfidic' may be a more realistic term that does not evoke high dissolved levels of ferrous iron, although we retain 'ferruginous' for continuity with the literature. Similarly, 'euxinic' does not denote absolute sulfide concentrations but rather enough sulfide present to pyritize the majority of reactive iron. To transform these values into more concrete determinations of paleoredox conditions, the results can be plotted in "iron space" (Fig. 2A), based on a set of empirically-derived threshold values that have been calibrated using ancient and modern marine environments. For the redox determinations made in this study, we use values of  $Fe_{HR}/Fe_T > 0.38$  to distinguish anoxic conditions and  $Fe_{py}/Fe_{HR}>0.7$  to indicate euxinic conditions, as these have been well-established in the literature (see Raiswell et al., 2018; Poulton, 2021 for further discussion).

It is important to recognize, however, that these values are indicative rather than prescriptive thresholds and there are a number of factors that can influence interpretation. Estuarine sediments can trap iron oxides and result in a false 'anoxic' signature (Poulton and Raiswell,

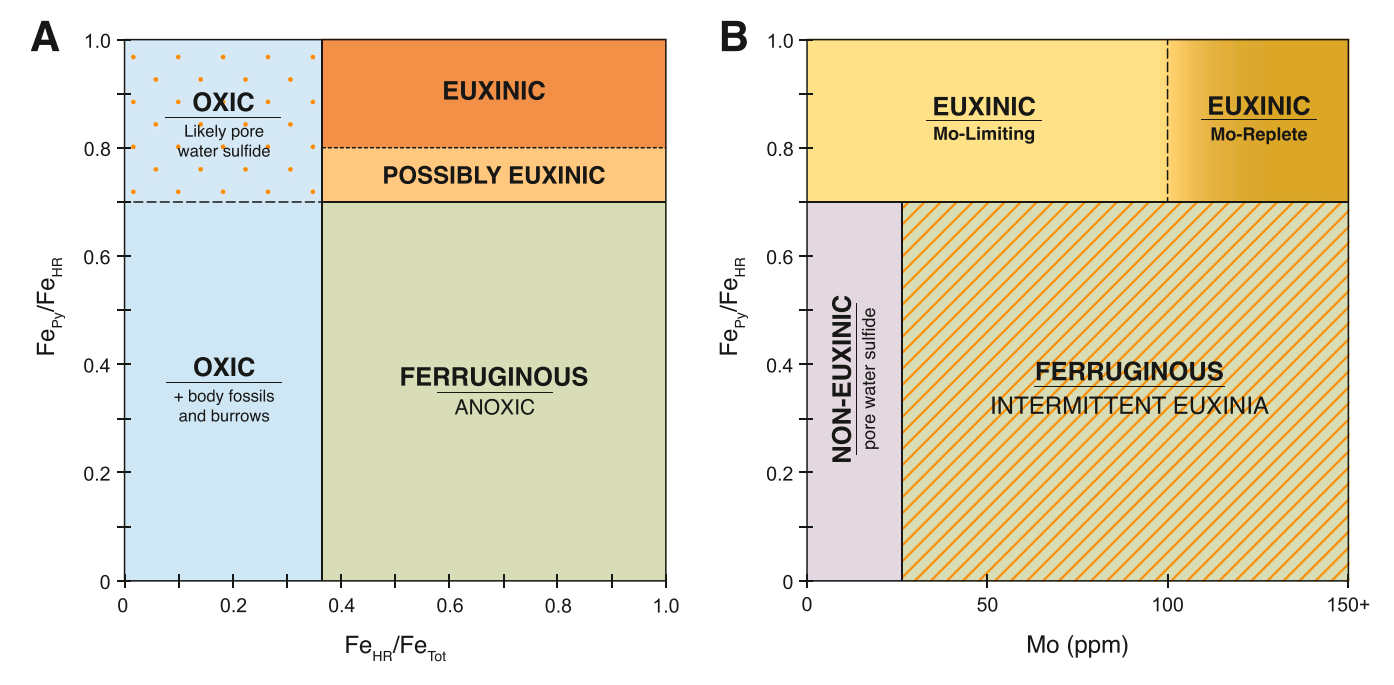


Fig. 2. Iron speciation proxy and molybdenum proxy composite interpretation plot (after Poulton and Canfield, 2011; Scott and Lyons, 2012; Sperling et al., 2015). Part A shows interpretations of redox conditions for sample values plotted in "iron-space." This iron space shows the contributions of highly reactive iron ( $Fe_{HR}$ ) compared to total iron ( $Fe_{T}$ ) on the x-axis and pyrite iron ( $Fe_{PY}$ ) compared to highly reactive iron on the y-axis. Part B is an extension of the interpretation achieved from part A with consideration of molybdenum values to determine a more specific interpretation of redox conditions. Divisions are based on empirical values from Raiswell and Canfield (1998) and Scott and Lyons (2012).

2002). Rapid deposition (such as in turbidites) can dilute highly reactive iron enrichments and/or not allow sufficient time for them to form (Raiswell and Canfield, 1998), leading to false 'oxic' values. Consequently, a lower FeHR/FeT interpretive threshold of 0.22 is commonly used to distinguish 'unequivocally' oxic samples from equivocal samples (Poulton and Canfield, 2011). It has also been recently recognized that some modern samples deposited under an oxygenated water column have relatively high Fe<sub>HR</sub>/Fe<sub>T</sub> values that are above 0.38 (Pasquier et al., 2022), which may be due to inclusion of inappropriate samples according to the criteria of (Raiswell et al., 2018), but may also be because the current sequential extraction protocol differs from the protocol used to establish the interpretive baselines (discussed in Farrell et al., 2013). In either case, these interpretive baselines may be revised in the future. Finally, samples with low total iron contents are more easily pyritized within the sediment porewater environment, thus leading to false 'euxinic' water column interpretations (Hutchings and Turchyn, 2021). Thus, results should ideally be analyzed in conjunction with sedimentology and geochemical context data and supported by other independent proxies. For instance, combining iron speciation data with assessments of authigenic enrichment of RSMs such as molybdenum can helpfully distinguish the presence and intensity of euxinia (Fig. 2B).

#### 2.2. RSM proxies: Molybdenum

A number of elements have been identified which exhibit variable but predictable behavior (by changing solubility or complexing patterns) as a function of redox potential, known collectively as redox-sensitive trace metals (RSMs). As with iron speciation, RSM proxies are not without caveats. Relevant to this study is the recognition that rapid changes in sedimentation rate can affect the magnitude of authigenic enrichment, as demonstrated by Crombez et al. (2020), who show that order-of-magnitude changes in sedimentation will dramatically alter the interpretation of trace metal patterns. While this can be mitigated by calculating trace element enrichment as mass accumulation rates, the cores investigated here do not have the detailed age models that would allow for these calculations; consequently, we have aimed to

interpret trace metal trends at a fairly broad scale.

Molybdenum is the most abundant redox sensitive trace metal in the modern ocean (~ 105 nM) and has a residence time (~450 kyr; Miller et al., 2011) that is orders of magnitude greater than the mixing time of the ocean, making it especially useful in understanding oxygenation dynamics within ocean basins. Present as the soluble molybdate anion in oxic and low-H<sub>2</sub>S environments, it is slowly removed to the sediment by adsorption to Fe- and Mn- (oxy)hydroxides in the form of Mn-nodules and ferromanganese crusts (Bertine and Turekian, 1973; Scott and Lyons, 2012). In well-oxygenated oceans like the modern, this mechanism can be responsible for the removal of 35-40% of the total seawater Mo inventory (Scott and Lyons, 2012). Under anoxic conditions where sulfide concentrations reach levels greater than  ${\sim}11~\mu\text{M}$ , molybdate undergoes nearly quantitative reduction to its particle-reactive thiomolybdate form, allowing for rapid sequestration in the sediment by binding to organic material and precipitation as authigenic sulfide minerals (Emerson and Huested, 1991; Erickson and Helz, 2000; Helz et al., 1996; Scott and Lyons, 2012). In the modern ocean, estimates of the seafloor fraction occupied by a euxinic water column or presence of pore water sulfide range from just 0.0005 to <0.02, yet this area accounts for up to 65% of the Mo sequestration from seawater (Scott et al., 2008; Scott and Lyons, 2012). This study follows the guidelines proposed by Scott and Lyons (2012) to interpret bulk Mo values >25 ppm to be enriched (relative to average oxygenated sediments) and thus, indicative of elevated water column sulfide concentrations. Enrichments between 25 and 100 ppm are considered to represent euxinic, Molimited environments, while enrichments >100 ppm are interpreted to indicate euxinic, Mo-replete environments (Fig. 2B).

We primarily focus here on interpretations of coupled iron speciation and molybdenum data (Fig. 2), but data for the redox-sensitive trace elements uranium and vanadium are plotted for additional geochemical context in Figs. 4–10. Both of these elements can be enriched under reducing but non-euxinic conditions via manganese cycling or reduction in sediment porewaters, making them potentially useful for identifying ferruginous conditions independent of the molybdenum proxy, which is more closely tied to sulfide (Algeo and Tribovillard, 2009; Algeo and

Liu, 2020; Tribovillard et al., 2006).

#### 2.3. Diagenetic and catagenetic effects on redox proxies

Post-depositional oxidation and weathering of samples can affect many reduced components in a shale, including TOC and pyrite sulfur (Petsch et al., 2000), which will in turn affect inferences from iron speciation (Ahm et al., 2017; Browne et al., 2020; Raiswell et al., 2018). Trace metals can also be lost (Perkins and Mason, 2015). Our samples all come from well-preserved and curated drill core, and thus these issues are avoided. The cores studied here range from thermally immature to thermally mature, and it is worthwhile to consider how processes of maturation/catagenesis will affect the sedimentary geochemical proxies. Most obviously, TOC loss during maturation means that proxies utilizing TOC in the proxy itself (e.g., Mo/TOC) must use reconstructed original TOC values (Hart and Hofmann, 2022), as we do here. Iron speciation analyses are unlikely to be affected by maturation, as the iron pools are not associated with TOC, and our samples are considerably lower grade than the true metamorphism required to affect this proxy (Raiswell et al., 2018; Slotznick et al., 2018). RSMs, however, are likely to be affected by maturation, as they are commonly hosted in organic matter and/or are affected by concentration changes if substantial TOC

loss occurs. Studies using both natural and artificial maturation have demonstrated that RSMs, and particularly Mo as discussed here, generally increase in concentration following maturation due to reduction in mass of the bulk rock (i.e., the metals are concentrated in the residue) (Dickson et al., 2020, 2022). Available data from artificial pyrolysis suggest Mo concentrations may increase between 6 and 57% depending on the rock (Dickson et al., 2020). Mo may also increase in specific horizons in thermally mature shales due to thermochemical sulfate reduction, which leads to hydrogen sulfide generation, pyrite formation and recrystallization, and the remobilization of Mo and precipitation of molybdenite (Ardakani et al., 2016). U also likely increases with maturation based on field tests (which rely on the assumption of similar initial geochemistry) (Dickson et al., 2022), but there are no studies using artificial maturation of the same sample. Other metals (particularly V and Ni; Lewan and Maynard (1982)) may alternatively be lost to the expelled oil. While processes associated with catagenesis and their effect on geochemical proxies are beginning to be understood, there is currently no accepted protocol to account for them. Given the limited stratigraphic distances we have investigated, RSM changes within a core are unlikely to be affected by maturation, but concentrations between cores likely will be (as discussed by Dickson et al., 2020). Cores/samples with higher thermal maturity and consequently higher

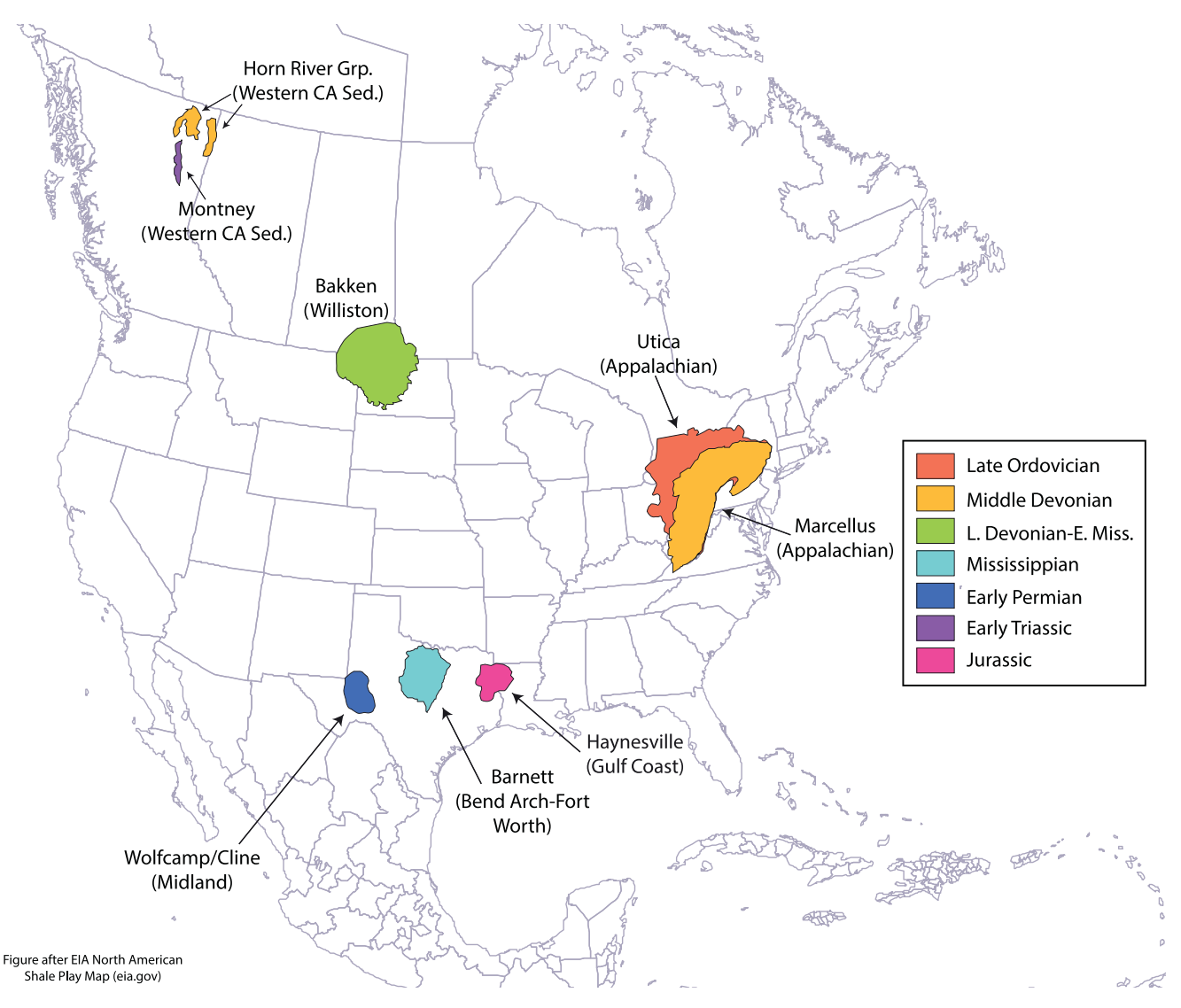


Fig. 3. Map of North American basins included in the present study. Map was modified from the North American Shale Play figure from EIA.gov. Note that the figure marks the general location of the economic plays as on the EIA figure rather than the exact location of our studied cores (specifically, the Kotaneelee YT I-48 core is from prospective areas of the Liard Basin in Yukon, not British Columbia).

mass loss of organic carbon will have over-estimated RSM contents compared to thermally immature cores/samples or samples with low generative potential (see programmed pyrolysis data in Supplementary Dataset S1).

#### 3. Materials and methods

#### 3.1. Study Sites and Geological Background

This work surveys a broad collection of North American black shale units, ranging in age from the Ordovician to the Jurassic (Fig. 3). Collectively, these strata were deposited in seven different sedimentary basins and comprise nine active resource plays. Table 1 provides a summary of the units included in this study along with sampling locations, well/core identifiers, geologic background, relevance to petroleum resources, and references for further information.

#### 3.2. Sample collection and preparation

The 793 individual samples included in this study were collected, prepared, and analyzed entirely or in-part by the authors. Almost all of the sampling and geochemical analyses were identical for all samples, but as a portion of the samples were contributed to the study by external collaborators or were used in previous studies, some aspects of the collection and preparation methods differ between sample sets; these are described below.

3.2.1. Marcellus, Utica, Barnett, Wolfcamp-Leonard and Cline formations Samples for these formations were collected by the first author (SRR) from a number of publicly accessible cores. The drill cores are housed at the West Virginia Geological and Economic Survey Core Repository in Morgantown, WV (Marcellus), ODNR Division of Geological Survey Horace R. Collins Laboratory in Delaware, OH (Utica), and the UT Bureau of Economic Geology Austin Core Research Center in Austin, TX (Barnett, Wolfcamp-Lower Leonard, Cline). Sampling methods used at each repository followed a similar procedure, as follows: cores were logged at roughly 0.25 m resolution for geological context, noting sedimentological and ichnological characteristics to identify lithofacies. Sampling resolution was determined on a by-core basis, generally ranging from 0.5 m to 1.5 m spacing. Samples from the core material were taken from depths interpreted to be fine-grained, minimally bioturbated, and free of weathered surfaces, secondary cements, nodules, or secondary pyrite accumulations, after the suggestions of Raiswell et al. (2018). Where possible, samples were collected using rock hammers and chisels or by selecting rock pieces from the core box. Where selfsampling was unavailable, samples were marked and cut by water-saw at the respective repositories. After collection, samples were cut at Stanford using a water-saw to ensure fresh material unaffected by oxidation and with minimal contamination from adhesive residue. Most samples were cut to a stratigraphic thickness of approx. 1 cm, and therefore represent a time-averaged value after homogenization (10<sup>3</sup> to 10<sup>4</sup> year scale, based on average shale deposition rates; though note there is high variability and also extensive and cryptic non-deposition in shales (Trabucho-Alexandre, 2015a, 2015b)). Samples were powdered using either a Spex Shatter Box and a tungsten carbide grinding vessel or by crushing to pea-sized gravel in a ceramic-walled benchtop jaw crusher followed by crushing in a Spex 8000D Mixer Mill benchtop ball mill in tungsten carbide vials.

#### 3.2.2. Montney/Doig formations

Samples for the Montney and Doig formations were provided by authors CMH and SS. The sample chips from core material were manually inspected for secondary calcite cements, phosphatic nodules, or secondary pyrite accumulations and those portions were removed. The remaining portion was powdered by hand using a ceramic mortar and pestle.

#### 3.2.3. Bakken Formation

Samples for the Bakken Formation were provided by Dr. Clint Scott (USGS). Samples were processed from core material using a ball mill with an aluminum vessel. Data for major and trace elements and TOC were taken from Scott et al. (2017).

#### 3.2.4. Besa River Formation

Samples from the Liard Basin (Besa River Formation; see discussion on stratigraphic nomenclature below) were collected from well-cuttings and were provided by author TF. A portion of the samples were powdered by the Yukon Geologic Survey using a steel crushing vessel prior to arrival at Stanford. Data for major and trace elements, TOC, programmed pyrolysis, and the analytical methods associated with these data are reported in Hutchison (2016). We note that these samples were analyzed for major- and trace-elements at Bureau Veritas using the LF202 package, which uses a lithium tetraborate fusion (followed by ICP-OES analysis) for major oxides, and an aqua regia digestion followed by ICP-MS analysis for the trace elements Mo, Cu, Pb, Zn, Ni, As, Cd, Sb, Bi, Ag, Au, Hg, Tl, Se. Although the aqua regia digestion releases most of the authigenic trace metals, it is not as aggressive as the four-acid digestion used for the majority of our samples (see below). We analyzed three samples including the USGS SBC-1 standard using both methods and found Mo to be 20% lower on average using the aqua regia digestion. The remaining portion of the sample set was manually powdered at Stanford using a ceramic mortar and pestle.

#### 3.2.5. Haynesville Formation

Samples for the Haynesville Formation were provided by Drs. Mark Zoback and Fatemeh Rassouli (Stanford University). Samples were processed from confidential core material and were received at Stanford pre-powdered (powdering method unknown).

#### 3.3. Analytical methods

All of the following analyses for this study were run concurrently with the samples analyzed by Sperling et al. (2021) and the detailed estimates of accuracy and precision reported in the supplement to that paper are applicable here.

### 3.3.1. Determination of highly-reactive iron (Fe $_{HR}$ ) contents

Roughly 0.1–0.2 g aliquots of the sample powders were weighed into a 15 mL centrifuge tube and subjected to the following sequential extractions according to the protocol developed by Poulton and Canfield (2005).

- 1.) 10 mL of 1 M sodium acetate solution of pH 4.5 was reacted with the sample powder by shaking for 48 h at 50 °C to extract any carbonate-bound iron (Fe<sub>carb</sub>)
- 2.) 10 mL of a 50 g/L sodium dithionite solution of pH 4.8 was reacted with the residual sample powder by shaking for 2 h at room temperature to extract iron oxide minerals ( $Fe_{ox}$ )
- 3.) 10 mL of a 0.2 M ammonium oxalate, 0.17 M oxalic acid solution of pH 3.2 was reacted with the residual sample powder by shaking for 6 h at room temperature to extract any magnetite-bound iron (Fe $_{mag}$ )

At the end of each extraction step, samples were centrifuged and 100  $\mu$ L aliquots were promptly taken from the overlying solution and used to quantify the extracted iron contents using the Ferrozine spectrophotometer method (Stookey, 1970; Viollier et al., 2000), with color allowed to develop overnight. This method may slightly under-estimate the Fe<sub>mag</sub> pool relative to other analytical methods (Alcott et al., 2020), but given this pool is minor in our samples (Table 3) the expected error is also minor. Between each of the above extraction steps, the remaining sample powders were rinsed with deionized water to a near-neutral pH and were left to dry overnight at 50 °C and then used for the next

Table 1
Geological background information for sample sets included in this work. Specific information is provided for sampled cores where available. References in parentheses: 1) Arens and Cuffey (1989), 2) Ettensohn (2004), 3) Ettensohn and Lierman (2012), 4) Hickman et al. (2015) 5) Smith and Leone (2014), 6) Enomoto et al. (2019), 7) Ryder et al. (1998), 8) Ryder (2008), 9) Ettensohn (1987), 10) Faill (1985), 11) Ferrill and Thomas (1988), 12) Rast and Skehan (1993), 13) Byers (1977), 14) Heckel and Wetzke (1979), 15) Werne et al. (2002), 16) (Sageman et al., 2003), 17) Arthur and Sageman (2005), 18) Chen and Sharma (2016), 19) Higley et al. (2019), 20) Carter et al. (2011), 21) Monger and Price (1979), 22) Leslie-Panek and McMechan (2021), 23) Cobbett et al. (2020), 24) Ferri et al. (2015), 25) National Energy Board (2016), 26) Kent et al. (1994), 27) Smith and Bustin (1998), 28) Scott et al. (2017), 29) Gaswirth et al. (2013), 30) Sonnenberg et al. (2017), 31) Loucks and Ruppel (2007), 32) Jarvie et al. (2007), 33) Rowe et al. (2008), 34) Gambacorta et al. (2016), 35) Gutschick and Sandberg (1983), 36) Marra et al. (2015), 37) Ruppel (2019), 38) Hamlin and Baumgardner (2012), 39) Fielding et al. (2008), 40) Peng et al. (2020), 41) Gaswirth (2017), 42) Rohais et al. (2018), 43) Schoepfer

and Henderson (2022), 44) Golding et al. (2016), 45) Ferri and Zonneveld (2008), 46) Zonneveld and Moslow (2018), 47) Moslow et al. (2018), 48) Crombez et al.

(2017), 49) Walsh et al. (2006), 50) Hammes et al. (2011), 51) Paxton et al. (2017).

Play / Basin Formation		General Locality	Paleo-location	Available Well I	nformation	General age	Absolute age
Utica-Point Pleasant	Appalachian Basin	New York, Pennsylvania, Ohio	20–25° S of paleoequator	Name: API #: Lat./Long.: Name: API #: Lat./Long.:	Farley #1305 3416729720 39.619014, -81.419167 Prudential #1-A 3410120196 40.587287, -83.240461	Upper Ordovician	455–449 Ma
Marcellus	Appalachian Basin	New York, Pennsylvania, West Virginia, Ohio	30° S of paleoequator	Name: API #: Lat./Long.: Name: API #: Lat./Long.:	WV-7 4710300645 39.678248, -80.8237619 Nathan Goff #55 4703305106 39.281368, -80.3926913	Middle Devonian	388–385 Ma
Besa River	Western Canadian Sedimentary Basin (Liard sub-basin)	British Columbia, Yukon, Northwest Territory	10–20° S of paleoequator	Name: Lat./Long.:	KOTANEELEE YT I-48 60.126644, –124.126792	Middle Devonian to Lower Mississippian	386–349 Ma
Bakken	Williston Basin	Eastern Montana, Western North Dakota, Western South Dakota, Southern Saskatchewan	5–10° N of paleoequator	Name: API #: Lat./Long.:	BN 1-23H (B832) 3300700666 47.194467,-103.568295	Upper Devonian to Lower Mississippian	356–351 Ma
Barnett	Bend Arch-Fort Worth Basin	North Central Texas	15–20° S of paleoequator	Name: API #: Lat./Long.:	Blakely #1 424973304100 33.005619,-97.399429	Middle Mississippian	354–323 Ma
Wolfcamp- Cline	Permian Basin (Midland sub-basins)	West Texas	5–10° N of paleoequator	Name: API #: Name: API #:	O.L. Greer #1 4238310189 O.L. Greer #2 4238310575	Upper Pennsylvanian to Permian	301–290 Ma
Montney- Doig	Western Canadian Sedimentary Basin (Peace River sub- basin)	Western Alberta, Eastern British Columbia	30° N of paleoequator	Name:	Progress Graham c-65-F	Upper Permian to Middle Triassic	252–246.8 Ma
Haynesville	Gulf of Mexico Basin	East Texas Louisiana		Name:	Confidential	Upper Jurassic	157–151 Ma

Play/ Formation	Basin type and geometry	Type section lithology	Organic matter preservation style and hypotheses	Relevance to petroleum exploration
Utica-Point Pleasant	Foreland basin (1–3)	Point Pleasant is a calcareous black to grey shale with interbedded fossiliferous limestone and minor siltstone; Utica is also calcareous black to brown shale with more localized fossiliferous horizons, usually laminated with some bioturbation and sedimentary structures indicative of storm activity.	Sea level rise and inundation causing restricted circulation plus influx of organic material allowing for the development of anoxic conditions (4–5).	Estimated to contain approx. 117 tcf natural gas and 1.8 billion barrels of oil as an unconventional source rock reservoir (6). Also serves as source rock for Upper Cambrian Copper Ridge dolomite and Upper Silurian Lockport dolomite (7, 8).
Marcellus	Retroarc foreland basin (2, 3; 9–12)	Muddy, dark grey to black laminated pyritic, carbonaceous units with occasional interbedded silt. Upper (Oatka Creek) and lower (Union Springs) portions are separated by thin carbonate intervals (Purcell and Cherry Valley limestones). The Union Springs unit is generally more organic carbon-rich. Oatka Creek is generally more clay-rich.	Somewhat disputed, interpretations include the presence of a "permanent pycnocline" with dominant stratification and anoxia at depth (14, 15), or seasonal stratification (15–17). Nutrient regeneration may also have played a role (18).	TOC up to 9% (this study). It is currently one of the largest shale gas producing formations in the world (19, 20).
Besa River	Extensional basin on the tectonically active NW Laurentian margin (21–23)	Predominantly carbonaceous, siliceous black shale and dark grey siltstone.	Deep-water shale deposition in anoxic waters (24).	The combined Exshaw and Patry shales likely contain 219 tcf of marketable natural gas (25).
Bakken	Intracratonic basin or sag (26).	Consists of a lower and upper organic-rich, fine-grained black shale facies, divided by a dominantly silty limestone and sandstone middle member.	Somewhat disputed; estuarine-like upwelling in a relatively deep environment to increase primary productivity and anoxia (27) or hypereuxinia into photic zone in shallow setting achieves optimal production of organic matter and minimal travel time to burial (28).	TOC contents of up to 35%. Considered to be the largest continuous petroleum system in North America (29). Unconventional reservoir and source rock for Three Forks and Lodgepole fms. (30).
Barnett	Deep water foreland basin, bounded in all directions by uplift (31).	Comprises three general lithofacies, including laminated siliceous mudstone, laminated argillaceous lime mudstone (marl), and skeletal, argillaceous lime packstone, interrupted by occasional event beds. Bioturbation is rare. Abundant small framboidal pyrite and phosphate (apatite) throughout. (31,32)	Restricted, deep water setting with low water col. turnover rates and severe Felimitation promoted stratification and persistent euxinia, precluding OM degredation (31, 33, 34). Possible additional OM supply from upwelling-induced algal blooms (35).	TOC ranges from 3 to 13%. Oil- to mixed- oil-gas-prone source charges most Paleozoic reservoirs in the basin. USGS estimated total mean undiscovered shale gas resource of 53 tcf, 172 million barrels shale oil, and 176 million barrels natural gas liquids (36)
Wolfcamp- Cline	Foreland basin (37)	Four major facies types include siliceous mudstone, calcareous mudstone, muddy carbonate-clast conglomerate, and skeletal packstone-grainstone (38).	Restricted inter-platform setting with glacially-driven sea level changes (39), also with enhanced phosphorus recycling (40).	Carbonate reservoirs since 1950's, now researched for unconventional properties. Contains up to 20 billion barrels of oil and 16 tcf of associated gas (41).
Montney- Doig	Back-arc basin (42–43) transitioning to retroarc foreland at time of deposition (44–47).	Predominantly muddy siltstone with rare carbonates and phosphatic zones associated with rise and fall of local sea level and local accommodation changes (47).	Multiple controls including dilution, anoxia/preservation, and production (48)	Holds a combined estimate of 900 tcf of natural gas-in-place (49).
Haynesville	Passive margin, continental shelf (50)	Generally silty, argillaceous mudstones, silty calcareous mudstones, dolomitic mudstones and dolostones.	Restriction by carbonate platforms, oolitic shoals, and paleo Gulf of Mexico created frequent anoxic/euxinic conditions, combined with variable burial rates and carbonate production to preserve OM (50, 51).	Estimated reserves of 1.1 billion barrels of oil and 196 tcf of gas (51).

extraction step. Samples were compared against a set of internal standards included in each run. Precision varied with the amount of iron in each extraction, with standard errors generally <5% for extraction pools with >0.3 wt% iron (Sperling et al., 2021).

#### 3.3.2. Determination of pyrite-bound iron ( $Fe_{py}$ ) and sulfur contents

Extraction and quantification of pyrite-bound sulfur and iron contents of the samples was done following the chromium reduction method developed by Canfield et al. (1986). Aliquots of sample powder (usually between 0.1 and 0.2 g, variable depending on the assumed pyrite contents of a given formation) were reacted with 20 mL of 1 M chromous chloride solution and 20 mL of 6 N HCl by heating under a nitrogen atmosphere for 2 h in a specialized distillation line at Stanford University. Within the distillation line, liberated sulfide was transported with the  $\rm N_2$  carrier gas as hydrogen sulfide and trapped in culture tubes containing a 0.24 M zinc acetate solution as zinc sulfide (ZnS). ZnS was then precipitated as solid silver sulfide (Ag<sub>2</sub>S) by the addition of 0.18 M AgNO<sub>3</sub> solution (typically 500–750  $\mu$ L, adjusted to ensure completeness of reaction as determined by solution color and clarity). The Ag<sub>2</sub>S

precipitate was isolated by filtration onto 20  $\mu m$  Millipore filters and left to dry for  $\sim$ 24 h at room temperature. Pyrite sulfur concentrations were determined by gravimetric analysis of the dried precipitate and from these values, pyrite iron (FeS<sub>2</sub>; Fe<sub>py</sub>) contents were calculated assuming a 2:1 (S:Fe) stoichiometry. Samples were compared against a set of internal laboratory standards included in each run, with relative standard deviation of 7.0% and average standard error of 1.5% (Sperling et al., 2021).

# 3.3.3. Determination of total iron (Fe $_{\rm T}$ ) contents and major, minor, and trace elemental composition

Following a standard four-acid digestion, values for total iron (Fe<sub>T</sub>) and other major elements were determined using a SPECTRO ARCOS ICP-OES and values for minor and trace elements were determined using a PerkinElmer Elan 9000 ICP-MS. Both sets of measurements were completed externally at Bureau Veritas/ACME Laboratories North America (MA-200 package). Samples were compared against USGS standards SBC-1 and SGR-1 and internal Bureau Veritas standards. Full details are available in the supplement to Sperling et al. (2021;

specifically Table S3 of that paper), with accuracy and precision (respectively) analyzed across all standards estimated as Al: (4.6%, 3.7%), Fe: (-1.9%, 3.2%), Mo: (-5.0%, 6.7%), Ni: (1.1%, 3.3%), U: (-2.0%, 5.1%), V: (-1.5%, 3.6%).

#### 3.3.4. Determination of total organic carbon (TOC) contents

For each sample, roughly 1-2 g of powder was weighed into a 15 mL centrifuge tube. Sample powders were acidified by adding ~10 mL of 3 N HCl and left to react for 48 h to ensure complete removal of carbonate carbon from the sample. After acidification, samples were rinsed with deionized water two or more times, then dried and reweighed to calculate mass loss, which is reported as percent carbonate. The remaining decalcified powder was homogenized by hand using a ceramic mortar and pestle and approximately 20 mg was weighed into tin capsules for TOC analysis using a Carlo Erba NA 1500 Elemental Analyzer (EA) in the EM-1 lab at Stanford. Samples were compared against a standard (USGS SBC-1) prepared using the above methodology and included in each EA run. Replicate analyses of SBC-1 yielded a TOC weight percent of 1.13 (S.D. = 0.06, n = 10). This is slightly low (~9%) on average compared to the reported USGS value of 1.23 wt% or samples that were similarly acidified but analyzed on a mass spectrometer (Strauss et al., 2020).

### 3.3.5. Programmed pyrolysis and reconstruction of original TOC contents $(TOC_{\Omega})$

Thermal maturity parameters (T<sub>max</sub>), indicators of organic matter quality (e.g., HI) and other measures of source rock generative potential (e.g., S1, S2) were determined for a subset of the samples in this study via programmed pyrolysis (n = 381). Briefly, S1 represents free hydrocarbons in the rock (in mg of hydrocarbons (HC) per gram of rock), S2 is the present-day amount of convertible hydrocarbons in the rock (in mg HC /g rock),  $T_{\text{max}}$  is the temperature corresponding to the maximum release of hydrocarbons (the S2 peak), and Hydrogen Index (HI) is the S2 peak normalized to TOC (in mg HC / g TOC) (reviewed by Hart and Steen, 2015). Aliquots of sample powder were packaged and sent to GeoMark Research, Ltd. for external analysis via HAWK programmed pyrolysis. Results from the pyrolysis experiments (and published data from Hutchison (2016) for the Besa River Formation) were then used to compute reconstructed values for original TOC content (TOCo) of the samples, which is necessary for paleoenvironmental proxies such as the Mo/TOC restriction proxy (Algeo and Lyons, 2006; Hart and Hofmann, 2022). These calculations were performed according to the methodology and assumptions outlined by Jarvie (2012), using the following equation, which is derived from the information in Table 2 of that paper.

$$TOCo = \left[TOC_{pd} - 0.085^* \left(S1_{pd} + S2_{pd}\right) - \left(HIo^* \ 0.0008\right)\right] \Big/ [1 - \left(HIo/1177\right)], \tag{1}$$

where subscript "pd" denotes a present-day measured value and

**Table 2**Formation- and play-specific estimates of HIo used in Eq. (1) to calculate original TOC (TOCo) for samples in this study. Note that the estimate for the Besa River Formation from Jarvie (2012) was specifically for the Muskwa (in the Horn River Group) and may be a relatively poor fit across the entire Kotaneelee YT I-48 core given its geochemical heterogeneity.

Formation/Play	Est. HIo	Reference		
Bakken	580	Jin and Sonnenberg, 2013		
Barnett	434	Jarvie, 2012		
Haynesville	722	Jarvie, 2012		
Marcellus	507	Jarvie, 2012		
Besa River	532	Jarvie, 2012		
Montney	354	Jarvie, 2012		
Utica	379	Jarvie, 2012		
Wolfcamp A	594	Baskoro et al., 2023		
Wolfcamp B	508	Baskoro et al., 2023		
Wolfcamp D/Cline	329	Baskoro et al., 2023		

subscript "o" denotes an original value. TOC, S1, S2, and HI as defined above.

Input values for  $TOC_{pd}$ ,  $S1_{pd}$  and  $S2_{pd}$  are determined directly from measurements made using the elemental analyzer and programmed pyrolysis methods described in earlier sections. In contrast, prescribing one or more input values for original hydrogen index ( $HI_O$ ) is often more difficult, as this value can change dramatically between formations or in a single core. In the absence of local, coeval, immature samples, selecting input values for  $HI_O$  is based on ranges observed in similar depositional systems (Espitalié et al., 1984; Jarvie, 2012; Jarvie et al., 2007; Langford and Blanc-Valleron, 1990). Here we assign each formation a specific value for  $HI_O$  (Table 2), ranging from 329 to 722, based on values reported in published references (Baskoro et al., 2023; Jarvie, 2012; Jin and Sonnenberg, 2013).

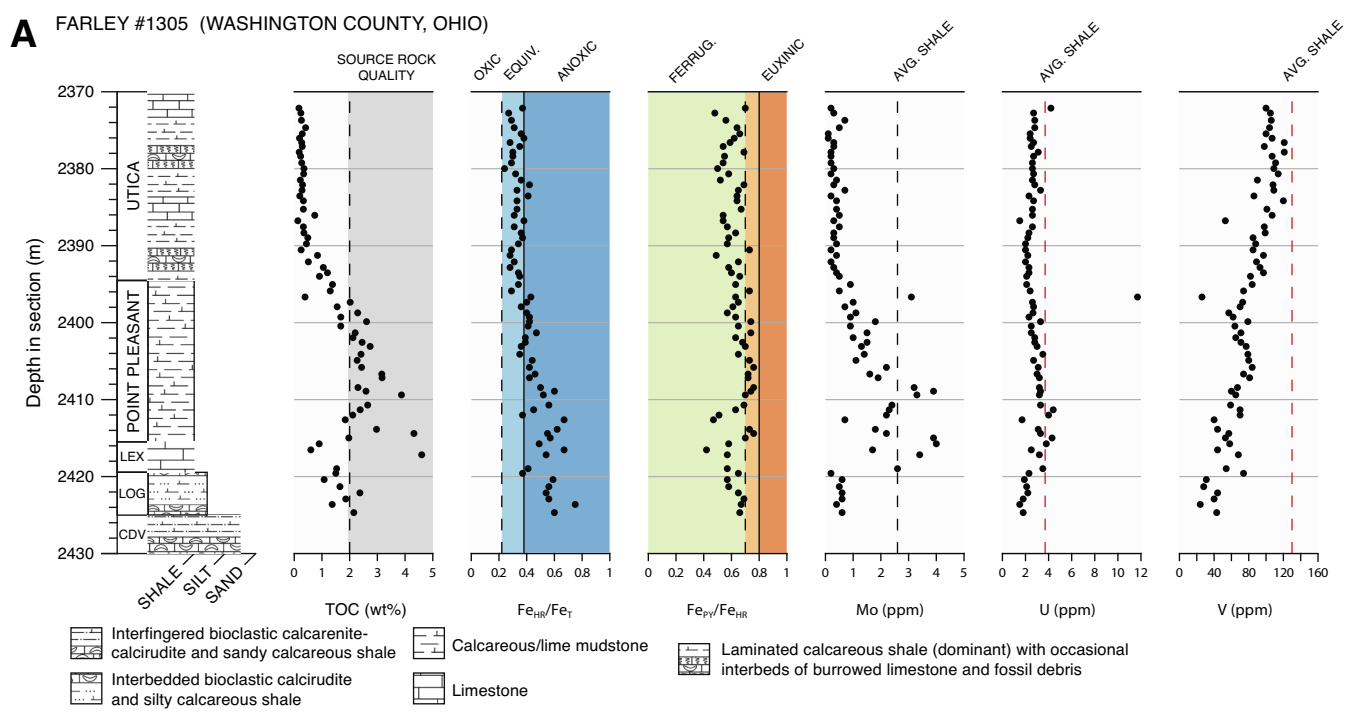
#### 4. Results: By formation/play and their interpretation

We first aim to evaluate the black shale units in this study on an individual basis, interpreting the geochemical data within a stratigraphic framework and within the context of any current and previous depositional models. Importantly, understanding the geochemical development and depositional history of each formation independently is prerequisite to drawing meaningful comparisons between basins. The scale of this study, however, is such that presenting and discussing all geochemical results and stratigraphic trends is not practical. Instead, summaries of all data presented in Figs. 4-10, for all sample units included in this study, can be found in Table 3. Bottom-water redox conditions are generally interpreted according to the literature-based interpretive scheme developed in Fig. 2 using iron speciation and Mo abundance data; U and V abundances are plotted for additional context and summarized in Table 3 but not discussed at length. In many cases these data represent the first multi-proxy sedimentary geochemical study of these units, and from that perspective the interpretations represent the most current understanding of redox conditions during deposition. Nonetheless, given that our study is primarily based on single-core studies, and redox conditions likely varied in space and time (e.g., Li et al., 2010; Poulton et al., 2010; Sahoo et al., 2023), understanding of redox conditions in these basins (and the local controls) will undoubtedly improve with additional stratigraphic geochemical study and the application of additional redox proxies.

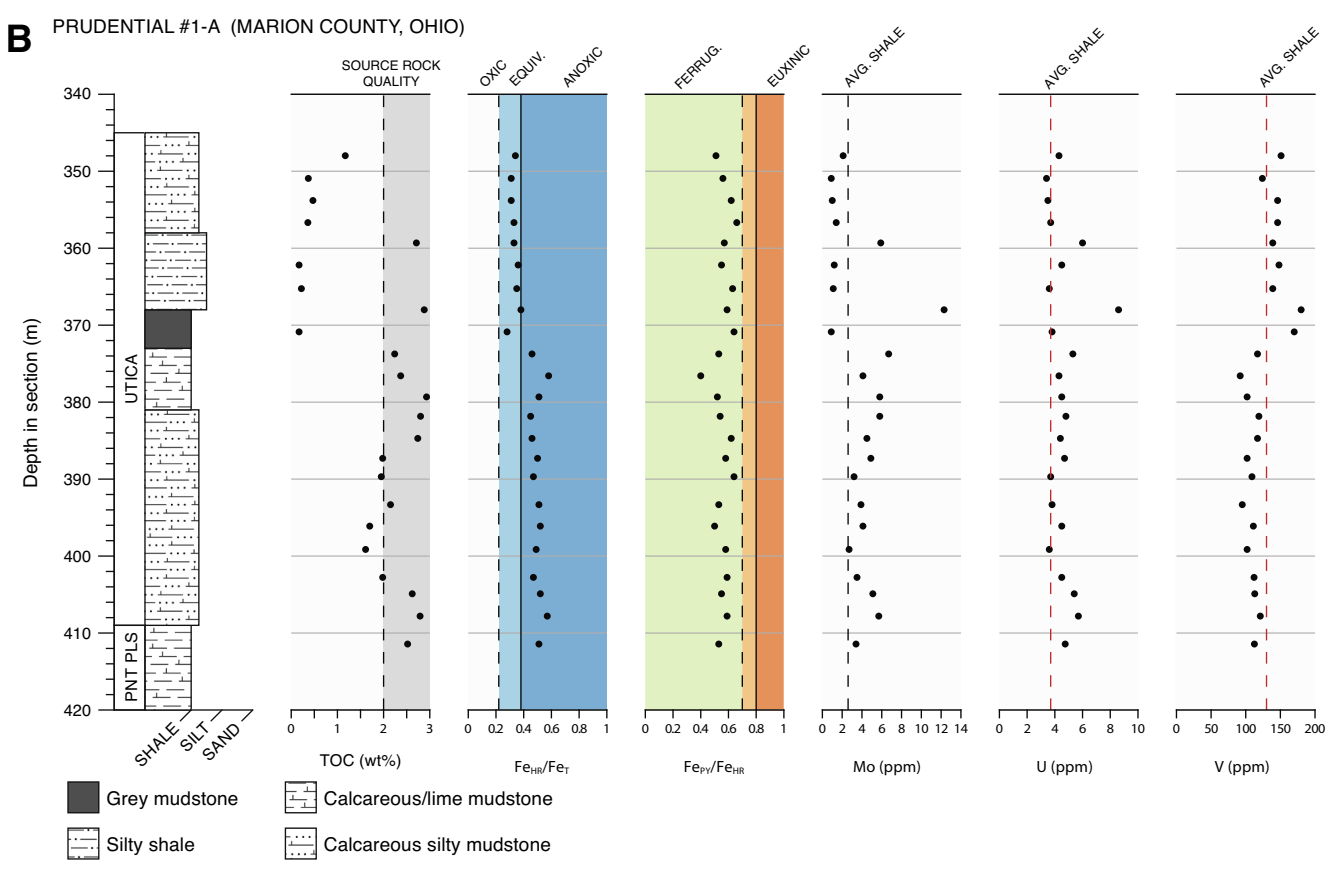
# 4.1. The Upper Ordovician (Sandbian-Katian) Point Pleasant and Utica formations

The Point Pleasant Formation and Utica Shale (as well as parts of the underlying Curdsville member, Logana member, and Lexington Formation) were investigated in the Farley #1305 and Prudential #1-A wells from central Ohio (Fig. 4). The Farley #1305 core (Fig. 4A) is characterized by a decrease in TOC from ~1-3 wt% in the Logana, Lexington and Point Pleasant to values generally <1 wt% in the uppermost Point Pleasant and Utica Shale. Present-day TOC is ~83% of reconstructed original TOC. The observed TOC decrease up core coincides with a change in FeHR/FeT ratios at or above 0.38 to between 0.2 and 0.38 (i.e., from the 'anoxic' iron speciation field to 'equivocal'). These are some of the rare samples in our study where iron speciation data do not indicate stratigraphically persistent anoxic conditions. Fepy/ FeHR values generally fall just below the euxinic-ferruginous threshold (average = 0.63) although occasionally reaching values > 0.7, with a maximum value of 0.77. Mo values are very low (1.1 ppm average, 4.6 ppm maximum), with little obvious change through the core. We did not observe any high Mo outliers (Ardakani et al., 2016).

The Prudential #1-A core (Fig. 4B), which covers the Point Pleasant-Utica contact at a more marginal location in the basin, has a similar geochemical signature. This core shows TOC values of 1.5–3 wt% in the lower part of the Utica before transitioning to values near 0 in the upper part of that unit. Because the Prudential #1-A core is thermally



CDV = Curdsville Mbr., LOG = Logana Mbr., LEX = Undifferentiated Lexington Mbr. of the Lexington/Trenton Group Limestone



PNT PLS = Point Pleasant Formation

(caption on next page)

Fig. 4. (A) Stratigraphic section and geochemical data plots for the Utica and Point Pleasant formations (and underlying stratigraphic units) from the Farley #1305 core. (B) Stratigraphic section and geochemical data plots for the Utica and Point Pleasant formations from the Prudential #1-A core. Reading from left to right, each panel illustrates the following;

- 1) Stratigraphic column.
- 2) Total Organic Carbon (TOC) contents in weight percent.
- 3) Iron paleoredox proxy ratio of highly-reactive iron to total iron ( $Fe_{HR}/Fe_T$ ), where values <0.22 suggest oxic conditions, values between 0.22 and 0.38 are considered "equivocal" and values >0.38 suggest anoxic conditions.
- 4) Iron paleoredox proxy ratio of pyrite-bound iron to highly-reactive iron ( $Fe_{PY}/Fe_{HR}$ ), where values <0.7 suggest ferruginous conditions, values between 0.7 and 0.8 suggest possible or intermittent euxinia, and values >0.8 suggest euxinic conditions.
- 5) Bulk values of molybdenum in ppm, with values <25 likely representing non-euxinic conditions, values >25 ppm suggesting euxinic, Mo-limiting conditions, and values >100 ppm suggesting euxinic, Mo-replete conditions. Dashed black line represents average shale value of 2.6 ppm from Wedepohl (1971).
- 6) Bulk values of uranium in ppm, a redox-sensitive trace metal that is not influenced by the amount of sulfide in the system. Dashed red line represents average shale value of 3.7 ppm from Wedepohl (1971).
- 7) Bulk values of vanadium in ppm, a redox-sensitive trace metal that can be enriched to moderate levels in the absence of sulfide but may reach "hyper-enrichments" in strongly euxinic systems (Scott et al., 2017). Dashed red line represents average shale value of 130 ppm from Wedepohl (1971). A small number of trace metal outliers in Figs. 4–10 were not plotted to maintain figure clarity; highest values are summarized in Table 3 and all values are included in Supplementary Dataset 1. (For interpretation of the references to color in this figure legend, the reader is referred to the web version of this article.)

immature (average Tmax = 431 °C), present-day TOC will be similar to original TOC. We see the same decrease in Fe<sub>HR</sub>/Fe<sub>T</sub> values coupled with decreasing TOC, although this occurs higher from a lithostratigraphic perspective, in the Utica Formation rather than the uppermost Point Pleasant. Fe<sub>Py</sub>/Fe<sub>HR</sub> values are similarly close to, but not over, the 0.7 threshold for euxinia or pore-water sulfide (average = 0.57), and RSMs are also low (average Mo = 4.35 ppm). We see one anomalous Mo value (42.6 ppm at 410.83 m core depth), but given this core is thermally immature, this is unlikely to represent thermochemical sulfate reduction (e.g., Ardakani et al. (2016)).

Interpretation of the slightly elevated  $Fe_{HR}/Fe_{T}$  values based on strict adherence to the established thresholds would suggest that these localities experienced significant periods of anoxic deposition. In reality, however, these thresholds are intended to be indicative rather than strictly diagnostic, and without any demonstrable RSM enrichments, much of the geochemical data remains truly 'equivocal.' For instance, muted authigenic trace metal enrichments can appear under both dysoxic and ferruginous conditions, and are difficult to distinguish without detailed knowledge of detrital flux in the basin (e.g., Sperling et al., 2018).

Both the Farley #1305 and Prudential #1-A cores exhibit characteristic benthic fossil assemblages which serve to provide additional clues about their redox environments. The unslabbed Prudential #1-A core, being a more shallow-water expression of the Point Pleasant and Utica formations, is especially fruitful in terms of providing wellpreserved, intact specimens along many of the bedding planes. Some of the fossils observed in the Prudential #1-A section include potentially phosphatized beds crowded with small bivalved ostracods that appear intact and preserve both valves, associated with a ~ 60 mm section of the core that is notably lighter in color and more massive than the dark shale above and below this interval. There is no sedimentological evidence to suggest this lithological change was the result of a transport event, but more likely a transient increase in O2, that allowed for colonization of the basin floor and inhibited enhanced preservation of organic matter. This is further supported by a decrease in TOC beginning at this point in the section (~378 m). There are also several instances of small lingulid brachiopods which were tentatively identified as Leptobolus sp., and a few rare trilobites (likely Triarthrus sp.). Importantly, Leptobolus and Triarthrus are thought to be low O2 specialists, or are at least tolerant of such environments (Boyer and Mitchell, 2017; Brett et al., 2020; Farrell et al., 2011). The deeper Farley #1305 core also contains significant shelly material (though largely in the form of transported debris), and has a more notable abundance of vertical and lateral burrows that vary greatly in size and density through the section.

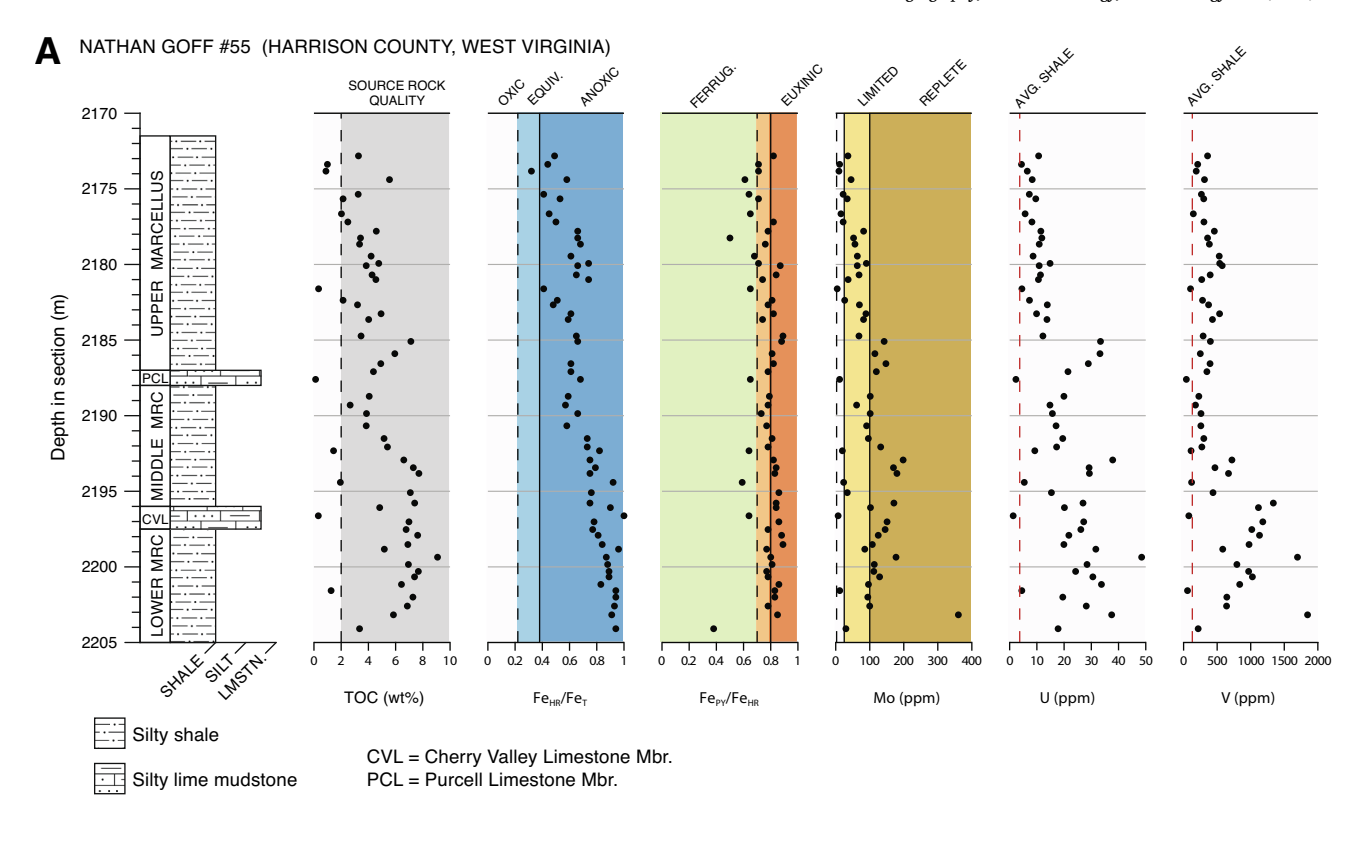
The combined geochemical and paleontological data most likely represent a mixture of dysoxic, suboxic, and anoxic bottom water conditions. Rapid redox fluctuations from anoxic to weakly oxic may have occurred at timescales more rapid than the integrated time covered by our samples (which span 1–3 cm of stratigraphy, e.g., Dahl et al., 2019), allowing for benthic organisms to transiently colonize the seafloor on ecological timescales. Finally, although anoxic bottom waters were likely dominantly ferruginous, the relatively high  $Fe_{py}/Fe_{HR}$  ratios suggest that sulfidic porewaters near the sediment-water interface or even weakly sulfidic bottom-waters may have been present at times. It is also possible that more intensely sulfidic conditions were present at times, but with basin restriction resulting in low trace metal abundances. However, pyrite framboid studies of the Point Pleasant have also been interpreted as representing a dysoxic water column (Blood et al., 2019). Thus, the combined data likely rule out persistent and high levels of sulfide; rather, these results point to a depositional environment that is precariously situated at the edge of oxic, euxinic and ferruginous environmental conditions.

#### 4.2. The Middle Devonian (Givetian) Marcellus Formation

The Marcellus Shale was investigated in the Nathan Goff #55 core (NG-55; Fig. 5A) from Harrison County, West Virginia, USA and the WV-7 core (Fig. 5B) from Wetzel County, West Virginia, USA. The Nathan Goff #55 core comprises roughly 33 m of dark grey to black silty shale. This black shale interval is split into three units (here referred to as the Lower, Middle, and Upper Marcellus) by two characteristic, thin ( $\sim 1~{\rm m}$  or less) beds of silty lime mudstone; the lower of the two limestone intervals separating the Lower and Middle Marcellus is the Cherry Valley Limestone, and the upper bed separating the Middle and Upper Marcellus intervals is commonly referred to as the Purcell Limestone. These informal units have not been recognized in the WV-7 core, and given the greater data density in the NG-55 core we focus our discussion there.

The NG-55 core exhibits variable total organic carbon (TOC) values throughout the section. The lowest values occur in the two limestone units, reaching 0.12 wt% in the Purcell. For the black shale intervals, TOC values range from 0.34 wt% to a maximum of 9.08 wt% in the Lower Marcellus. Over the entire interval, TOC contents display an oscillatory, potentially cyclical, trend, with a wavelength of approximately 5 m. TOC generally decreases up-section, with the Lower Marcellus Member exhibiting consistently high TOC contents throughout ( $\sim$ 7–8 wt%), while the Middle Marcellus Member shows a decreasing trend, reaching values near 4 wt% at the Middle Marcellus-Purcell contact. Above the Purcell, in the Upper Marcellus member, TOC values return to high values similar to those seen in the Lower Marcellus, but decrease in an oscillatory fashion to values below 2 wt% towards the top of the section. Present-day TOC in this core is on average  $\sim$  61% of reconstructed original TOC values.

Throughout the NG-55 section,  $Fe_{HR}/Fe_{T}$  ratios are consistently above 0.38 with the exception of a single sample in the Upper Marcellus, suggesting deposition under anoxic bottom water conditions for the duration of the interval. Intriguingly,  $Fe_{HR}/Fe_{T}$  values seem to follow a



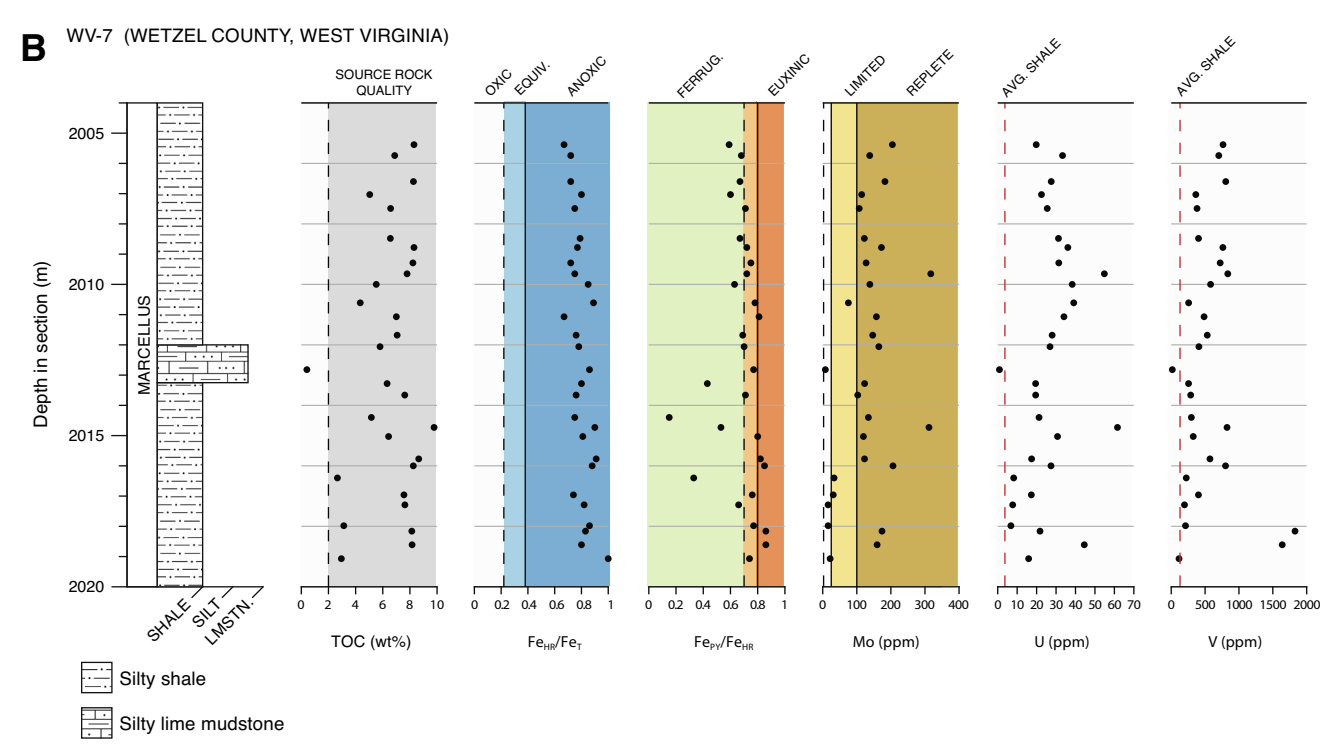


Fig. 5. (A) Stratigraphic section and geochemical data plots for the Marcellus formation and regionally recognized limestone members from the Nathan Goff #55 core. (B) Stratigraphic section and geochemical data plots for the Marcellus formation from the WV-7 core. Geochemical plots follow Fig. 4.

trend similar to that of TOC, decreasing up-section. While values of the  $Fe_{HR}/Fe_{T}$  ratio are typically interpreted relative to thresholds, rather than as an absolute or relative measure of anoxia, the covariation with other geochemical proxies indicates either a decrease in delivery of highly reactive iron to the site of deposition, or an increasing sedimentation rate that diluted all proxies.  $Fe_{py}/Fe_{HR}$  values are generally

higher than 0.7 and average 0.76 for all samples in the section, indicating that redox conditions at the sediment-water interface were at least intermittently euxinic across the depositional time span. However, 12 of 58 samples (~20%) do fall below this threshold, suggesting that bottom waters were not persistently euxinic and deposition under ferruginous conditions did occur. Many of the instances in which Fe $_{\rm py}/{\rm Fe}_{\rm HR}$ 

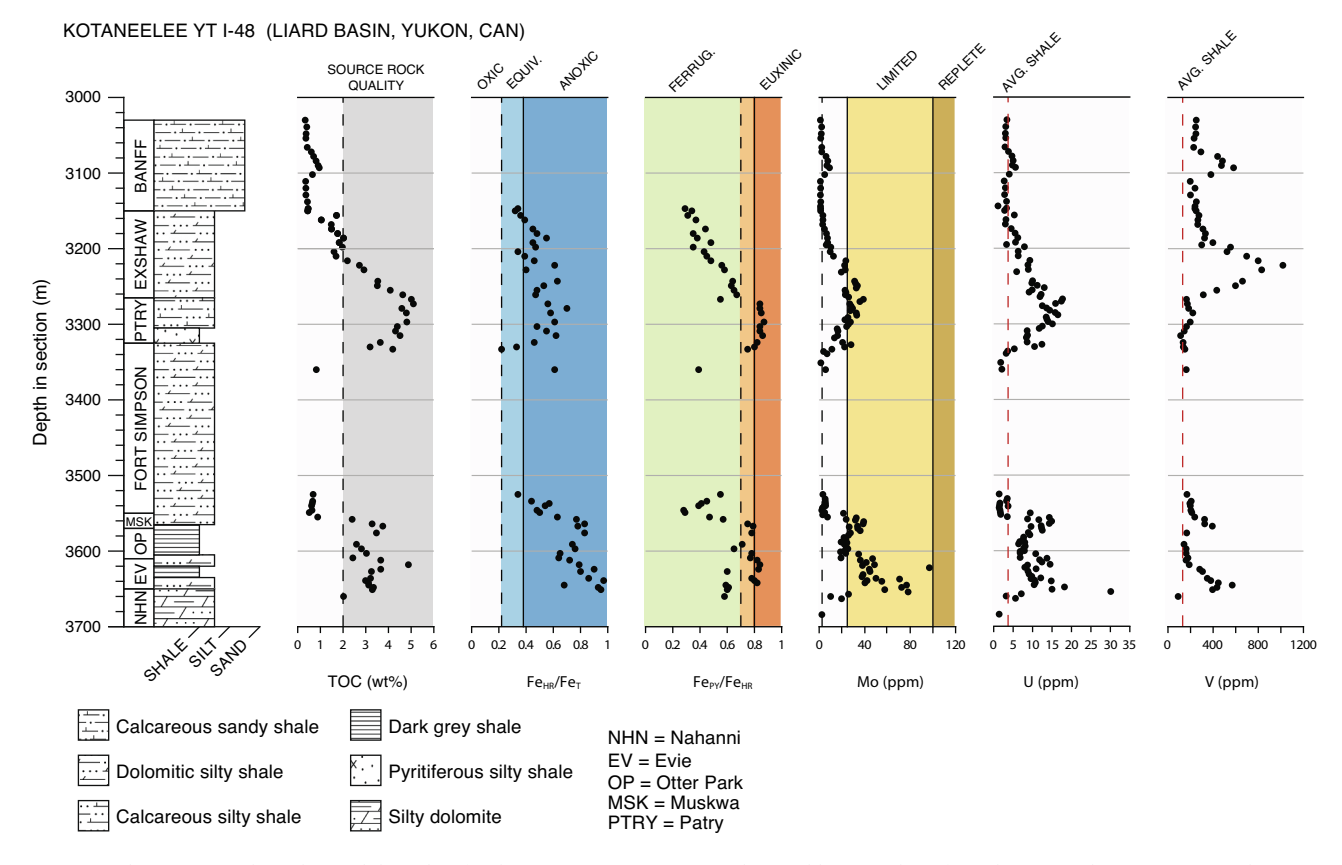


Fig. 6. Stratigraphic section and geochemical data plots for the Besa River Formation in the Liard basin (Yukon) from the Kotaneelee YT I-48 core. The Evie, Otter Park, and Muskwa represent the Horn River Group in British Columbia. Geochemical plots follow Fig. 4.

values fall below the 0.7 threshold occur in conjunction with relative lows in TOC and Mo content and tend to be located towards the top of the core.

Throughout the section, trends in the concentration of various redoxsensitive trace elements (Mo, U, V) largely mimic each other, as well as trends in TOC contents, suggesting that bottom water redox conditions (or alternatively sedimentation rate) were a dominant control on organic matter burial and preservation in the Marcellus. Mo values are consistently enriched above crustal averages and reach values as high as 360 ppm in the Lower Marcellus. Over the entire core Mo concentration averages ~87 ppm, with values consistently ranging from 100 to 200 ppm in the Lower and Middle Marcellus and the lowest 3 m of the Upper Marcellus, before steadily decreasing through the Upper Marcellus to values under 25 ppm at the top of the section. The enrichment exhibited in the Mo concentrations serves to reinforce the interpretation that euxinic conditions predominated for much of this time interval. Values above or around 100 ppm in the Lower and Middle Marcellus (in samples with euxinic iron speciation signatures) indicate that the basin was likely in communication with the open ocean and that deep-water renewal and replenishment of the aqueous trace metal reservoir occurred at least intermittently (using the model of Algeo and Lyons, 2006). A decrease to values below 100 ppm in the Upper Marcellus suggests that either water column sulfide reached the concentrations required for Mo reduction less frequently, or for shorter durations, limiting sedimentary Mo sequestration. Alternatively, the aqueous Mo reservoir may have been progressively depleted, via increasing restriction of the basin and/or globally widespread reducing conditions. Mo/ TOCo ratios rise from  $\sim$ 5–10 at the base of the NG-55 core, to  $\sim$ 10–15 in the middle (with maximum values for samples with sufficient TOC up to 18), and then back to  $\sim$ 5–10 at the top. Although the possibility of global trace metal drawdown in the Givetian-Frasnian must be considered, using the framework of (Algeo and Lyons, 2006), these Mo/TOCo

values indicate strong restriction at the base of the Marcellus (between Black Sea and Framvaren Fjord modern analogues), a less restricted setting (between Framvaren and Cariaco basin analogues), and then back to strong restriction.

Taken together, our geochemical data from core NG-55 for the Marcellus is in good agreement with that of other workers (e.g., Chen and Sharma, 2016; Lash and Blood, 2014; Sageman et al., 2003; Werne et al., 2002), demonstrating dominantly euxinic conditions but with clear non-euxinic intervals on short stratigraphic scales. All measured indicators (TOC,  $Fe_{HR}/Fe_{T}$  and  $Fe_{py}/Fe_{HR}$ , Mo, U, and V abundances) decrease throughout the core, most easily explained by less reducing conditions through time. Core WV-7 shows similar results, albeit covering a shorter stratigraphic interval of the Marcellus.

#### 4.3. The Upper Devonian to Carboniferous Besa River Formation

The Kotaneelee YT I-48 core (Fig. 6) from the Liard Basin in Yukon, Canada, covers nearly 7000 ft (as originally measured; ~2100 m) of stratigraphy and covers eight different lithostratigraphic units (Hutchison, 2018). As noted by Fiess et al. (2015) and Hutchison (2018), different stratigraphic nomenclature has been used for the Devonian-Carboniferous stratigraphy of the Liard Basin in the three neighboring jurisdictions of Yukon, British Columbia, and Northwest Territories. Here we use the term 'Besa River Formation' (the lithostratigraphic term that has traditionally been used in Yukon) while recognizing the nomenclatural confusion and using informal member/formation names following the National Energy Board (2016). Essentially, the Besa River Formation in Yukon is recognized to represent distal, time-equivalent shale to the Horn River Group and Fort Simpson, Kotcho, Exshaw, Banff, Prophet, and Golata formations in northeastern British Columbia (National Energy Board, 2016). The lowest of our studied units (below the Besa River Formation) is the Nahanni Formation, which grades from

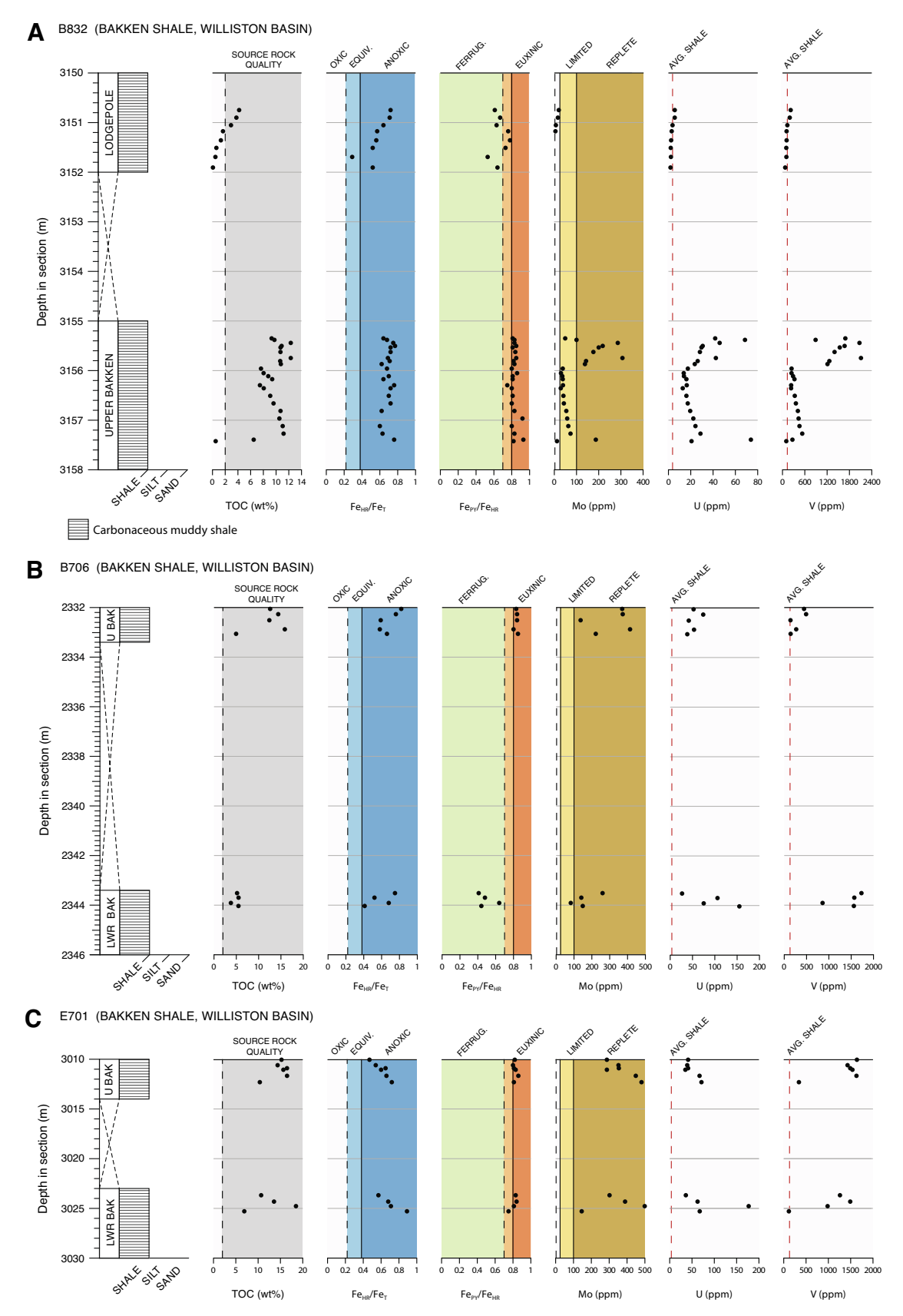


Fig. 7. Stratigraphic sections and geochemical data plots for the Bakken Formation from (A) the B832 core, (B) the B706 core, and (C) the E701 core. Geochemical plots follow Fig. 4.

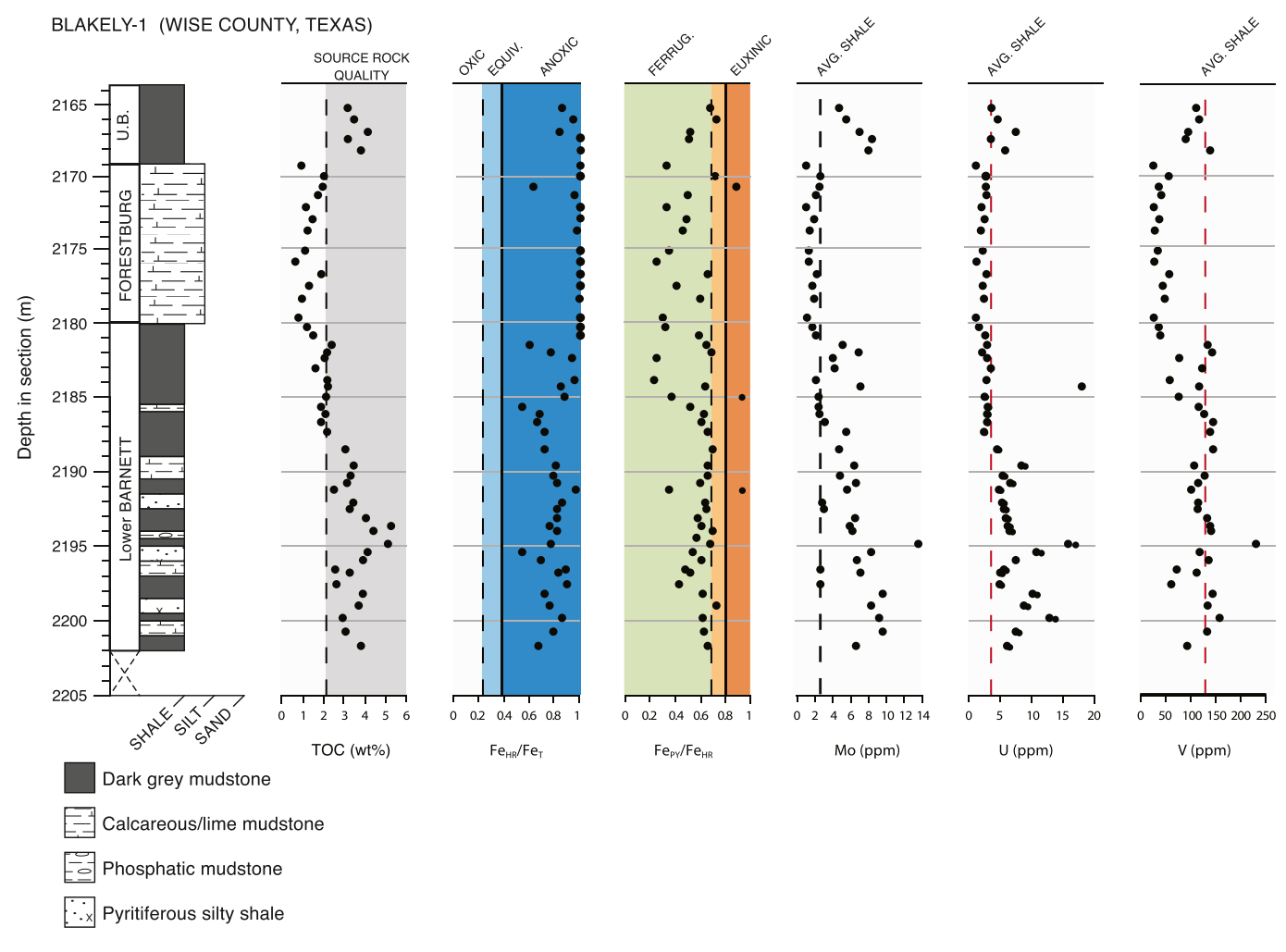


Fig. 8. Stratigraphic section and geochemical data plots for the Barnett Formation from the Blakely-1 core. Geochemical plots follow Fig. 4. Note that a number of samples in the Forestburg Limestone had  $Fe_{HR}/Fe_T$  values slightly >1.0, likely due to increased error in limestones with relatively low total iron (Clarkson et al., 2014). See Supplemental Dataset S1 for exact values. U.B. = Upper Barnett.

light grey silty dolomite into the overlying dark grey dolomitic silty shale facies of the Evie shale. Overlying the Evie shale, the Otter Park shale remains a dark grey shale, but is less dolomitic. Above the Otter Park, the Muskwa shale and Fort Simpson become lighter grey in color, and again exhibit higher dolomitic content with intervals of pyrite throughout. The Evie, Otter Park, and Muskwa comprise the Horn River Group in British Columbia, which has been extensively studied as a shale gas play. The lowermost portion of the Patry shale also exhibits a pyritic silty shale facies that transitions to dark grey calcareous shale and then to the grey dolomitic silty shales of the Exshaw shale before finally coarsening to a light grey calcareous sandy shale in the uppermost Banff. For ease of discussion, samples from the Nahanni, Evie, Otter Park, Muskwa, and lowermost Fort Simpson will be referred to as the lower group and samples from the uppermost Fort Simpson, Patry, Exshaw and Banff will be referred to as the upper group.

Throughout the entire Kotaneelee core, TOC ranges from 0.33 to 5.48 wt% and averages 2.72 wt%. Present-day TOC is on average 33% of reconstructed original TOC, with high variance. Much of the core exhibits TOC contents above 2 wt%, with the exception of the Fort Simpson, the upper portion of the Exshaw, and the Banff. There are no readily observable trends in the TOC values of the lower group, except for a sharp decrease from values around 3-4 wt% to values around 0.5 wt% across the Muskwa and into the TOC-lean Fort Simpson. The upper group exhibits a steady increase in TOC from the Fort Simpson through the Patry, which has the highest observed TOC values. TOC contents

begin to decrease at the Patry-Exshaw boundary, eventually reaching the lowest observed values in the Banff. TOC contents across this depositional interval are generally higher in more fine-grained sediments and decrease with coarser grain sizes.

Among 77 samples in the Kotaneelee core for which Fe-speciation data is available, nearly all samples (70 of 77, ~91%) exhibit FeHR/ Fe<sub>T</sub> values above 0.38, suggesting that the water column during this time was predominantly anoxic. Of the 7 samples that fall below the Fe<sub>HR</sub>/Fe<sub>T</sub> anoxic threshold of 0.38, all remain above the lower baseline of 0.22 and may still represent deposition under an anoxic water column. Fe<sub>nv</sub>/Fe<sub>HR</sub> trends exhibit a number of transitions across the threshold of 0.7, suggesting that bottom waters experienced extended periods of both ironreplete, ferruginous conditions as well as sulfidic, euxinic conditions. Interpretation of these transitions in light of Mo concentration data (discussed below) suggests that the Evie and portions of the Patry and Exshaw were indeed deposited under dominantly euxinic conditions, while the Otter Park and lowermost Patry probably experienced at least intermittently euxinic bottom waters. The Nahanni, Muskwa, Fort Simpson, upper Exshaw and Banff appear to have been deposited under dominantly ferruginous water columns.

Mo values throughout the section range from near average shale (2.6 ppm) to relatively high enrichments of up to 98 ppm, with an average of  $\sim$ 22 ppm. The highest enrichments occur in the Evie, likely as a function of deposition under a generally euxinic water column. While Mo concentrations within this interval reach 98 ppm, the majority of samples

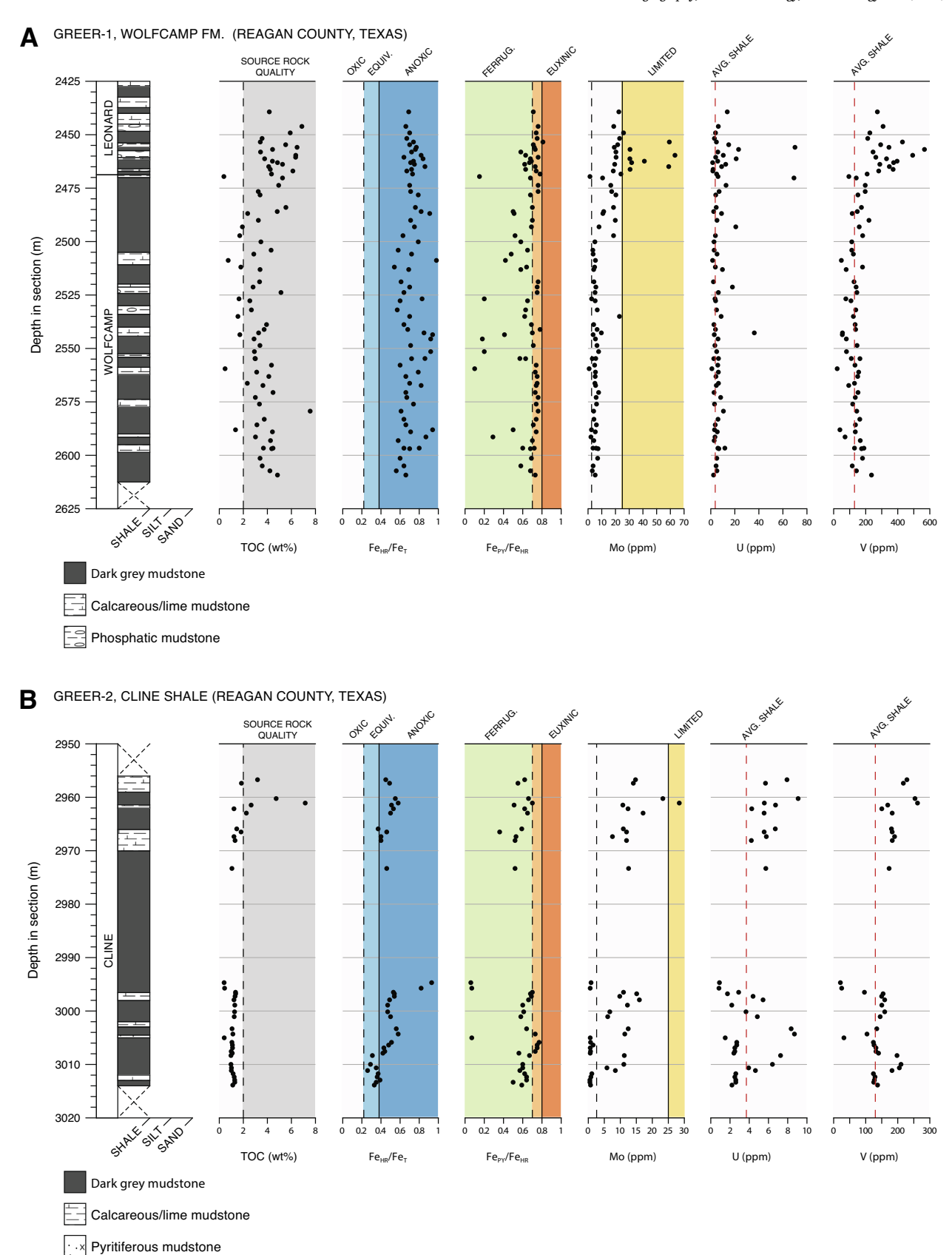


Fig. 9. (A) Stratigraphic section and geochemical data plots for the Wolfcamp and Lower Leonard formations from the Greer-1 core. (B) Stratigraphic section and geochemical data plots for the Cline Shale from the Greer-2 core. Geochemical plots follow Fig. 4.

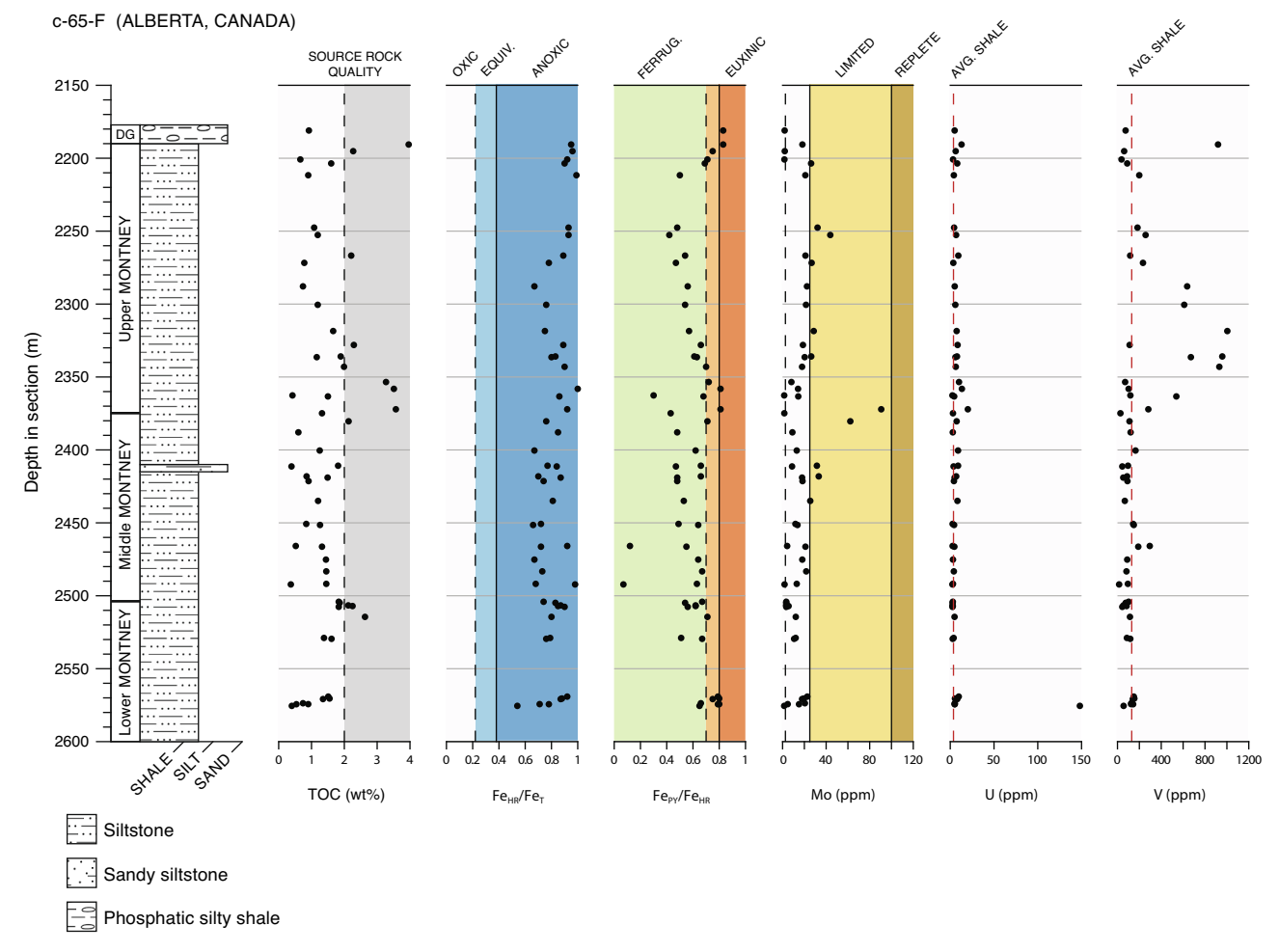


Fig. 10. Stratigraphic section and geochemical plots for the Montney and Doig formations from the c-65-F core. Geochemical plots follow Fig. 4.

show values in the range of 40 to 60 ppm. Further, the 98 ppm sample is also characterized by relatively low U (8 ppm) and a high Mo<sub>auth</sub>/U<sub>auth</sub> ratio of 15.2, suggesting that the high Mo in this case resulted from the operation of an Mn shuttle and a fluctuating chemocline (Algeo and Tribovillard, 2009). Mo/TOCo ratios of confirmed euxinic samples in the Evie/Otter Park/Muskwa based on iron speciation are 6.4  $\pm$  1.4 This suggests that the basin experienced a moderate degree of hydrographic restriction during this time, similar to or slightly more restricted than the Framvaren Fjord modern analogue. The upper portion of the Patry also shows moderate enrichment in Mo, with values ranging from ~20-40 ppm. In this interval, confirmed euxinic samples based on iron speciation have Mo/TOCo ratios of 3.2  $\pm$  0.7, essentially at the Black Sea modern analogue. However, in both these cases the intersection of local and global signals make it difficult to infer the extent of basinal restriction across this time interval; although anoxia in the Middle-Late Devonian may have been more diachronous than previously believed (Hedhli et al., 2023), there was still certainly the opportunity for global trace-metal drawdown due to widespread anoxia (Elrick et al., 2022).

To summarize, the Devonian-Carboniferous units in the Liard Basin exhibit values for  $Fe_{HR}/Fe_T$  that are stratigraphically variable but consistent with anoxic deposition. Ratios of  $Fe_{py}/Fe_{HR}$  are similarly variable, and suggest the periodic development of euxinia in a predominantly ferruginous water column. Low to moderate Mo enrichments throughout the section, only briefly plotting in the Mo-limited regime (25–100 ppm; Scott and Lyons, 2012), are consistent with intervals of euxinia from iron speciation data. Low Mo/TOCo ratios suggest the plausibility of hydrographic restriction as a cause for the development of anoxia.

### 4.4. The Upper Devonian to Lower Mississippian (Famennian-Tournaisian) Bakken Formation

Here, we present new iron speciation data from three cores (Fig. 7) taken from the central part of the Williston Basin (North Dakota and Montana) along with previously published trace metal and TOC data (Scott et al., 2017). The Bakken succession is typically divided into three stratigraphic intervals; the lithologically similar Lower and Upper organic-rich (black) mudstones, separated by a Middle member composed of grey mudstone, siltstone and fine sandstone facies (Smith and Bustin, 1996). Sampling for this study focused primarily on the highly productive Lower Bakken (LB) and Upper Bakken (UB) members, as well as the overlying basal shale of the Lodgepole Formation (sometimes referred to as the "false Bakken" or FB).

TOC concentrations in the LB and UB units are high, averaging 10.43 and 9.95 wt%, respectively (see Scott et al., 2017 for additional discussion). Values in the UB reach as high as 18.92 wt%. TOC values from the FB or basal Lodgepole shale are lower, averaging 1.87 wt%. Present-day TOC values for Bakken samples are on average  $\sim$  68% of reconstructed original values. Fe-speciation data for all three cores places LB and UB deposition firmly under persistent anoxic conditions (Fe $_{\rm HR}/{\rm Fe}_{\rm T}>0.38$  for all samples). The FB also appears to have been deposited under dominantly anoxic conditions (5 of 6 samples show Fe $_{\rm HR}/{\rm Fe}_{\rm T}>0.38$ , all samples have Fe $_{\rm HR}/{\rm Fe}_{\rm T}>0.22$ ). However, values for Fe $_{\rm py}/{\rm Fe}_{\rm HR}$  are variable across the LB, UB and FB, as well as among the different cores, indicating that the redox architecture of the Williston Basin may have been rather complex with respect to the spatial and temporal distribution of ferruginous vs. euxinic conditions at the sediment-water

Palaeogeography, Palaeoclimatology, Palaeoecology 649 (2024) 112266

Table 3
Summarized results of all geochemical analyses presented in Figs. 4–10 of this work. Sample observations are grouped by play (all results in bold), by section or core (all results in italics), and by formation (all results in plain text). Results are summarized as a count of all samples included for an analysis, the average of all results, minimum and maximum values, and the 95% confidence interval of the results.

Play   Section	TOC	(all in	wt%)		Fe-S	peciatio	n Pool A	Average	es (%) Rec	ox Clas	sification	ı (%)	Мо (	(all in pp	om)		U (a	ll in pp	m)		V (a	ll in ppm)	)	
Formation	(n	Avg.	Min Max.	95% CI	(n	FeCarb	FeOx	FeMag	g FePy (n	Oxic	Ferrug	. Euxinio	c (n	Avg.	Min Max.	95% CI	(n	Avg.	Min Max.	95% CI	(n	Avg.	Min Max.	95% CI
	=)	_			=)				=)		_		=)	-			=)	_			=)	-		
Utica-Pt. Pleasant	93	1.51	0.13-4.6	1.28-1.74	117	27.41	5.36	7.44	59.78 117	36.7	5 50.38	12.82	119	2.47	0.1-42.6	1.62-3.17	119	3.49	0.7-13.2	3.16-3.83	119	84.55	7–180	78.54–90.56
Prudential	23	1.78	0.17-2.93	1.34-2.21	46	31.86	7.54	5.99	54.62 46	19.57	76.09	4.35	47	4.53	0.7-42.6	2.72-6.34	47	4.51	0.7 - 13.2	3.88-5.14	47	95.29	7–180	83.24-107.33
TH-F1305	70	1.42	0.13-4.6	1.15-1.69	71	24.52	3.96	8.37	63.12 71	47.89	36.62	15.49	72	1.13	0.1-4.6	0.87-1.39	72	2.83	1.5-11.7	2.54-3.12	72	77.54	24-121	71.75-83.33
Utica Shale	52	0.97	0.13 - 2.93	0.71-1.24	65	27.2	6.46	8.68	57.67 65	58.46	6 41.53	0	65	1.12	0.2 - 3.4	0.54-1.69	65	3.55	1.5-8.6	3.23-3.86	65	107.69	53-180	102.36-113.02
Point Pleasant Fm.	31	2.29	0.39-4.32	2.01-2.58	39	26.17	4.26	5.82	63.69 39	15.38	3 51.28	33.33	41	3.06	0.5-42.6	1.03-5.09	41	3.81	1.7 - 13.2	3.01-4.62	41	62.26	13-112.5	56.44-68.08
Curdsville/Logana/ Lex.	10	1.87	0.6–4.6	1.1-2.65	13	32.13	3.19	6.06	58.58 13	7.69	92.31	0	13	2.38	0.1-12.3	1.71–3.05	13	2.22	0.7–3.5	1.78-2.67	13	39.15	7–74	27.73–50.58
Marcellus	90	5.2	0.12 - 9.78	4.8-5.61	87	16.15	7.35	3	73.47 87	1.15	41.38	57.47	91	100.61	0.9-360.46	88.72-112.5	91	20.48	0.9-61.6	18.4-22.56	91	517.51	16-1847	450.31-584.7
Nathan Goff #55	61	4.59	0.12-9.08	4.13-5.05	58	15.83	4.77	3	76.36 58	1.72	31.03	67.24	62	87.37	4.33-360.46	5 74.64–100.1	62	17.66	1.3-48.49	15.51–19.8	62	501.56	41–1847	421.06-582.07
WV-7	29	6.5	0.41-9.78	5.85-7.15	29	16.75	12.34	2.99	67.87 29	0	62.07	37.93	29	128.92	0.9–317.09	105.29-152.54	29	26.52	0.9-61.6	22.38-30.66	29	551.59	16-1828	428.33-674.85
Besa River	104	2.72	0.33-5.48	2.46-2.98	77	26.29	6.19	5.06	62.36 77	9.09	53.25	37.66	164	21.95	1.1-98	19.58-24.32	164	7.93	0.8-30.1	7.29-8.57	162	265.59	10-1018	243.28-287.91
Banff fm.	16	0.53	0.33-0.95	0.44-0.61	2	41.67	5.45	10.34	42.5 2	50	50	0	17	3.14	1.1 - 9.2	2.07-4.22	17	3.51	1.1 - 5.6	3.08-3.93	17	311	202-584	264.44-357.56
Exshaw shale	22	2.62	0.44-4.98	2.17 - 3.07	19	35.81	5.82	10.14	48.21 19	15.79	84.21	0	25	16.98	1.3-34	13.29-20.67	25	7.57	2.8-13	6.56-8.57	25	506	254-1018	432.03-579.97
Patry shale	19	4.57	3.64-5.2	4.39-4.74	9	14.98	2.3	1.51	81.22 9	0	11.11	88.89	20	26.66	13.6-39.9	23.9-29.43	20	13.32	8.4–17.7	12.24–14.4	20	168.3	110-251	154.62-181.98
Fort Simpson fm.	12	1.14	0.51 - 4.19	0.56-1.72	12	38.72	5.6	6.43	49.08 12	25	66.67	8.33	20	5.91	1.5-22.6	4.21-7.6	20	3.23	1.4–10.5	2.45-4.01	20	189.05	136-255	176.32-201.78
Muskwa shale	7	2.92	0.88 - 4.38	2.14-3.69	6	28.83	4.76	5.58	60.83 6	0	50	50	10	26.86	3.1 - 39.6	20.22-33.5	10	10.6	1.8 - 15.3	8.12-13.08	10	321.1	227-393	293.17-349.03
Otter Park shale	10	3.27	2.43-4.84	2.85-3.7	13	17.85	4.24	1.39	76.38 13	0	30.77	69.23	29	25.19	17.3–47.5	23.15-27.23	29	8.54	5.2 - 13.7	7.9–9.19	29	165.76	142–191	161.56-169.95
Evie shale	16	3.64	2.99-5.48	3.37-3.91	10	16.29	10.37	1.89	71.45 10	0	30	70	24	50.67	22.6-98	45.17-56.18	24	11.84	8-25.2	10.61-13.08	24	344.58	132-580	306.25-382.92
Nahanni Fm.	2	2.66	2.02-3.29	1.61-3.7	6	17.23	12.6	3.01	66.5 6	0	83.33	16.67	19	13.45	1.5–79.1	5.47-21.43	19	4.37	0.8 - 30.1	1.7–7.05	17	97.29	10-395	47.35–147.24
Bakken	114	9.59	0.07-18.92	8.94–10.25	50	17.37	2.95	2.29	77.36 50	2	18	80	110	263.61	3–1810	226.51-300.71	114	51.71	1.85-296	44.72-58.71	114	850.78	73–2540	758.22-943.34
B706	11	8.86	3.78–15.87	6.66–11.05	9	21.92	7.81	2.09	68.11 9	0	44.44	55.56	11	381.73	82–1810	140.64–622.82	11	86.75	26.6-296	47.71–125.8	11	756.82	140–1730	453.98–1059.65
B832	31	7.44	0.07-12.31		31	16.87	2	2.45	78.68 31	3.23	16.13	80.65	27	89.11	5–307	61.74–116.49	31	21.83	1.85-73.9	16.52-27.13	31	623.77	73–2110	435.15-812.4
E701	17	13.57	4.95–18.92	11.97–15.18	3 10	14.79	1.54		81.6 10	0	0	100	17		146–596	306.47-420.82	17	61.47	22.4–177	47.53–75.42			115–1820	937.77-1379.76
'False' Bakken	8	1.87	0.07-4.19	0.96-2.78	8	26	2.79	4.37	66.88 8	12.5	62.5	25	4	12	5–20	6.11–17.89	8	3.3	1.85-5.65	2.4-4.2	8	130.88	73–220	101.6–160.15
Upper Bakken	56	9.95	0.5–18.92	9.05–10.84		13.7		1.84	82.74 34	0	0	100	56		3–596	143.23-209.99			2.19–74	28.25-36.61		861.09	80-2170	713.6–1008.58
Lower Bakken	50			9.63–11.24		24.33	8.68	2.1	65 8	0	50	50	50		34–1810	319.33-443.03	50	81.06	19.1–296	69.05–93.06		954.42	115–2540	842.61–1066.23
Barnett	52		0.65-5.26		51	36.8	5.93		55.71 51		86.27	13.73	52	4.64	1–13.6	3.84-5.44	52	4.95	1.1–18.1	3.95-5.94	52	96.1	25-231	83.19–109
Barnett Shale (upp. + low.)	38	3.12	1.51–5.26	2.82–3.43	37		6.34		58.58 37		82.05	17.95	38	5.73	2.1–13.6	4.87–6.58	38	6	2.1–18.1	4.8–7.2	38	117.79		106.77–128.81
Forestburg Limestone	14		0.65-2.03	1.07–1.58	14				47.93 14			14.29	14	1.69	1–2.6	1.39–2.0	14		1.1–2.8	1.72–2.45	14	37.21	25–57	30.96–43.47
Wolfcamp-Cline	113		0.38-7.56			27.63			61.72 113					11.49	0.5-63.36	9.67–13.3		6.98	0.85-70.05			171.73		157.47–185.98
Greer-1	<i>75</i>		0.38–7.56	3.45–4	<i>75</i>	27.37		0.98	63.77 75	0	80	20	<i>7</i> 5	13	0.8-63.36	10.48–15.52	<i>7</i> 5	8.31	0.9–70.05	6.09–10.53	<i>75</i>	181.5	22–566.57	161.48–201.53
Greer-2	38		0.4–7.15	1.19–1.84	38			7.83	57.66 38			7.89	38	8.5	0.5–28.42	6.64–10.35	38	4.36	0.85-9.08	3.76-4.96	38		21–261.64	138.13–166.74
Cline Shale	38	1.52	0.4–7.15	1.19–1.84	38	28.15		7.83	57.66 38		8 68.42		38	8.5	0.5–28.42	6.64–10.35	38	4.36	0.85-9.08	3.76-4.96	38	152.44	21–261.64	138.13–166.74
Leonard Fm.	18	4.96	3.41–6.87	4.51–5.41	18	23.44		0.78	70.33 18	0	77.78	22.22	18	30.85	18.4-63.36		18		1.55-70.05		18	335.7	212.57–566.57	
Wolfcamp Fm.	57	3.33	0.38-7.56	3.05-3.62	57		8.64		61.7 57	0	80.7	19.3	57	7.36	0.8–23.95	6.16–8.57	57	7.19	0.9-69.19	5.02–9.36	57	132.81	22-236	122.99-142.63
Montney	56	1.47	0.28-3.96	1.29-1.65	55	35.68			60.75 55	0		18.18		17.43	0.5-90.6	14.01–20.85	55	8.17	0.7–148.1	3.84-12.5	55	212.49		156.2–268.78
Doig Fm.	2	2.44	0.92-3.96	10164	2			1.42	83 2	0	0	100	2	10.05	1.9–18.2	145 01 50	2	8.95	5–12.9	4.60.6.00	2	496.5	74–919	140.00.050.05
Montney Fm.	52	1.47	0.37-3.57	1.3–1.64	52	37.51		1.25	59.56 52	0	84.62	15.38	52	18.04	0.7–90.6	14.5–21.58	52	5.45	0.7–20.1	4.68-6.22	52		15–1004	149.88–259.27
Belloy Fm.	2	0.34	0.28-0.4	0 =1 1 (=	1	9.48		11.11		0	100	0	1	0.5	0.4.0.	1 =1 0 =6	1	148.1	0660	1 00 0 00	1	56	11 110	50.04.0F.0
Haynesville	12	1.08	0.33 - 2.19	0.71-1.45	15	35.18	4.59	3.7	56.4 15	13.3	3 60	26.67	15	2.73	0.4-9.7	1.71-3.76	15	2.61	0.6 - 6.3	1.89-3.33	15	70.07	11–119	52.34-87.8

interface. Recently, Sahoo et al. (2023) mapped the distribution of euxinic bottom waters through the Williston Basin using data from 90 wells. This demonstrated that, through the development of the LB, euxinia (as proxied by Mo and V abundances) began in the basin center and progressively onlapped the basin margins through time. Euxinic conditions were not uniform, and were not present on the eastern and southern margins at the close of LB deposition. This is verified by our iron speciation data (Fig. 7B and C), with Fe-speciation values from core E701 (the more centrally-located, basinal core) (Fe $_{\rm py}$ /Fe $_{\rm HR}$  > 0.7) indicating deposition under a euxinic water column, but in core B706 (a more marginal section from the northeastern margin), Fe $_{\rm py}$ /Fe $_{\rm HR}$  values are consistently below the 0.7 threshold.

In summary,  $Fe_{HR}/Fe_{T}$  and  $Fe_{py}/Fe_{HR}$  values for the LB and UB Bakken Formation units place deposition firmly in an anoxic, persistently-euxinic regime in the basin center, and there is evidence for a shallow-chemocline and intensely sulfidic conditions during deposition of the UB (Scott et al., 2017). The results also imply that while sulfidic bottom water and/or pore water conditions were common in the Williston Basin during Bakken time, some of these occurrences may have been transient or short-lived, especially at the margins and during deposition of the LB (based on current sampling). The basal Lodgepole shale or 'False Bakken' also likely saw the development of ferruginous bottom-water conditions. The basin was likely subject to some amount of hydrographic restriction or dampened circulation, evidenced by low but stable enrichments of Mo (for instance in the UB of core B832 where Mo/TOCo ratios of  $3.1 \pm 0.5$  are maintained between core heights of 3157.27 and 3155.96 m).

### 4.5. The Middle to Upper Mississippian (Visean-Serpukhovian) Barnett Formation

The Barnett Formation was studied in the Blakely-1 well (Fig. 8); this is the same core from Wise County, Texas, that was analyzed by Rowe et al. (2008), and a detailed core description can be found in Loucks and Ruppel (2007). The lower portion of the core consists of massive black shale with occasional carbonate layers and pyritized fossil compressions. Moving upwards, the core exhibits more massive units with layers of carbonate-rich sediment; intermittently, light grey carbonate-rich layers and lenses are observed (the Forestburg Limestone). Continuing towards shallower depths, the core transitions into fissile intervals, accompanied by variations in sediment composition. Some intervals show black shale with limited carbonate cement, while others display small pyrite crystals. The shallowest portion of the core consists of broken up, finegrained black shale with very fine silt/clay-sized pyrite grains. Consistent with Rowe et al. (2008), our TOC measurements were ~ 4 wt% at the base of the core and  $\sim 2\%$  at the top (average = 2.61%) (with present-day TOC ~70% of reconstructed original TOC). In contrast, we found higher values (maximum 5.26 wt%) in the 2195-2193 m core depth. Also consistent with the previous study, we found that a significant fraction of highly reactive iron is present in non-pyritized phases. Specifically, we found that 55.7% of highly reactive iron was present as pyrite, and that the remainder was dominantly present in the iron-carbonate (acetate extractable) pool (36.8%) followed by the iron oxide (dithionite extractable) pool (5.9%) and the magnetite (oxalate extractable) pool (1.5%) (note there is not a perfect correspondence between the chemical extraction and extracted mineralogy (Slotznick et al., 2020)). All investigated samples have Fe<sub>HR</sub>/Fe<sub>T</sub> values indicating deposition under anoxic conditions. Most have Fepy/FeHR values suggesting ferruginous rather than euxinic conditions, though some values plot within the 'equivocal' interpretive space and two samples plot in the euxinic zone, with all samples close to the 0.7 interpretive threshold. Consequently, it is likely that sulfide may have developed in the pore waters or water column during some of the period of deposition, but our results do not support persistent sulfidic conditions. Mo contents are low (averaging 4.6 ppm, with a maximum of 13.6 ppm and a generally decreasing trend through the core). These low Mo contents were

interpreted by Rowe et al. (2008) as representing extreme restriction of the Barnett seaway, following the conceptual model of Algeo and Lyons (2006). However, in light of the ferruginous iron speciation signature, we interpret these values as more simply representing a lack of water column sulfide (e.g., <11 µM (Erickson and Helz, 2000; Helz et al., 1996)) that was insufficient to reduce molybdenum (discussed below).

### 4.6. The Upper Pennsylvanian to Lower Permian Cline Shale (Gzhelian) and Wolfcamp and Lower Leonard Formations (Asselian-Sakmarian)

The upper Wolfcamp and lower Leonard formations were studied in the Greer-1 core, from Reagan County, Texas (Fig. 9A). This core, and some TOC and handheld XRF elemental data derived from it, have previously been described and reported by Baumgardner et al. (2014) and Hamlin and Baumgardner (2012), although the data are not presently publicly available. The Wolfcamp Formation ranges from very fine grained dark grey carbonaceous shale in the lower portion to massive dark grey to brown mudstone towards the middle and top of the core section, with notable intervals around 2335 m, 2302 m, and 2294 m that display a brown to bluish mottled appearance. The Lower Leonard Formation still contains mudstone but is characterized by a dominance of calcareous mudrock. Turbiditic conglomerates are found through the Wolfcamp Formation, while finer-grained calciturbidites are found in the Leonard (see Hamlin and Baumgardner, (2012) for detailed description). TOC in the studied core interval averages 3.72 wt%, with a noticeable increase right below the stratigraphic contact with the Lower Leonard Formation (around 2475 m), where TOC values shift from ∼3 wt% to ~6 wt%. Present-day TOC is on average ~ 88% of reconstructed original TOC. Iron speciation data for the Wolfcamp and Lower Leonard formations strongly suggest deposition under an anoxic water column, however, it is less clear whether ferruginous or euxinic conditions were dominant. While all values for FeHR/FeT fall far beyond the anoxic threshold, Fepv/FeHR values are more enigmatic, plotting almost entirely in the "equivocal zone" with a smaller, but still substantial, population clearly indicative of ferruginous conditions. Notably, the number of clear ferruginous data points decreases in the same stratigraphic interval where TOC increases. There is very little sedimentary Mo enrichment in the lower two-thirds of the studied core, plotting consistently near crustal levels in the Wolfcamp until  $\sim\!2500$  m core depth, when Mo increases to  $\sim 10$ –20 ppm. Mo levels then increase again near the Wolfcamp-Lower Leonard contact (i.e. at the same level where TOC and Fe<sub>pv</sub>/Fe<sub>HR</sub> values change), to values of at least 20 ppm and with occasional higher values up to 63.4 ppm. U and V values also increase at this stratigraphic interval.

Interpretations of bottom-water redox state in the Greer-1 core are complicated, as much of the data do fall in the 'equivocal' interpretive zones. Like the intervals of the Utica/Point Pleasant formations discussed above, the intervals in the Wolfcamp with  $\text{Fe}_{\text{py}}/\text{Fe}_{\text{HR}}$  between 0.7 and 0.8 but with Mo  $\sim$ 2 ppm likely represent ferruginous bottom water conditions, with sulfide perhaps developing in pore waters. The interval near the Wolfcamp-Lower Leonard contact, with higher Mo (and other trace element) enrichments more plausibly indicates sulfidic water column conditions, although this may have been a dynamic environment. The presence of small trace fossils in the Lower Leonard indicates that conditions were at least intermittently oxygenated as well, suggesting there may have been rapid redox changes between oxic, ferruginous, and euxinic bottom waters that occurred more rapidly than the time-averaged interval of our stratigraphic sampling (e.g., Dahl et al., 2019)).

The Cline Shale (or "Wolfcamp D") was studied in the Greer-2 core, also from Reagan County, Texas (Fig. 9 B). Lithologically, the core is largely composed of massive fine grained black mudstone with sparse shelly intervals and occasional lenticular carbonate lenses. The intervals of shelly matter become less frequent and disappear towards the middle portion of the core where the mudstone is more carbonaceous, then return towards the top of the core section as the mudstone again

becomes more calcareous. TOC contents are relatively low through the studied interval (averaging 1.92 wt%, with low values from  $\sim\!\!1-\!1.5\%$  throughout most of the core and a much more enriched interval up to 7.15% at the top of the core). Present-day TOC is  $\sim\!\!88\%$  of reconstructed TOC. Fe\_HR/Fe\_T values are in the 'equivocal' interpretation space at the base of the core, but samples shallower than 3008 m depth are essentially all in the anoxic field. Fe\_py/Fe\_HR values are generally in the ferruginous interpretive field, although some points around 3008–3004 m are in the equivocal field. This interval, however, has no authigenic Mo enrichment, and consequently we do not see evidence for the presence of sulfidic water-column conditions. Indeed, Mo concentrations are quite low throughout the core (averaging 8.5 ppm; maximum 28.4 ppm) and consequently the mudstones in this core were likely dominantly deposited under ferruginous bottom waters.

# 4.7. The uppermost Permian to middle Triassic (Changhsingian-Anisian) Montney and Doig Formations

The Montney and Doig formations are represented in the c-65-F core from Alberta, Canada (Fig. 10). The core contains 395 m of strata, and a detailed ITRAX core scan (cm-scale; calibrated to ICP-MS data) study of the core has been published by Schoepfer et al. (2024). The core includes 5 m of the cherty, uppermost Permian Belloy Formation, and the entirety of the overlying Montney Formation, composed of variably dolomitic siltstone to fine sandstone, with distinct beds of algal dolostone and bioclastic tempestites. The Montney Formation is divided by two prominent sequence boundaries into a 'Lower Montney' succession, representing the Griesbachian and Dienerian, the 'Middle Montney' correlated with the Smithian substage of the Lower Triassic, and an 'Upper Montney' succession, representing the Spathian substage (Zonneveld and Moslow, 2018). The core also includes the basal 25 m of the overlying Doig Formation, composed of Anisian phosphatic sandstones (Moslow et al., 2018). TOC values in the core average 1.5 wt%, with occasional values as high as 4 wt%. FeHR/FeT ratios within the Montney Formation are consistently well above the 0.38 threshold, suggesting its deposition under a persistently anoxic water column. This contrasts with paleontological evidence, including biostromes of the bivalve Claraia in the Dienerian interval (the informally termed 'Pocketknife member'), as well as intervals with trace fossils, particularly in the upper Spathian (Moslow et al., 2018). Although Claraia is commonly described as being hypoxia tolerant, and thus the water column need not have been fully oxygenated, the abundance of biotic evidence for aerobic organisms (especially compared to other cores studied here) suggest that, while bottom waters may have been 'anoxic' on average, there was also considerable time when the basin was oxygenated. Fepv/FeHR values throughout the section are generally <0.7, suggesting predominantly ferruginous conditions when conditions were anoxic, with periodic excursions towards euxinia demonstrated by values surpassing 0.8. These euxinic intervals are broadly correlative with the Permian-Triassic boundary, the phosphatic earliest Spathian, and the transition into the Anisian, consistent with high-resolution ITRAX XRF data from this core (Schoepfer et al., 2024) and other regional data (Grasby et al., 2016). A lack of concurrent enrichment in Mo and U during the lower- and uppermost euxinic periods may suggest some aspect of water-mass restriction was at play (Schoepfer and Henderson, 2022). However, with other geochemical and sedimentological indicators remaining relatively stable across these intervals and in light of paleontological evidence for mass extinction of marine biota that was likely driven by temperaturedependent hypoxia (Payne and Clapham, 2012; Penn et al., 2018), U isotope evidence for expanded euxinia (Lau et al., 2016; Zhang et al., 2018), and biomarker evidence for photic-zone euxinia (Grice et al., 2005), perhaps a more plausible explanation is the occurrence of widespread anoxia/euxinia and a drawdown of the global marine trace metal inventory. The only enrichment of TOC to source rock quantities (> 2 wt%) is also correspondent to these excursions towards euxinia, implying that the net effect of redox on OM generation and preservation was likely a controlling factor.

#### 4.8. The Upper Jurassic (Tithonian) Haynesville Formation

The samples from the Haynesville Formation were provided from a confidential well with no stratigraphic context or locality information; thus, they are not plotted stratigraphically. The iron speciation geochemistry generally suggests deposition under oxygenated conditions, and the limited trace metal enrichment and relatively low TOC values (avg. 1.07 wt%) do not necessarily refute this hypothesis. Although these samples are included in our compilation and statistical analyses, given the small number of samples and lack of stratigraphic context these results should not be considered indicative of the Haynesville Formation more broadly.

# 5. Results: Bottom-water redox conditions and TOC during deposition of North American black shales

#### 5.1. Redox heterogeneity between basins and targets

With respect to redox conditions in North American black shales deposited from the Late Ordovician to the Jurassic, several conclusions can be drawn from the data. Results from the Williston, Appalachian, Midland, Liard, Peace River, Fort Worth, and Gulf Coast basins suggest that almost all investigated units were deposited under generally anoxic depositional conditions. This is not unexpected given previous geochemical studies of these units and the fact that we were targeting black shales in general (Wignall, 1994). Such units are defined by their dark color resulting from organic matter enrichment and their general lack of in-situ benthic body and trace fossils. Of the cores we investigated, body fossils were only found in the Utica-Point Pleasant cores and Montney cores (along with associated trace fossils) and small trace fossils were found in the Lower Leonard. Otherwise, the cores exhibited a laminated or massive nature and bottom water redox conditions were clearly excluding a benthic fauna (note that paleontological/ichnological observations were not possible in the I-48 core, which was analyzed from cuttings, and the Haynesville samples, which were previously powdered).

While these cores exhibit consistent geochemical signatures of anoxic bottom waters, the biogeochemical nature of anoxia varied greatly within and among basins, specifically in the proportion of sulfidized reactive iron, i.e. whether the overlying water column was ferruginous (sulfide-limited) or euxinic (iron-limited). It is clear that euxinia was not ubiquitous throughout deposition of these units; rather, our results show that an increased emphasis must be placed on the likelihood that any given organic-rich shale was deposited under ferruginous conditions. Fig. 11 illustrates that a significant portion of our samples were deposited under ferruginous, or at least oscillatory, redox conditions. This interpretation stands in contrast to older models of source rock development under predominantly euxinic conditions. Most likely there is a spectrum of broadly discrete states that can be used to characterize these units, for example fully ferruginous (Cline Shale), poised at the tipping point between several redox states (Utica Shale), ferruginous but with some euxinic intervals (Wolfcamp), dominantly euxinic but with some ferruginous oscillations (Marcellus Shale), or dominantly euxinic (Bakken Formation depocenter).

#### 5.2. Total organic carbon versus redox state

These data suggest a significantly higher TOC content in euxinic settings compared to ferruginous settings (Fig. 12). Specifically, looking across all formations, samples defined as euxinic based on iron speciation have a median TOC of 4.39 wt% (average = 5.35 wt%) as compared to a ferruginous median TOC of 2.02 wt% (average = 2.42 wt%) and oxic median TOC of 0.6 wt% (average = 0.93 wt%) (Fig. 12). The significance of the difference between the euxinic and ferruginous samples

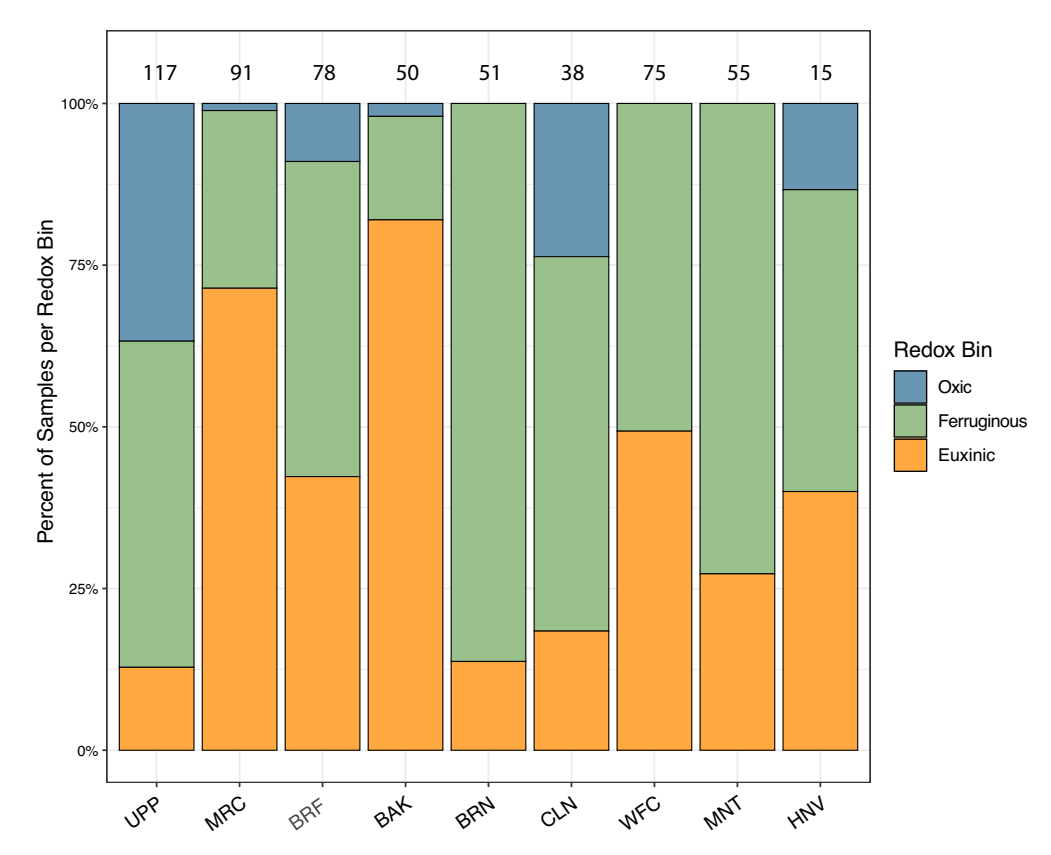


Fig. 11. Proportionalities of observed redox conditions for each of the investigated plays based on interpretations from iron speciation paleoredox proxy results. Individual basins/plays are listed from left to right from oldest to youngest. UPP = Utica-Point Pleasant, MRC = Marcellus, BRF = Besa River Formation, BAK = Bakken, BRN = Barnett, CLN = Cline, WFC = Wolfcamp/Leonard, MNT = Montney-Doig, HNV = Haynesville. Numbers at top of columns represent the number of analyzed samples.

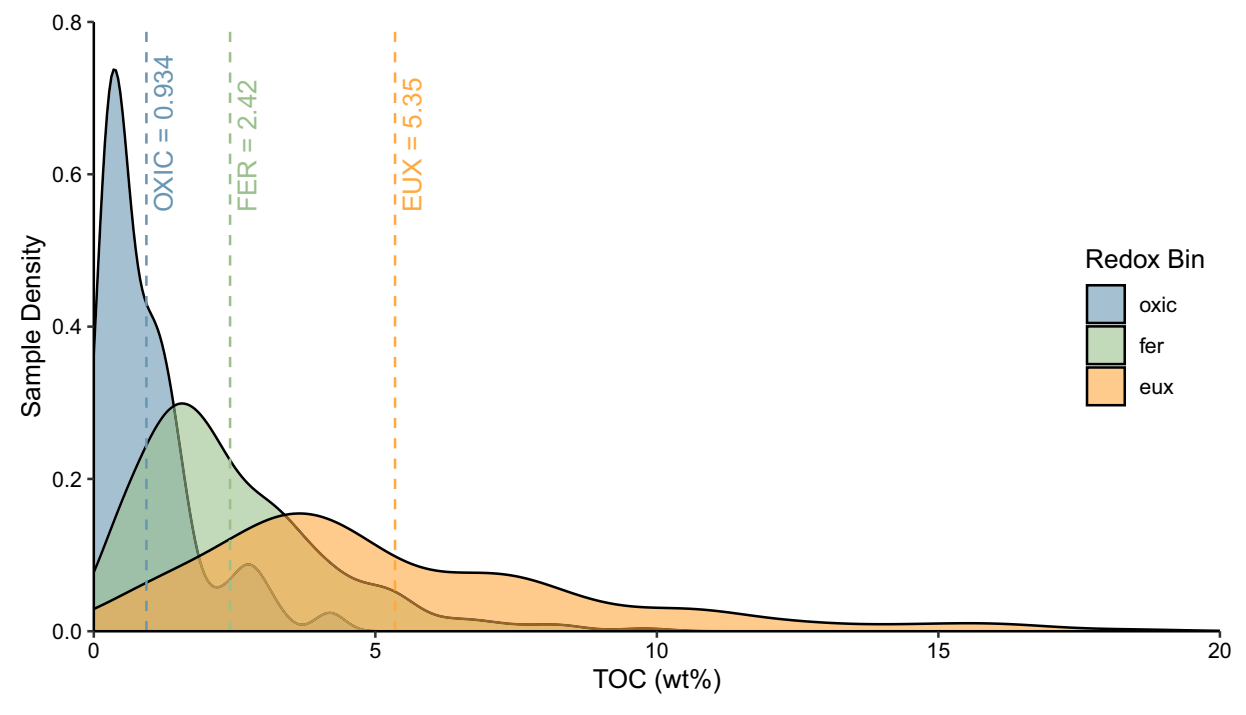


Fig. 12. Density distribution plots of total organic carbon (TOC) values across all basins in the study, divided into oxic ( $Fe_{HR}/Fe_T < 0.38$ ; blue), ferruginous ( $Fe_{HR}/Fe_T > 0.38$  and  $Fe_{PY}/Fe_{HR} < 0.7$ ; green), and euxinic ( $Fe_{HR}/Fe_T > 0.38$  and  $Fe_{PY}/Fe_{HR} > 0.7$ ; orange) populations. Dashed lines represent mean TOC values for each population in weight percent. Statistical significance test results confirm that TOC contents are higher in euxinic samples than in ferruginous samples (Table 4). (For interpretation of the references to color in this figure legend, the reader is referred to the web version of this article.)

Table 4

Statistical analyses of TOC and TOCo versus redox categories. Each analysis shows the number of samples in each redox bin, the results of the Kruskal-Wallis test (one-way ANOVA on ranks), and the p-values of pairwise Wilcoxon tests between different redox categories. Eux. = euxinic. Fer. = ferruginous.

TOC by redox bin					
Number of samples	Total	Oxic	Ferruginous	Euxinic	
	570	63	281	226	
Kruskal-Wallis test	Chi-squared	df 2	p-value 2.62E-42		
Pairwise Wilcoxon test	FerrEux. 8.16E-15	Oxic-Eux. 2.88E-26	FerrOxic 2.88E-26		

#### TOCo by redox bin

Number of samples	Total	Oxic	Ferruginous	Euxinic
	420	53	192	175
Kruskal-Wallis test	Chi-squared	df 2	p-value 2.16E-39	
Pairwise Wilcoxon test	FerrEux. 4.43E-16	Oxic-Eux. 1.58E-24	FerrOxic 4.97E-23	

was assessed using both a Pairwise Wilcoxon test and Kruskal-Wallis rank sum test (non-parametric three-way ANOVA), with both methods returning p-values << 0.05 (Table 4). Importantly, many of the 'oxic' points (for instance from the Utica Shale) actually fall in the 'equivocal' space and, based on their  $Fe_{PY}/Fe_{HR}$  values, may actually represent ferruginous bottom water conditions. In this case, the TOC difference between euxinic and ferruginous samples would be even more dramatic given the low TOC contents of 'oxic' sediments.

After applying Eq. (1) to the subset of samples with programmed pyrolysis data using the estimates for HIo from Table 2, original TOC values were reconstructed for comparison with measured (present-day)

TOC. TOCo results were also compared by redox group (Fig. 13). As in the TOC analysis, TOCo is significantly higher in euxinic settings than in ferruginous settings (Table 4). Samples defined as euxinic based on iron speciation have a median TOCo of 7.34 wt% (average = 8.34 wt%) as compared to a ferruginous median TOCo of 3.12 wt% (average = 3.79 wt%) and oxic median TOCo of 0.49 wt% (average = 0.95 wt%) (Fig. 13). Significance between the redox bins was again assessed using both a Pairwise Wilcoxon test and Kruskal-Wallis rank sum test (non-parametric three-way ANOVA), with both methods returning p-values <<0.05 (Table 4). The reconstruction of original TOC content thus produces a similar but slightly more pronounced difference in organic content between euxinic and ferruginous environments (a median difference of 54% for TOCpD versus 57% for TOCo). This fact strongly implies a predictable relationship between euxinia and extremely high levels of organic richness.

#### 6. Discussion

#### 6.1. Redox controls on organic matter accumulation

Given the exponential decay of organic matter settling through an oxygenated water column (Marsay et al., 2015), a rapid settling time between the oxic portion of the water column and a strong chemocline is one of the key controls on the quantity and quality of preserved organic matter (Katsev and Crowe, 2015; Pichevin et al., 2004). The effect of the chemistry of waters below the chemocline (i.e., ferruginous versus euxinic) on TOC preservation has been less well explored (Johnston et al., 2010; Poulton et al., 2010). A statistical TOC difference between redox states has been demonstrated in the Neoproterozoic Fifteenmile Group (Sperling et al., 2013) and qualitatively in Chuar Group (Johnston et al., 2010), but not across basins, in the Phanerozoic, or in stratigraphic targets of economic interest. The results described in Section 5.2 clearly demonstrate higher TOC in samples deposited under euxinic bottom-waters, consistent with the previous single-basin

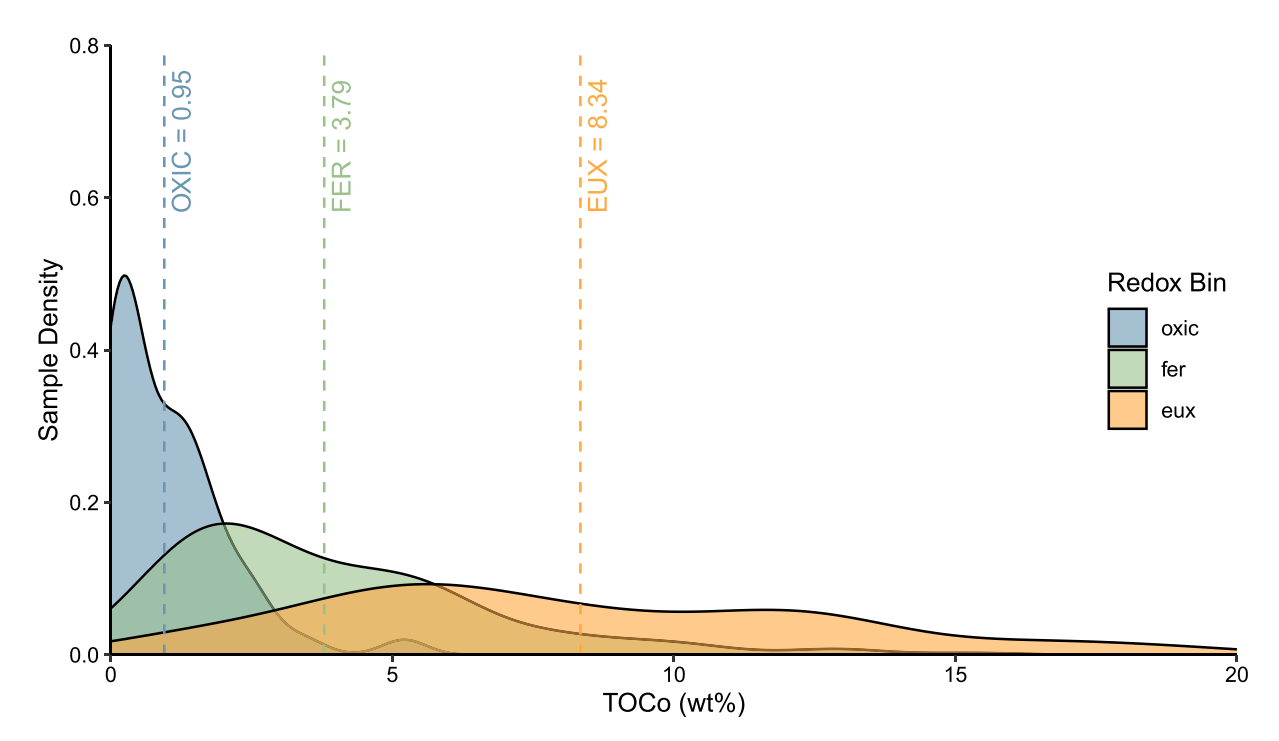


Fig. 13. Density distribution plots of reconstructed values of original total organic carbon (TOCo) for a subset of samples in the study with available pyrolysis data. Samples are divided into oxic ( $Fe_{HR}/Fe_T < 0.38$ ; blue), ferruginous ( $Fe_{HR}/Fe_T > 0.38$  and  $Fe_{PY}/Fe_{HR} < 0.7$ ; green), and euxinic ( $Fe_{HR}/Fe_T > 0.38$  and  $Fe_{PY}/Fe_{HR} > 0.7$ ; orange) populations. Dashed lines represent mean TOCo values for each population in weight percent. Statistical significance test results confirm that TOCo contents are higher in euxinic samples than in ferruginous samples (Table 4). (For interpretation of the references to color in this figure legend, the reader is referred to the web version of this article.)

Neoproterozoic case studies.

Like the broader question of preservation versus productivity in TOC accumulation (Katz, 2005; Tyson, 2005), this observed relationship likely has different causes in different basins. In many cases, this difference may be simply explained by biogeochemical controls on the distribution of euxinia. In other words, high levels of primary productivity and organic carbon export production are a necessary factor for driving marine waters below the chemocline towards euxinic conditions (Johnston et al., 2010), and thus high TOC would predictably be associated with euxinia (i.e., a production control—high preserved TOC despite high levels of organic matter remineralization).

Alternatively, higher TOC in euxinic samples could be a consequence of that redox state. For instance, the model developed by Scott et al. (2017) for the Bakken Formation involved organic matter descending through a very short oxygenated water column before reaching a shallow, hyper-sulfidic chemocline. If euxinia reaches the photic zone, organic matter can even be produced by phototrophic sulfide oxidizing bacteria without ever passing through an oxygenated water column (i.e. a preservational control—high preserved TOC due to lower levels of organic matter remineralization).

Higher TOC in euxinic settings may also be related to preservation via sulfurization of OM. Sulfur-rich OM is relatively resistant to biodegradation (Sinninghe Damste and De Leeuw, 1990) and is second only to pyrite as a sink for reduced sulfur (Berner and Raiswell, 1983). Like pyrite, the organically-bound sulfur (OS) pool is most enriched in euxinic settings, specifically where free sulfide remains after scavenging by available highly-reactive Fe (Tribovillard et al., 2004; Zaback and Pratt, 1992). A portion of this excess reduced sulfur can be incorporated into organic matter, primarily through abiotic reactions in the porewater during diagenesis (Sinninghe Damste and De Leeuw, 1990; Werne et al., 2003, 2008), though there is evidence that in certain conditions, water column sulfurization can occur and compete with remineralization for labile OM (Raven et al., 2016; Sinninghe Damsté et al., 1988). The occurrence of water column and/or sediment sulfurization, likely under euxinic, Fe-limited scenarios, may explain hyper-enrichments of OM in some source rocks even if Type II-S kerogens do not fully develop (Raven et al., 2018).

While the causative control(s) are likely different in different basins, euxinic conditions are statistically correlated with higher TOC. Nonetheless, from an economic perspective, despite this clear statistical relationship between redox state and TOC, it is worth emphasizing that the median/average TOC content associated with either ferruginous or euxinic bottom water redox condition is well beyond the requirement for generative potential. It is obvious that ferruginous bottom waters are no impediment to economic production (e.g., Barnett, Utica, and Cline Shale). On the other hand, the recognition that many exceptional shale plays (Marcellus, Bakken) or drilling targets within formations (Wolfcamp-Lower Leonard contact) appear to be associated with euxinic conditions suggest there may be a link between sulfidic conditions and the highest likelihood of economical hydrocarbons. This may be at the level of increased TOC quantity (e.g., Figs. 12 and 13), but could also be related to TOC quality. It is likely that exposure to more reduced anoxic conditions (euxinic as opposed to ferruginous) promotes the preservation of higher quality organic matter (higher HI), just as decreasing exposure to oxygenated conditions promotes higher quality organic matter in the oxic realm (Gélinas et al., 2001). Although this hypothesis remains to be tested in thermally immature samples with paired organic and inorganic geochemical data from the same samples, this effect can be seen qualitatively by comparing our summary results in Fig. 11 with the initial HI estimates in Table 2. Formations/plays associated with euxinic depositional conditions (e.g., Bakken, Marcellus, Besa River Formation) have higher HIo than those deposited under ferruginous conditions (e.g., Montney, Utica, Cline Shale).

6.2. Undoing assumptions of euxinic prevalence and updating proxy interpretations to consider ferruginous cases

The recognition that many black shales were deposited under ferruginous conditions has important implications for the way we interpret geochemical data from these units. For instance, ratios of Mo to initial TOC are commonly used as a proxy for paleohydrographic restriction within a basin, based on comparison to modern euxinic analogues (Algeo and Lyons, 2006). This proxy has been employed to suggest (based on very low Mo/TOC ratios) that the Barnett Formation (Gambacorta et al., 2016; Rowe et al., 2008) and Wolfcamp Formation (Baumgardner et al., 2014; Peng et al., 2020) were deposited in very restricted conditions, likely more restricted than the modern Black Sea. However, the results here suggest these two formations were deposited under dominantly ferruginous conditions, and the low levels of Mo in samples was likely due to low sulfide during deposition rather than low aqueous Mo concentrations in the basin resulting from severe restriction. Indeed, across all our samples, samples with a ferruginous bottom water signature and enough TOCo for good estimation of this ratio  $(Fe_{pv}/Fe_{HR} < 0.7; TOCo > 0.5 wt\%)$  have a Mo/TOCo value of 5.8 (interquartile range of 1.4 to 8.0, with a maximum of 32). In other words, all ferruginous samples would have had to been deposited in incredibly restricted settings (Algeo and Lyons, 2006). In contrast, euxinic samples have a significantly higher Mo/TOCo value of 11.4 (inter-quartile range of 3.0 to 18.6, with a maximum of 61.7). This indicates a more reasonable spread of basinal restriction across samples—including some strongly restricted basins (not surprising given the relationship between restriction and the development of reducing conditions) but also some more open settings, similar to Framvaren Fiord or Cariaco Basin, and a few instances similar to the modern unrestricted Saanich Inlet. The euxinic and ferruginous populations are significantly different (Wilcoxon test, W = 20,250,  $p = 3.15 \times 10^{-7}$ ), and the results suggest that either euxinic bottom waters preferentially develop in less restricted settings, or more simply that ferruginous bottom waters did not have enough sulfide to generate comparable Mo enrichments. A low Mo/TOC ratio can develop from multiple drivers: either due to low Mo (due to restriction) or due to ferruginous (or oxic) conditions. Thus, the application of the Mo/TOC restriction proxy and other paleoenvironmental proxies that rely on the presence of euxinic conditions should thus only be applied after independent geochemical confirmation of euxinia.

#### 7. Conclusions

This study provides a detailed analysis of North American black shales using a consistent geochemical dataset. This work reveals a surprising prevalence of ferruginous conditions (>50% of samples) in these stratigraphic units. These findings affirm the importance of anoxia but challenge the idea that euxinia is a pre-requisite for organic-rich deposition, or further, that it is even the dominant condition under which source rocks/black shales typically develop. These results suggests that we may be underestimating the extent or importance of ferruginous (or more broadly, anoxic and non-sulfidic) deposition in the sedimentary record. While this work does highlight the potential importance of ferruginous environments in economically important shale units, the data show that TOC contents are, in fact, significantly higher in euxinic settings. It remains unclear whether higher TOC in euxinic conditions is a cause or consequence of this redox state (likely both in different settings), but this robust finding lays the groundwork for future investigations of biogeochemistry and carbon cycling in reducing basins.

#### CRediT authorship contribution statement

**Samantha R. Ritzer:** Conceptualization, Data curation, Formal analysis, Investigation, Methodology, Resources, Writing – original draft, Writing – review & editing, Visualization, Supervision. **Shane Schoepfer:** Resources, Writing – review & editing, **Bella Bussian:** 

Investigation. Una C. Farrell: Data curation, Investigation, Supervision. Tiffani Fraser: Resources, Writing – review & editing. Charles M. Henderson: Resources, Writing – review & editing. Junyao Kang: Investigation, Writing – review & editing. Chiza N. Mwinde: Investigation. Austin Patch: Investigation. Erik A. Sperling: Conceptualization, Formal analysis, Funding acquisition, Project administration, Resources, Supervision, Writing – review & editing.

#### Declaration of competing interest

The authors declare the following financial interests/personal relationships which may be considered as potential competing interests:

Erik Sperling reports financial support was provided by National Science Foundation. Erik Sperling reports financial support was provided by American Chemical Society. Samantha Ritzer reports financial support was provided by American Association of Petroleum Geologists Foundation. Charles Henderson reports equipment, drugs, or supplies was provided by Petronas Canada Ltd. If there are other authors, they declare that they have no known competing financial interests or personal relationships that could have appeared to influence the work reported in this paper.

#### Data availability

Data has been provided as a supplemental data file

#### Acknowledgements

We thank Nathan Ivicic and Brandon Williamson at the Austin Core Research Center, Phil Dinterman at the West Virginia Geological and Economic Survey, and Jeffrey Deisher at the Ohio Department of Natural Resources H.R. Collins Laboratory for assistance sampling cores. We thank Clint Scott for providing samples of the Bakken Formation and Mark Zoback and Fatemeh Rassouli for providing samples of the Haynesville Formation. The authors would like to express their gratitude to Petronas Canada Ltd. (formerly Progress Energy Canada Ltd.), especially to Gerald Nyberg, Matt Adams, and Wayne Hovdebo, and Sasol Exploration and Production Ltd. for providing us with access to the c-65-F core. We thank Doug Turner, Austin Miller, Maoli Vizcaíno, Tessa Browne, Cecilia Endriga, Sabrina Tecklenberg, and Juan Pacheco Lezama for help with laboratory analyses, and Kate French, Ned Frost, Ben Gill, Steve Graham, Allegra Hosford Scheirer, Matt Hutchison, Swapan Sahoo, Clint Scott, and Morgan Raven for helpful discussion. BB thanks the Witter Grant at Colorado College. EAS thanks the donors of The American Chemical Society Petroleum Research Fund for partial support of this research (61017-ND2) and National Science Foundation grants EAR-2143164 and EAR-1922966. EAS and SRR thank the affiliates of the Stanford Program on Deepwater Depositional Systems and the Stanford Natural Gas Initiative for funding. SRR thanks the Stanford-USGS fellowship, the McGee-Levorsen fund, and an AAPG student research grant for funding support.

#### Appendix A. Supplementary data

Supplementary data to this article can be found online at https://doi.org/10.1016/j.palaeo.2024.112266.

#### References

- Ahm, A.-S.C., Bjerrum, C.J., Hammarlund, E.U., 2017. Disentangling the record of diagenesis, local redox conditions, and global seawater chemistry during the latest Ordovician glaciation. Earth Planet. Sci. Lett. 459, 145–156. https://doi.org/ 10.1016/j.epsl.2016.09.049.
- Alcott, L.J., Krause, A.J., Hammarlund, E.U., Bjerrum, C.J., Scholz, F., Xiong, Y., Hobson, A.J., Neve, L., Mills, B.J., März, C., Schnetger, B., Bekker, A., Poulton, S.W., 2020. Development of iron speciation reference materials for palaeoredox analysis. Geostand. Geoanal. Res. 44, 581–591.

- Algeo, T.J., 2004. Can marine anoxic events draw down the trace element inventory of seawater? Geology 32, 1057–1060.
- Algeo, T.J., Liu, J., 2020. A re-assessment of elemental proxies for paleoredox analysis. Chem. Geol. 119549.
- Algeo, T.J., Lyons, T.W., 2006. Mo-total organic carbon covariation in modern anoxic marine environments: Implications for analysis of paleoredox and paleohydrographic conditions. Paleoceanography 21, PA1016.
- Algeo, T.J., Rowe, H., 2012. Paleoceanographic applications of trace-metal concentration data. In: Chemical Geology, 324–325, pp. 6–18. https://doi.org/10.1016/j. chemgeo.2011.09.002.
- Algeo, T.J., Tribovillard, N., 2009. Environmental analysis of paleoceanographic systems based on molybdenum-uranium covariation. Chem. Geol. 268, 211–225. https:// doi.org/10.1016/j.chemgeo.2009.09.001.
- Anderson, T.F., Raiswell, R., 2004. Sources and mechanisms for the enrichment of highly reactive iron in euxinic Black Sea sediments. Am. J. Sci. 304, 203–233. https://doi. org/10.2475/ais.304.3.203.
- Anttila, E.S.C., Macdonald, F.A., Szymanowski, D., Schoene, B., Kylander-Clark, A., Danhof, C., Jones, D.S., 2023. Timing and tempo of organic carbon burial in the Monterey Formation of the Santa Barbara Basin and relationships with Miocene climate. Earth Planet. Sci. Lett. 620, 118343 https://doi.org/10.1016/j.epsl.2023.118343.
- Ardakani, O.H., Chappaz, A., Sanei, H., Mayer, B., 2016. Effect of thermal maturity on remobilization of molybdenum in black shales. Earth Planet. Sci. Lett. 449, 311–320. https://doi.org/10.1016/j.epsl.2016.06.004.
- Arens, N.C., Cuffey, R.J., 1989. Shallow and stormy: late Middle Ordovician paleoenvironments in Central Pennsylvania. Northeast. Geol. 11, 218–224.
- Arthur, M.A., Sageman, B.B., 2005. Sea-Level control on source-rock development: Perspectives from the Holocene Black Sea, the Mid-Cretaceous Western Interior Basin of North America, and the Late Devonian Appalachian Basin. In: Harris, N.B. (Ed.), the Deposition of Organic-Carbon-Rich Sediments: Models, Mechanisms, and Consequences. SEPM Society for Sedimentary Geology, pp. 35–60. https://doi. org/10.2110/pec.05.82.0035.
- Baskoro, A.S., Baur, F., Yu, A.Z., Grossman, E.L., 2023. Restoring source rock initial quality and quantity with kinetic-based inversion - Applied to the Wolfcamp play in the Permian Delaware Basin. Mar. Pet. Geol. 150, 106143 https://doi.org/10.1016/ i.maroetgeo.2023.106143.
- Baumgardner, R.W., Hamlin, H.S., Rowe, H.D., 2014. High-Resolution Core Studies of Wolfcamp/Leonard Basinal Facies, Southern Midland Basin, Texas. AAPG Search Discov. 10607, 1–4.
- Berner, R.A., Raiswell, R., 1983. Burial of organic carbon and pyrite sulfur in sediments over Phanerozoic time: a new theory. Geochim. Cosmochim. Acta 47, 855–862. https://doi.org/10.1016/0016-7037(83)90151-5.
- Bertine, K.K., Turekian, K.K., 1973. Molybdenum in marine deposits. Geochim. Cosmochim. Acta 37, 1415–1434.
- Blood, D.R., Schlaegle, S., Hefferan, C.M., Vazquez, A., McAllister, D., 2019. Chapter 5: Diagenetic pyrite morphology in mudstones of the Upper Ordovician Point Pleasant Limestone. In: Appalachian Basin: Evidence for Dysoxic Deposition, pp. 69–82. https://doi.org/10.1306/13672211M1213822
- Boyer, D.L., Mitchell, C.E., 2017. Aligned trace fossils from the Utica Shale: implications for mode of life and feeding in the trilobite Triarthrus beckii. Lethaia 50, 69–78. https://doi.org/10.1111/let.12177.
- Brett, C.E., Aucoin, C.D., Dattilo, B.F., Freeman, R.L., Hartshorn, K.R., McLaughlin, P.I., Schwalbach, C.E., 2020. Revised sequence stratigraphy of the upper Katian Stage (Cincinnatian) strata in the Cincinnati Arch reference area: Geological and paleontological implications. Palaeogeogr. Palaeoclimatol. Palaeoecol. 540, 109483 https://doi.org/10.1016/j.palaeo.2019.109483.
- Browne, T.N., Hofmann, M.H., Malkowski, M.A., Wei, J., Sperling, E.A., 2020. Redox and paleoenvironmental conditions of the Devonian-Carboniferous Sappington Formation, southwestern Montana, and comparison to the Bakken Formation, Williston Basin. Palaeogeogr. Palaeoclimatol. Palaeoecol. 560, 110025 https://doi.org/10.1016/j.palaeo.2020.110025.
- Byers, C.W., 1977. Biofacies patterns in Euxinic Basins: A general model. In: Cook, H.E., Enos, P. (Eds.), Deep-Water Carbonate Environments. SEPM Society for Sedimentary Geology, pp. 5–17. https://doi.org/10.2110/pec.77.25.0005.
- Canfield, D.E., 1989. Reactive iron in marine sediments. Geochim. Cosmochim. Acta 53, 619–632. https://doi.org/10.1016/0016-7037(89)90005-7.
- Canfield, D.E., Raiswell, R., Westrich, J.T., Reaves, C.M., Berner, R.A., 1986. The use of chromium reduction in the analysis of reduced inorganic sulfur in sediments and shales. Chem. Geol. 54, 149–155. https://doi.org/10.1016/0009-2541(86)90078-1.
- Canfield, D.E., Poulton, S.W., Knoll, A.H., Narbonne, G.M., Ross, G., Goldberg, T., Strauss, H., 2008. Ferruginous conditions dominated later Neoproterozoic deepwater chemistry. Science 321, 949–952. https://doi.org/10.1126/science.1154499.
- Carter, K.M., Harper, J.A., Schmid, K.W., Kostelnik, J., 2011. Unconventional natural gas resources in Pennsylvania: the backstory of the modern Marcellus Shale play. Environ. Geosci. 18, 217–257. https://doi.org/10.1306/eg.09281111008.
- Chen, R., Sharma, S., 2016. Role of alternating redox conditions in the formation of organic-rich interval in the Middle Devonian Marcellus Shale, Appalachian Basin, USA. Palaeogeogr. Palaeoclimatol. Palaeoecol. 446, 85–97. https://doi.org/ 10.1016/j.palaeo.2016.01.016.
- Clarkson, M.O., Poulton, S.W., Guilbaud, R., Wood, R.A., 2014. Assessing the utility of Fe/Al and Fe-speciation to record water column redox conditions in carbonate-rich sediments. Chem. Geol. 382, 111–122.
- Cobbett, R.N., Colpron, M., Crowley, J.L., Cordey, F., Blodgett, R.B., Orchard, M.J., 2020. Late Devonian magmatism and clastic deposition in the upper Earn Group (Central Yukon, Canada) mark the transition from passive to active margin along western Laurentia. Can. J. Earth Sci. 58, 471–494. https://doi.org/10.1139/cjes-2020-0161.

- Cole, D.B., Zhang, S., Planavsky, N.J., 2017. A new estimate of detrital redox-sensitive metal concentrations and variability in fluxes to marine sediments. Geochimica et Cosmochimica Acta 215, 337–353.
- Crombez, V., Baudin, F., Rohais, S., Riquier, L., Euzen, T., Pauthier, S., Ducros, M., Caron, B., Vaisblat, N., 2017. Basin scale distribution of organic matter in marine fine-grained sedimentary rocks: Insight from sequence stratigraphy and multiproxies analysis in the Montney and Doig Formations. Mar. Pet. Geol. 83, 382–401. https://doi.org/10.1016/j.marpetgeo.2016.10.013.
- Crombez, V., Rohais, S., Euzen, T., Riquier, L., Baudin, F., Hernandez-Bilbao, E., 2020. Trace metal elements as paleoenvironmental proxies: why should we account for sedimentation rate variations? Geology 48, 839–843. https://doi.org/10.1130/ G47150.1
- Dahl, T.W., Siggaard-Andersen, M.-L., Schovsbo, N.H., Persson, D.O., Husted, S., Hougård, I.W., Dickson, A.J., Kjær, K., Nielsen, A.T., 2019. Brief oxygenation events in locally anoxic oceans during the Cambrian solves the animal breathing paradox. Sci. Rep. 9, 11669. https://doi.org/10.1038/s41598-019-48123-2.
- Dickson, A.J., Idiz, E., Porcelli, D., van den Boorn, S.H.J.M., 2020. The influence of thermal maturity on the stable isotope compositions and concentrations of molybdenum, zinc and cadmium in organic-rich marine mudrocks. Geochim. Cosmochim. Acta, New develop. Geochem. Proxies Paleoceanogr. Res. 287, 205–220. https://doi.org/10.1016/j.gca.2019.11.001.
- Dickson, A.J., Idiz, E., Porcelli, D., Murphy, M.J., Celestino, R., Jenkyns, H.C., Poulton, S. W., Hesselbo, S.P., Hooker, J.N., Ruhl, M., van den Boorn, S.H.J.M., 2022. No effect of thermal maturity on the Mo, U, Cd, and Zn isotope compositions of lower Jurassic organic-rich sediments. Geology 50, 598–602. https://doi.org/10.1130/G49724.1.
- Elrick, M., Gilleaudeau, G.J., Romaniello, S.J., Algeo, T.J., Morford, J.L., Sabbatino, M., Goepfert, T.J., Cleal, C., Cascales-Miñana, B., Chernyavskiy, P., 2022. Major Early-Middle Devonian oceanic oxygenation linked to early land plant evolution detected using high-resolution U isotopes of marine limestones. Earth Planet. Sci. Lett. 581, 117410 https://doi.org/10.1016/j.epsl.2022.117410.
- Emerson, S.R., Huested, S.S., 1991. Ocean anoxia and the concentrations of molybdenum and vanadium in seawater. Mar. Chem. 34, 177–196. https://doi.org/10.1016/0304-4203(91)90002-E
- Enomoto, C.B., Trippi, M.H., Higley, D.K., Ii, R.M.D., Gaswirth, S.B., Mercier, T.J., Brownfield, M.E., Leathers-Miller, H.M., Le, P.A., Marra, K.R., Tennyson, M.E., Woodall, C.A., Schenk, C.J., 2019. Assessment of undiscovered continuous oil and gas resources in the Upper Ordovician Point Pleasant Formation and Utica Shale of the Appalachian Basin Province, 2019 (Fact Sheet no. 2019–3044), Fact Sheet. U.S. Geological Survey. https://doi.org/10.3133/fs20193044.
- Erickson, B.E., Helz, G.R., 2000. Molybdenum(VI) speciation in sulfidic waters: stability and lability of thiomolybdates. Geochim. Cosmochim. Acta 64, 1149–1158. https:// doi.org/10.1016/S0016-7037(99)00423-8.
- Espitalié, J., Marquis, F., Barsony, İ., 1984. Geochemical logging. In: Analytical Pyrolysis. Elsevier, pp. 276–304.
- Ettensohn, F.R., 1987. Rates of relative plate motion during the Acadian Orogeny based on the spatial distribution of black shales. J. Geol. 95, 572–582. https://doi.org/10.1086/629150.
- Ettensohn, F.R., 2004. Modeling the nature and development of major Paleozoic clastic wedges in the Appalachian Basin, USA. J. Geodynam. Tecton. Appal. Belt 37, 657–681. https://doi.org/10.1016/j.jog.2004.02.009.
- Ettensohn, F.R., Lierman, R.T., 2012. Large-scale tectonic controls on the origin of Paleozoic dark-shale source-rock Basins: examples from the Appalachian Foreland Basin, Eastern United States. AAPG Mem. 100, 95–124. https://doi.org/10.1306/ 13351549M1003529.
- Faill, R.T., 1985. The Acadian orogeny and the Catskill Delta. In: Woodrow, D.L., Sevon, W.D. (Eds.), The Catskill Delta. Geological Society of America, pp. 15–37. https://doi.org/10.1130/SPE201-p15.
- Farrell, U.C., Briggs, D.E.G., Gaines, R.R., 2011. Paleoecology of the olenid trilobite Triarthrus: New evidence from Beecher's Trilobite Bed and other sites of pyritization. Palaios 26, 730–742.
- Farrell, Ú.C., Briggs, D.E.G., Hammarlund, E.U., Sperling, E.A., Gaines, R.R., 2013. Paleoredox and pyritization of soft-bodied fossils in the Ordovician Frankfort Shale of New York. Am. J. Sci. 313, 452–489.
- Ferri, F., Zonneveld, J.-P., 2008. Were Triassic rocks of the Western Canada Sedimentary Basin deposited in a Foreland? Can. Soc. Petrol. Geol. Reserv. 35, 12–14.
- Ferri, F., McMechan, M., Creaser, R., 2015. The Besa River Formation in Liard Basin, British Columbia. In: Oil and Gas Reports, BC Ministry of Natural Gas Development, nn. 1–27
- Ferrill, B.A., Thomas, W.A., 1988. Acadian dextral transpression and synorogenic sedimentary successions in the Appalachians. Geology 16, 604–608. https://doi.org/ 10.1130/0091-7613(1988)016<0604:ADTASS>2.3.CO;2.
- Fielding, C.R., Frank, T.D., Isbell, J.L., 2008. The late Paleozoic ice age—A review of current understanding and synthesis of global climate patterns. In: Fielding, C.R., Frank, T.D., Isbell, J.L. (Eds.), Resolving the Late Paleozoic Ice Age in Time and Space. Geological Society of America, pp. 343–354. https://doi.org/10.1130/ 2008.2441(24).
- Fiess, K.M., Ferri, F., Fraser, T.A., Pyle, L.J., Rocheleau, J., 2015. Liard Basin Hydrocarbon Project: Shale gas potential of Devonian-Carboniferous strata in the Northwest Territories, Yukon and Northeastern British Columbia; #10706 (2015). AAPG Search and Discovery Article #10706.
- Gambacorta, G., Trincianti, E., Torricelli, S., 2016. Anoxia controlled by relative sealevel changes: an example from the Mississippian Barnett Shale Formation. Palaeogeogr. Palaeoclimatol. Palaeoecol. 459, 306–320. https://doi.org/10.1016/j.palaeo.2016.07.015.
- Gaswirth, S.B., 2017. Assessment of continuous oil resources in the Wolfcamp shale of the Midland Basin, Permian Basin Province, Texas, 2016 (Open-File Report no.

- 2017–1013), Open-File Report. U.S. Geological Survey. https://doi.org/10.3133/ofr20171013
- Gaswirth, S.B., Marra, K.R., Cook, T.A., Charpentier, R.R., Gautier, D.L., Higley, D.K., Klett, T.R., Lewan, M.D., Lillis, P.G., Schenk, C.J., Tennyson, M.E., Whidden, K.J., 2013. Assessment of Undiscovered Oil Resources in the Bakken and Three Forks Formations, Williston Basin Province, Montana, North Dakota, and South Dakota, 2013 (Fact Sheet No. 2013–3013), Fact Sheet. U.S. Geological Survey. https://doi.org/10.3133/fs20133013.
- Gélinas, Y., Baldock, J.A., Hedges, J.I., 2001. Organic carbon composition of marine sediments: effect of oxygen exposure on oil generation potential. Science 294, 145–148. https://doi.org/10.1126/science.1062363.
- Gill, B.C., Lyons, T.W., Young, S.A., Kump, L.R., Knoll, A.H., Saltzman, M.R., 2011. Geochemical evidence for widespread euxinia in the later Cambrian Ocean. Nature 469, 80–83. https://doi.org/10.1038/nature09700.
- Golding, M.L., Mortensen, J.K., Ferri, F., Zonneveld, J.-P., Orchard, M.J., 2016. Determining the provenance of Triassic sedimentary rocks in northeastern British Columbia and western Alberta using detrital zircon geochronology, with implications for regional tectonics. Can. J. Earth Sci. 53, 140–155. https://doi.org/ 10.1139/cjes-2015-0082.
- Grasby, S.E., Beauchamp, B., Knies, J., 2016. Early Triassic productivity crises delayed recovery from world's worst mass extinction. Geology 44, 779–782. https://doi.org/ 10.1130/G38141.1.
- Grice, K., Cao, C., Love, G.D., Böttcher, M.E., Twitchett, R.J., Grosjean, E., Summons, R. E., Turgeon, S.C., Dunning, W., Jin, Y., 2005. Photic Zone euxinia during the Permian-Triassic superanoxic event. Science 307, 706–709. https://doi.org/10.1126/science.1104323.
- Guilbaud, R., Poulton, S.W., Butterfield, N.J., Zhu, M., Shields-Zhou, G.A., 2015. A global transition to ferruginous conditions in the early Neoproterozoic oceans. Nat. Geosci. 8, 466–470. https://doi.org/10.1038/ngeo2434.
- Gutschick, R.C., Sandberg, C.A., 1983. Mississippian continental margins of the conterminous USA. SEPM Spec. Publ. 33, 79–96.
- Hamlin, H.S., Baumgardner, R.W., 2012. Wolfberry (Wolfcampian-Leonardian) deepwater depositional systems in the Midland Basin: Stratigraphy, lithofacies, reservoirs, and source rocks. Bureau Econ. Geol. Rep. Investigat. 277, 1–72.
- Hammes, U., Hamlin, H.S., Ewing, T.E., 2011. Geologic analysis of the Upper Jurassic Haynesville Shale in East Texas and West Louisiana. AAPG Bull. 95, 1643–1666. https://doi.org/10.1306/0214110128.
- Hancock, L.G., Hardisty, D.S., Behl, R.J., Lyons, T.W., 2019. A multi-basin redox reconstruction for the Miocene Monterey Formation, California, USA. Palaeogeogr. Palaeoclimatol. Palaeoecol. 520, 114–127. https://doi.org/10.1016/j. palaeo.2019.01.031.
- Hart, B.S., Hofmann, M.H., 2022. Revisiting paleoenvironmental analyses and interpretations of organic-rich deposits: the importance of TOC corrections. Org. Geochem. 170. 104434 https://doi.org/10.1016/j.orggochem.2022.104434.
- Hart, B.S., Steen, A.S., 2015. Programmed pyrolysis (Rock-Eval) data and shale paleoenvironmental analyses: a review. Interpretation 3, SH41–SH58. https://doi. org/10.1190/INT-2014-0168.1.
- Heckel, P., Wetzke, B.J., 1979. Devonian world palaeogeography determined from distribution of carbonates and related lithic paleoclimatic indicators. Spec. Pap. Palaeontol. 23, 99–123.
- Hedhli, M., Grasby, S.E., Henderson, C.M., Davis, B.J., 2023. Multiple diachronous "Black Seas" mimic global ocean anoxia during the latest Devonian. Geology. https://doi.org/10.1130/G51394.1.
- Helz, G.R., Miller, C.V., Charnock, J.M., Mosselmans, J.F.W., Pattrick, R.A.D., Garner, C. D., Vaughan, D.J., 1996. Mechanism of molybdenum removal from the sea and its concentration in black shales: EXAFS evidence. Geochim. Cosmochim. Acta 60, 3631–3642. https://doi.org/10.1016/0016-7037(96)00195-0.
- Hickman, J., Eble, C., Riley, R., Erenpreiss, M., Carter, K., Harper, J., Dunst, B., Smith, L., Cooney, M., Soeder, D., Metzger, G., Moore, J., Hohn, M., Pool, S., Saucer, J., Patchen, D., 2015. A geologic play book for Utica Shale Appalachian Basin exploration. Appal. Oil Nat. Gas Res. Consort. 2, 1–187.
- Higley, D.K., Enomoto, C.B., Leathers-Miller, H.M., Ellis, G.S., Mercier, T.J., Schenk, C.J., Trippi, M.H., Le, P.A., Brownfield, M.E., Woodall, C.A., Marra, K.R., Tennyson, M.E., 2019. Assessment of undiscovered gas resources in the Middle Devonian Marcellus Shale of the Appalachian Basin Province, 2019 (Fact Sheet No. 2019–3050), Fact Sheet. U.S. Geological Survey. https://doi.org/10.3133/fs20193050.
- Hutchings, A.M., Turchyn, A.V., 2021. A quantification of the effect of diagenesis on the paleoredox record in mid-Proterozoic sedimentary rocks. Geology 49, 1143–1147. https://doi.org/10.1130/G48774.1.
- Hutchison, M.P., 2016. Analytical methods and non-interpretative data compilation for unconventional shale plays of Yukon's Liard basin. In: Yukon Geological Survey Open File 2016–33, pp. 1–13.
- Hutchison, M.P., 2018. An appraisal of Devonian-Mississippian shale strata in Yukon's Liard basin. Yukon Explor. Geol. 2017, 69–88.
- Jarvie, D.M., 2012. Shale Resource Systems for oil and gas: Part 1—Shale-Gas Resource Systems. AAPG Memoir 97, 69–87. https://doi.org/10.1306/13321446M973489.
- Jarvie, D.M., Hill, R.J., Ruble, T.E., Pollastro, R.M., 2007. Unconventional shale-gas systems: the Mississippian Barnett Shale of north-Central Texas as one model for thermogenic shale-gas assessment. AAPG Bull. 91, 475–499. https://doi.org/ 10.1306/12190606068.
- Jin, H., Sonnenberg, S.A., 2013. Characterization for source rock potential of the Bakken Shales in the Williston Basin, North Dakota and Montana. In: Unconventional Resources Technology Conference, Denver, Colorado, 12–14 August 2013. SEG Global Meeting Abstracts. Society of Exploration Geophysicists, American Association of Petroleum Geologists, Society of Petroleum Engineers, pp. 117–126. https://doi.org/10.1190/urtec2013-013.

- Johnston, D.T., Poulton, S.W., Dehler, C., Porter, S., Husson, J., Canfield, D.E., Knoll, A. H., 2010. An emerging picture of Neoproterozoic ocean chemistry: Insights from the Chuar Group, Grand Canyon, USA. Earth Planet. Sci. Lett. 290, 64–73. https://doi.org/10.1016/j.epsl.2009.11.059.
- Katsev, S., Crowe, S.A., 2015. Organic carbon burial efficiencies in sediments: the power law of mineralization revisited. Geology 43, 607–610. https://doi.org/10.1130/ G36626.1.
- Katz, B.J., 2005. Controlling Factors on Source Rock Development—A Review of Productivity, Preservation, and Sedimentation Rate. SEPM Special Publications 82, 7–16.
- Kent, D.M., Christopher, J.E., Mossop, G., Shetsen, I., 1994. Geological history of the Williston Basin and Sweetgrass arch. In: Geological Atlas of the Western Canada Sedimentary Basin. CSPG and Alberta Research Council, pp. 421–429.
- Langford, F.F., Blanc-Valleron, M.-M., 1990. Interpreting Rock-Eval pyrolysis data using graphs of pyrolizable hydrocarbons vs. total organic carbon. AAPG Bull. 74, 799–804.
- Lash, G.G., Blood, D.R., 2014. Organic matter accumulation, redox, and diagenetic history of the Marcellus Formation, southwestern Pennsylvania, Appalachian basin. Mar. Pet. Geol. 57, 244–263. https://doi.org/10.1016/j.marpetgeo.2014.06.001.
- Lau, K.V., Maher, K., Altiner, D., Kelley, B.M., Kump, L.R., Lehrmann, D.J., Silva-Tamayo, J.C., Weaver, K.L., Yu, M., Payne, J.L., 2016. Marine anoxia and delayed Earth system recovery after the end-Permian extinction. PNAS 113, 2360–2365. https://doi.org/10.1073/pnas.1515080113.
- LeRoy, M.A., Gill, B.C., 2019. Evidence for the development of local anoxia during the Cambrian SPICE event in eastern North America. Geobiology 17, 381–400. https:// doi.org/10.1111/gbi.12334.
- Leslie-Panek, J., McMechan, M., 2021. A seismic structural overview of Liard Basin, Northeast British Columbia, Canada. Interpretation 9, T523–T532. https://doi.org/ 10.1190/INT-2020-0078.1
- Lewan, M.D., Maynard, J.B., 1982. Factors controlling enrichment of vanadium and nickel in the bitumen of organic sedimentary rocks. Geochim. Cosmochim. Acta 46, 2547–2560. https://doi.org/10.1016/0016-7037(82)90377-5.
- Li, C., Love, G.D., Lyons, T.W., Fike, D.A., Sessions, A.L., Chu, X., 2010. A stratified redox model for the Ediacaran Ocean. Science 328, 80–83.
- Loucks, R.G., Ruppel, S.C., 2007. Mississippian Barnett Shale: Lithofacies and depositional setting of a deep-water shale-gas succession in the Fort Worth Basin, Texas. AAPG Bull. 91, 579–601.
- Lyons, T.W., Severmann, S., 2006. A critical look at iron paleoredox proxies: New insights from modern euxinic marine basins. Geochim. Cosmochim. Acta, A Special Issue Dedicat. Robert A. Berner 70, 5698–5722. https://doi.org/10.1016/j. gca.2006.08.021.
- Marra, K.R., Charpentier, R.R., Schenk, C.J., Lewan, M.D., Leathers-Miller, H.M., Klett, T. R., Gaswirth, S.B., Le, P.A., Mercier, T.J., Pitman, J.K., Tennyson, M.E., 2015.
  Assessment of undiscovered shale gas and shale oil resources in the Mississippian Barnett Shale, Bend Arch–Fort Worth Basin Province, North-Central Texas (Fact Sheet No. 2015–3078), Fact Sheet. U.S. Geological Survey. https://doi.org/10.3133/fs20153078
- Marsay, C.M., Sanders, R.J., Henson, S.A., Pabortsava, K., Achterberg, E.P., Lampitt, R.S., 2015. Attenuation of sinking particulate organic carbon flux through the mesopelagic ocean. Proc. Natl. Acad. Sci. USA 112, 1089–1094. https://doi.org/ 10.1073/nnas.1415311112.
- Marz, C., Poulton, S.W., Beckmann, B., Kuster, K., Wagner, T., Kasten, S., 2008. Redox sensitivity of P cycling during marine black shale formation: Dynamics of sulfidic and anoxic, non-sulfidic bottom waters. Geochim. Cosmochim. Acta 72, 3703–3717.
- Miller, C.A., Peucker-Ehrenbrink, B., Walker, B.D., Marcantonio, F., 2011. Re-assessing the surface cycling of molybdenum and rhenium. Geochim. Cosmochim. Acta 75, 7146–7179. https://doi.org/10.1016/j.gca.2011.09.005.
- Monger, J.W.H., Price, R.A., 1979. Geodynamic evolution of the Canadian Cordillera progress and problems. Can. J. Earth Sci. 16, 770–791. https://doi.org/10.1139/
- Moslow, T.F., Haverslew, B., Henderson, C.M., 2018. Sedimentary facies, petrology, reservoir characteristics, conodont biostratigraphy and sequence stratigraphic framework of a continuous (395m) full diameter core of the lower Triassic Montney Fm, northeastern British Columbia. Bull. Can. Petrol. Geol. 66, 259–287.
- National Energy Board, 2016. The unconventional gas resources of Mississippian-Devonian shales in the Liard basin of British Columbia, the Northwest Territories and Yukon. In: Yukon Geological Survey Miscellaneous Report, 14.
- Pasquier, V., Fike, D.A., Révillon, S., Halevy, I., 2022. A global reassessment of the controls on iron speciation in modern sediments and sedimentary rocks: a dominant role for diagenesis. Geochim. Cosmochim. Acta 335, 211–230. https://doi.org/ 10.1016/j.gca.2022.08.037.
- Paxton, S.T., Pitman, J.K., Kinney, S.A., Gianoutsos, N.J., Pearson, O.N., Whidden, K.J., Dubiel, R.F., Schenk, C.J., Burke, L.A., Klett, T.R., Leathers-Miller, H.M., Mercier, T. J., Haines, S.S., Varela, B.A., Le, P.A., Finn, T.M., Gaswirth, S.B., Hawkins, S.J., Marra, K.R., Tennyson, M.E., 2017. Assessment of undiscovered oil and gas resources in the Haynesville Formation, U.S. Gulf Coast, 2016 (Fact Sheet no. 2017–3016), Fact Sheet. U.S. Geological Survey. https://doi.org/10.3133/fs20173016.
- Payne, J.L., Clapham, M.E., 2012. End-Permian mass extinction in the oceans: an ancient analog for the twenty-first century? Annu. Rev. Earth Planet. Sci. 40, 89–111.
- Peng, J., Fu, Q., Larson, T.E., Janson, X., 2020. Trace-elemental and petrographic constraints on the severity of hydrographic restriction in the silled Midland Basin during the late Paleozoic ice age. GSA Bull. https://doi.org/10.1130/B35336.1.
- Penn, J.L., Deutsch, C., Payne, J.L., Sperling, E.A., 2018. Temperature-dependent hypoxia explains biogeography and severity of end-Permian marine mass extinction. Science 362, eaat1327. https://doi.org/10.1126/science.aat1327.

- Perkins, R.B., Mason, C.E., 2015. The relative mobility of trace elements from short-term weathering of a black shale. Appl. Geochem. 56, 67–79. https://doi.org/10.1016/j. apgeochem.2015.01.014.
- Petsch, S.T., Berner, R.A., Eglinton, T.I., 2000. A field study of the chemical weathering of ancient sedimentary organic matter. Org. Geochem. 31, 475–487. https://doi.org/ 10.1016/S0146-6380(00)00014-0.
- Pichevin, L., Bertrand, P., Boussafir, M., Disnar, J.-R., 2004. Organic matter accumulation and preservation controls in a deep sea modern environment: an example from Namibian slope sediments. Org. Geochem. 35, 543–559. https://doi. org/10.1016/j.orggeochem.2004.01.018.
- Planavsky, N.J., McGoldrick, P., Scott, C.T., Li, C., Reinhard, C.T., Kelly, A.E., Chu, X., Bekker, A., Love, G.D., Lyons, T.W., 2011. Widespread iron-rich conditions in the mid-Proterozoic Ocean. Nature 477, 448–451.
- Poulton, S.W., 2021. The iron speciation paleoredox proxy. In: Elements in Geochemical Tracers in Earth System Science., pp. 1–25. https://doi.org/10.1017/ 0781108847148
- Poulton, S.W., Canfield, D.E., 2005. Development of a sequential extraction procedure for iron: implications for iron partitioning in continentally derived particulates. Chem. Geol. 214, 209–221. https://doi.org/10.1016/j.chemgeo.2004.09.003.
- Poulton, S.W., Canfield, D.E., 2011. Ferruginous conditions: a dominant feature of the ocean through earth's history. Elements 7, 107–112. https://doi.org/10.2113/ gselements.7.2.107.
- Poulton, S.W., Raiswell, R., 2002. The low-temperature geochemical cycle of iron: from continental fluxes to marine sediment deposition. Am. J. Sci. 302, 774–805. https:// doi.org/10.2475/ais.302.9.774
- Poulton, S.W., Fralick, P.W., Canfield, D.E., 2004. The transition to a sulphidic ocean 1.84 billion years ago. Nature 431, 173–177. https://doi.org/10.1038/nature02912.
- Poulton, S.W., Fralick, P.W., Canfield, D.E., 2010. Spatial variability in oceanic redox structure 1.8 billion years ago. Nat. Geosci. 3, 486–490. https://doi.org/10.1038/ ngeo889.
- Raiswell, R., Canfield, D.E., 1998. Sources of iron for pyrite formation in marine sediments. Am. J. Sci. 298, 219–245. https://doi.org/10.2475/ajs.298.3.219.
- Raiswell, R., Canfield, D.E., 2012. The iron biogeochemical cycle past and present. Geochem. Perspect. 1, 1–2.
- Raiswell, R., Canfield, D.E., Berner, R.A., 1994. A comparison of iron extraction methods for the determination of degree of pyritisation and the recognition of iron-limited pyrite formation. Chem. Geol. 111, 101–110. https://doi.org/10.1016/0009-2541 (94)90084-1.
- Raiswell, R., Newton, R., Wignall, P.B., 2001. An Indicator of Water-Column Anoxia: Resolution of Biofacies Variations in the Kimmeridge Clay (Upper Jurassic, U.K.). J. Sediment. Res. 71, 286–294. https://doi.org/10.1306/070300710286.
- Raiswell, R., Hardisty, D.S., Lyons, T.W., Canfield, D.E., Owens, J.D., Planavsky, N.J., Poulton, S.W., Reinhard, C.T., 2018. The iron paleoredox proxies: a guide to the pitfalls, problems and proper practice. Am. J. Sci. 318, 491–526. https://doi.org/10.2475/05.2018.03.
- Rast, N., Skehan, J.W., 1993. In: Roy, D.C., Skehan, J.W. (Eds.), The Acadian Orogeny: Recent Studies in New England, Maritime Canada, and the Autochthonous Foreland, 275. Geological Society of America Special Paper, pp. 1–25. https://doi.org/ 10.1130/SPE275-p1.
- Raven, M.R., Sessions, A.L., Adkins, J.F., Thunell, R.C., 2016. Rapid organic matter sulfurization in sinking particles from the Cariaco Basin water column. Geochim. Cosmochim. Acta 190, 175–190. https://doi.org/10.1016/j.gca.2016.06.030.
- Raven, M.R., Fike, D.A., Gomes, M.L., Webb, S.M., Bradley, A.S., McClelland, H.-L.O., 2018. Organic carbon burial during OAE2 driven by changes in the locus of organic matter sulfurization. Nat. Commun. 9, 3409. https://doi.org/10.1038/s41467-018-05943-6.
- Rohais, S., Crombez, V., Euzen, T., Zonneveld, J.-P., 2018. Subsidence dynamics of the Montney Formation (early Triassic, Western Canada Sedimentary Basin): insights for its geodynamic setting and wider implications. Bull. Can. Petrol. Geol. 66, 128–160.
- Rowe, H.D., Loucks, R.G., Ruppel, S.C., Rimmer, S.M., 2008. Mississippian Barnett Formation, Fort Worth Basin, Texas: Bulk geochemical inferences and Mo–TOC constraints on the severity of hydrographic restriction. Chem. Geol. 257, 16–25. https://doi.org/10.1016/j.chemgeo.2008.08.006.
- Ruppel, S.C., 2019. Anatomy of a Paleozoic basin: the Permian Basin, USA, AAPG Memoir. Bureau of Economic Geology, The University of Texas at Austin; American Association of Petroleum Geologists, Austin, TX, [Tulsa, Oklahoma].
- Ryder, R.T., 2008. Assessment of Appalachian Basin Oil and Gas Resources: Utica-Lower Paleozoic Total Petroleum System, Open File Report. U.S. Department of the Interior, U.S. Geological Survey.
- Ryder, R.T., Burruss, R.C., Hatch, J.R., 1998. Black shale source rocks and oil generation in the Cambrian and Ordovician of the Central Appalachian Basin, USA. AAPG Bull. 82, 412–441. https://doi.org/10.1306/1D9BC42B-172D-11D7-8645000102C1865D.
- Sageman, B.B., Murphy, A.E., Werne, J.P., Ver Straeten, C.A., Hollander, D.J., Lyons, T. W., 2003. A tale of shales: the relative roles of production, decomposition, and dilution in the accumulation of organic-rich strata, Middle–Upper Devonian, Appalachian basin. Chem. Geol. 195, 229–273.
- Sahoo, S.K., Gilleaudeau, G.J., Wilson, K., Hart, B., Barnes, B.D., Faison, T., Bowman, A. R., Larsen, T.E., Kaufman, A.J., 2023. Basin-scale reconstruction of euxinia and late Devonian mass extinctions. Nature 615, 640–645. https://doi.org/10.1038/s41586-023-05716-2.
- Schoepfer, S.D., Henderson, C.M., 2022. Paleogeographic implications of Open-Marine Anoxia in the Permian–Triassic Slide Mountain Ocean. In: Late Paleozoic and Early Mesozoic Tectonostratigraphy and Biostratigraphy of Western Pangea, SEPM Special Publication 113. Society for Sedimentary Geology, pp. 205–225.

- Schoepfer, S.D., Henderson, C.M., Moslow, T.F., Shen, C., 2024. Extremely high resolution XRF core scanning reveals the early Triassic depositional history of the Montney Formation in northeastern British Columbia, Canada. Palaeogeogr. Palaeoclimatol. Palaeoecol. 637, 112019 https://doi.org/10.1016/j. palaeo.2024.112019.
- Scott, C., Lyons, T.W., 2012. Contrasting molybdenum cycling and isotopic properties in euxinic versus non-euxinic sediments and sedimentary rocks: refining the paleoproxies. Chem. Geol. Special Issue Recent Adv. Trace Metal. Appl. Paleoceanogr. Stud. 324–325, 19–27. https://doi.org/10.1016/j. chemgeo.2012.05.012.
- Scott, C., Lyons, T.W., Bekker, A., Shen, Y., Poulton, S.W., Chu, X., Anbar, A.D., 2008. Tracing the stepwise oxygenation of the Proterozoic Ocean. Nature 452, 456–459. https://doi.org/10.1038/nature06811.
- Scott, C., Slack, J.F., Kelley, K.D., 2017. The hyper-enrichment of V and Zn in black shales of the late Devonian-early Mississippian Bakken Formation (USA). Chem. Geol. 452, 24–33. https://doi.org/10.1016/j.chemgeo.2017.01.026.
- Severmann, S., Lyons, T.W., Anbar, A., McManus, J., Gordon, G., 2008. Modern iron isotope perspective on the benthic iron shuttle and the redox evolution of ancient oceans. Geology 36, 487–490.
- Sinninghe Damste, J.S., De Leeuw, J.W., 1990. Analysis, structure and geochemical significance of organically-bound sulphur in the geosphere: State of the art and future research. In: Organic Geochemistry, Proceedings of the 14th International Meeting on Organic Geochemistry, 16, pp. 1077–1101. https://doi.org/10.1016/0146-6380(90)90145-P
- Sinninghe Damsté, J.S., Irene, W., Rijpstra, C., de Leeuw, J.W., Schenck, P.A., 1988. Origin of organic sulphur compounds and sulphur-containing high molecular weight substances in sediments and immature crude oils. In: Organic Geochemistry, Proceedings of the 13th International Meeting on Organic Geochemistry, 13, pp. 593–606. https://doi.org/10.1016/0146-6380(88)90079-4.
- Slotznick, S.P., Eiler, J.M., Fischer, W.W., 2018. The effects of metamorphism on iron mineralogy and the iron speciation redox proxy. Geochim. Cosmochim. Acta 224, 96–115. https://doi.org/10.1016/j.gca.2017.12.003.
- Slotznick, S.P., Sperling, E.A., Tosca, N.J., Miller, A.J., Clayton, K.E., van Helmond, N.A. G.M., Slomp, C.P., Swanson-Hysell, N.L., 2020. Unraveling the mineralogical complexity of sediment iron speciation using sequential extractions. Geochem. Geophys. Geosyst. 21, e2019GC008666 https://doi.org/10.1029/2019GC008666.
- Smith, M.G., Bustin, R.M., 1996. Lithofacies and paleoenvironments of the Upper Devonian and lower Mississippian Bakken Formation, Williston Basin. Bull. Can. Petrol. Geol. 44, 495–507.
- Smith, M.G., Bustin, R.M., 1998. Production and preservation of organic matter during deposition of the Bakken Formation (late Devonian and early Mississippian), Williston Basin. Palaeogeogr. Palaeoclimatol. Palaeoecol. 142, 185–200. https://doi. org/10.1016/S0031-0182/98)00063-7.
- Smith, T., Leone, J., 2014. Shallow onlap model for Ordovician and Devonian organic-rich shales. New York State, AAPG Search and Discovery Article, p. 50911.
- Sonnenberg, S.A., Theloy, C., Jin, H., 2017. The giant continuous oil accumulation in the Bakken Petroleum System, U.S. Williston Basin. AAPG Memoir 113, 91–119. https:// doi.org/10.1306/13572002M113508.
- Sperling, E.A., Halverson, G.P., Knoll, A.H., Macdonald, F.A., Johnston, D.T., 2013.
  A basin redox transect at the dawn of animal life. Earth Planet. Sci. Lett. 371–372, 143–155. https://doi.org/10.1016/j.epsl.2013.04.003.
- Sperling, E.A., Wolock, C.J., Morgan, A.S., Gill, B.C., Kunzmann, M., Halverson, G.P., Macdonald, F.A., Knoll, A.H., Johnston, D.T., 2015. Statistical analysis of iron geochemical data suggests limited late Proterozoic oxygenation. Nature 523, 451–454. https://doi.org/10.1038/nature14589.
- Sperling, E.A., Balthasar, U., Skovsted, C.B., 2018. On the edge of exceptional preservation: insights into the role of redox state in Burgess Shale-type taphonomic windows from the Mural Formation, Alberta, Canada. Emerg. Topics Life Sci. 2, 311–323. https://doi.org/10.1042/ETLS20170163.
- Sperling, E.A., Melchin, M.J., Fraser, T., Stockey, R.G., Farrell, U.C., Bhajan, L., Brunoir, T.N., Cole, D.B., Gill, B.C., Lenz, A., Loydell, D.K., Malinowski, J., Miller, A. J., Plaza-Torres, S., Bock, B., Rooney, A.D., Tecklenburg, S.A., Vogel, J.M., Planavsky, N.J., Strauss, J.V., 2021. A long-term record of early to mid-Paleozoic marine redox change. Sci. Adv. 7, eabf4382 https://doi.org/10.1126/sciadv.
- Stookey, L.L., 1970. Ferrozine—a new spectrophotometric reagent for iron. Anal. Chem. 42, 779–781. https://doi.org/10.1021/ac60289a016.

- Strauss, J.V., Fraser, T.A., Melchin, M.J., Allen, T., Malinowski, J., Feng, X., Taylor, J., Day, J., Gill, B.C., Sperling, E.A., 2020. The Road River Group of northern Yukon, Canada: early Paleozoic deep-water sedimentation within the Great American Carbonate Bank. Can. J. Earth Sci. 57, 1193–1219. https://doi.org/10.1139/cjes-2020.0017
- Trabucho-Alexandre, J., 2015a. Organic matter-rich shale depositional environments. In: Fundamentals of Gas Shale Reservoirs. John Wiley & Sons, Ltd, pp. 21–45. https://doi.org/10.1002/9781119039228.ch2.
- Trabucho-Alexandre, J., 2015b. More gaps than shale: erosion of mud and its effect on preserved geochemical and palaeobiological signals. Geol. Soc. Lond. Spec. Publ. 404, 251–270. https://doi.org/10.1144/SP404.10.
- Tribovillard, N., Riboulleau, A., Lyons, T., Baudin, F., 2004. Enhanced trapping of molybdenum by sulfurized marine organic matter of marine origin in Mesozoic limestones and shales. Chem. Geol. 213, 385–401. https://doi.org/10.1016/j. chemgeo.2004.08.011.
- Tribovillard, N., Algeo, T.J., Lyons, T., Riboulleau, A., 2006. Trace metals as paleoredox and paleoproductivity proxies: an update. Chem. Geol. 232, 12–32. https://doi.org/10.1016/j.chemgeo.2006.02.012.
- Tyson, R., 2005. The "Productivity Versus Preservation" Controversy: Cause, Flaws, and Resolution. SEPM Special Publication 82, 17–34. https://doi.org/10.2110/pec.05.82.0017.
- Van De Velde, S.J., Reinhard, C.T., Ridgwell, A., Meysman, F.R.J., 2020. Bistability in the redox chemistry of sediments and oceans. PNAS 117, 33043–33050.
- Viollier, E., Inglett, P.W., Hunter, K., Roychoudhury, A.N., Van Cappellen, P., 2000. The ferrozine method revisited: Fe(II)/Fe(III) determination in natural waters. Appl. Geochem. 15, 785–790. https://doi.org/10.1016/S0883-2927(99)00097-9.
- Walsh, W., Adams, A., Kerr, B., Korol, J., 2006. "Regional Shale Gas" potential of the Triassic Doig and Montney Formations, northeastern British Columbia. In: Ministry of Energy, Mines and Petroleum Resources, Oil and Gas Division, Resource Development and Geoscience Branch, British Columbia, Petroleum Geology Open File Open File 2006-02, pp. 1–19.
- Wedepohl, K.H., 1971. Environmental influences on the chemical composition of shales and clays. Phys. Chem. Earth 8, 305–333. https://doi.org/10.1016/0079-1946(71) 90020-6.
- Werne, J.P., Sageman, B.B., Lyons, T.W., Hollander, D.J., 2002. An integrated assessment of a "type euxinic" deposit: evidence for multiple controls on black shale deposition in the middle Devonian Oatka Creek formation. Am. J. Sci. 302, 110–143. https://doi.org/10.2475/ajs.302.2.110.
- Werne, J.P., Lyons, T.W., Hollander, D.J., Formolo, M.J., Sinninghe Damsté, J.S., 2003. Reduced sulfur in euxinic sediments of the Cariaco Basin: sulfur isotope constraints on organic sulfur formation. Chem. Geol. Isotop. Rec. Microb. Mediat. Proc. 195, 159–179. https://doi.org/10.1016/S0009-2541(02)00393-5.
- Werne, J.P., Lyons, T.W., Hollander, D.J., Schouten, S., Hopmans, E.C., Sinninghe Damsté, J.S., 2008. Investigating pathways of diagenetic organic matter sulfurization using compound-specific sulfur isotope analysis. Geochim. Cosmochim. Acta 72, 3489–3502. https://doi.org/10.1016/j.gca.2008.04.033.
- Wignall, P.B., 1994. Black Shales. Oxford University Press, Oxford, New York.
- Wijsman, J.W.M., Middelburg, J.J., Heip, C.H.R., 2001. Reactive iron in Black Sea Sediments: implications for iron cycling. Mar. Geol. 172, 167–180. https://doi.org/ 10.1016/S0025-3227(00)00122-5.
- Young, S.A., Benayoun, E., Kozik, N.P., Hints, O., Martma, T., Bergström, S.M., Owens, J. D., 2020. Marine redox variability from Baltica during extinction events in the latest Ordovician–early Silurian. Palaeogeogr. Palaeoclimatol. Palaeoecol. 554, 109792 https://doi.org/10.1016/j.palaeo.2020.109792.
- Zaback, D.A., Pratt, L.M., 1992. Isotopic composition and speciation of sulfur in the Miocene Monterey Formation: Reevaluation of sulfur reactions during early diagenesis in marine environments. Geochim. Cosmochim. Acta 56, 763–774. https://doi.org/10.1016/0016-7037(92)90096-2.
- Zhang, F., Romaniello, S.J., Algeo, T.J., Lau, K.V., Clapham, M.E., Richoz, S., Herrmann, A.D., Smith, H., Horacek, M., Anbar, A.D., 2018. Multiple episodes of extensive marine anoxia linked to global warming and continental weathering following the latest Permian mass extinction. Sci. Adv. 4, e1602921 https://doi.org/ 10.1126/sciadv.1602921.
- Zonneveld, J.-P., Moslow, T.F., 2018. Palaeogeographic setting, lithostratigraphy, and sedimentary framework of the lower Triassic Montney Formation of western Alberta and northeastern British Columbia. Bull. Can. Petrol. Geol. 66, 93–127.